Alma Mater Studiorum – Università di Bologna

DOTTORATO DI RICERCA IN

SCIENZE DELLA TERRA

Ciclo XXV

Settore Concorsuale di afferenza: 04/A2

Settore Scientifico disciplinare: GEO/01

CARBONATE CONICAL MOUNDS OF THE EASTERN ANTI-ATLAS (MOROCCO) AND THEIR RELATIONSHIP WITH POTENTIAL ANALOGUES ON MARS

Presentata da: **FULVIO FRANCHI**

Coordinatore Dottorato

Prof. Roberto Barbieri

Relatore

Prof. Roberto Barbieri

Co-Relatore

Dr.ssa Barbara Cavalazzi

Esame finale anno 2013

ABSTRACT

Longstanding debates concerning the origin of the Kess Kess Emsian carbonate mounds exposed at Hamar Laghdad Ridge in the eastern Anti-Atlas of Morocco centre around the processes that induced precipitation of carbonate mud and the preservation of the steep morphologies. Although in the last years an origin related to hydrothermalism seemed to be more likely, to date the Kess Kess are still considered unusual or controversial vent deposits, and their origin remains relevant to geoscientists.

This study combines in updated research review information from previous work and from results from detailed field observations and new analytical results to define a consistent framework and some new insight of current knowledge about the origin of the Emsian mounds. We obtain a complete minero-petrographic and palaeobiological data set and a detailed geochemical characterization of the different lithologies and facies of the Hamar Laghdad stratigraphic succession, including Kess Kess mounds, and we compared the results with the data from Maïder Basin mounds (Anti-Atlas, Morocco). Our data point out and support the hydrothermal model proposed for the genesis and development of the Kess Kess mounds. The mechanisms linked to the mounds formation and growth are discussed in the light of the new finding of fluid-sediment interaction within a scenario driven by late magmatic fluids circulation.

Conical mounds and other fluids related morphologies were also reported from Crommelin crater area (Arabia Terra, Mars). These mounds consist in meter-sized conical buildups hosted in the Equatorial Layered Deposits (ELDs) deposed during a regional groundwater fluid upwelling. The geometries and the geological conditions that might have controlled the development of such morphologies were discussed. According to our new data the morphological and stratigraphical characteristics of the mounds in the area of the Crommelin crater are most consistent with a formation by fluids advection.

Then we compare terrestrial and Martian data and examine the geological settings of hydrothermal mound occurrences on Earth in order to describe potential target areas for hydrothermal structures on Mars.

RIASSUNTO

Dal momento in cui sono stati descritti per la prima volta i *mound* conici affioranti nello Hamar Laghdad (Anti-Atlante, Marocco) e chiamati informalmente Kess Kess, hanno ricevuto interpretazioni discordanti. Ad oggi, sebbene sembri assodata una dipendenza dalla circolazione di fluidi idrotermali, la loro origine rimane problematica e sono pertanto definiti solo ambiguamente depositi di *vent*.

Questo progetto ha come obiettivo principale quello di fornire nuove evidenze della genesi dei Kess Kess e della loro interazione con fluidi idrotermali. A questo scopo è stata prodotta una dettagliata descrizione minero-petrografica, paleobiologica e geochimica di tutta la successione stratigrafica corrispondente ai Kess Kess (Merzane Group e Seheb el Rhassel Group). I dati così ottenuti sono stati confrontati con i dati provenienti da *mound* analoghi ai Kess Kess affioranti nel Maïder Basin per il quale è stata proposta un'origine non legata ad idrotermalismo. I dati in nostro possesso hanno confermato l'influenza di fluidi idrotermali durante la formazione dei Kess Kess e, come previsto il fattore che controlla la circolazione di fluidi all'interno dei sedimenti dello Hamar Laghdad è risultato essere un corpo vulcanico alla base dello successione stratigrafica.

In una seconda fase della ricerca sono stati descritti alcuni *mound* conici scoperti di recente sulla superficie marziana nell'area del cratere Crommelin (Arabia Terra, Marte). Questi corpi conici sono stati individuati all'interno dei così detti *Equatorial Layered Deposits* (ELDs) per i quali da tempo è stata suggerita un'origine legata a risalita di fluidi. I risultati ottenuti dalla descrizione di dettaglio dei *mound* e delle altre morfologie confermano la risalita di fluidi localizzata nelle depressioni costituite dai crateri da impatto come Crommelin. Questa risalita di fluidi oltre ad avere generato i *mound* e le altre morfologie descritte ha influenzato la geometria dei sedimenti all'interno dei crateri.

Il confronto fra *mound* terrestri e marziani e lo studio di dettaglio di particolari contesti geologici sulla Terra hanno permesso di ipotizzare potenziali aree affette da idrotermalismo e risalita di fluidi su Marte.

1. GENERAL INTRODUCTION

PREMISE

Mounds are peculiar geological bodies widespread in the geological record and described from different setting and environments from Paleozoic to Recent. Many of these geological bodies were generated under environmental conditions where the minerals precipitation was microbially mediated by communities of prokariotes. The mutual relationship between mounds and life could, therefore, be directly documented by the microbial signatures within rocks or could be indirectly inferred through the chemo-physical paleoenvironmental parameters preserved in the rocks.

The carbonate mud mounds were defined by Riding (2002) as *"carbonate mud-dominated deposits with topographic relief and few or no stromatolites, thrombolites or in place skeletons"*. The term mound, organic mound, or carbonate mound, filling the gaps between original definitions of reef and banks, became widely employed during the 1970s for many deposits, particularly of Palaeozoic age. The first formal definition of mound was by Toomey and Finks (1969): ''an organic carbonate buildup, commonly of relatively small size, devoid of obvious bedding features, and containing a biota different from the usually bedded surrounding sediments''. According to this definition carbonate mud mounds are rarely devoid of fossils, but these have often been regarded as too scarce to unequivocally account for mounds formation (Riding, 2002). The mud mounds development and its resistance to the water turbulence are due to genetic factors that triggered the early lithification of the carbonate. For example, in particular environmental conditions, precipitation of authigenic minerals, such as microbial carbonates, can be accounted for the early lithification of the sediments. This syndepositional lithification preserved precious environmental informations that could be investigated with geochemical tools.

The subject of this study is a family of Devonian carbonate conical mounds cropping out in the Eastern Anti-Atlas, Morocco. These mounds, known in the geological literature to as Kess Kess, have fueled a long and lively debate on their genesis and on the relationships with fluids advection. In a recent past, a large amount of energy was used in the geological study of these mounds that are characterized by a unique morphology and exceptional exposure. Despite the significant literature produced since the early 50s, however, only at the end of the last century a hydrothermal-related genesis was proposed (Belka, 1998; Mounji et al., 1998). Documented evidences of this hydrothermal origin, however, were still fragmentary and a complete genetic scenario was still lacking. Because of the presumed relationship with methane, and other fluids advection, and microbial activities, the Kess Kess mounds seem suitable for the study of some early life processes.

In addition, they have a potential primary interest for the astrobiological research for two main reasons: 1) their genetic link with methane and hydrothermal processes; 2) the recent discovery on Mars of conical mounds that, in several respects, they can be compared with the Kess Kess mounds.

The purposes of this thesis are (1) to describe the Devonian Kess Kess conical mounds and provide a detailed genetic model of these Moroccan mounds to answer questions that are still open, and (2) to use this model to improve the understanding of how certain conical mounds developed on Mars and what these mounds could potentially tell us on Early Mars habitability. The study of the Kess Kess mounds is thoroughly discussed in Chapter 2, where these mounds have been characterized from a geological, paleontological, and geochemical point of view. For comparative purposes with the Kess Kess mounds, Chapter 3 discusses the Devonian mounds of the Maïder Basin (Eastern Anti-Atlas) from a paleontological and paleoecological point of view. Chapter 4 is then devoted to further geochemical investigation on both the Kess Kess and Maïder mounds. Finally, Chapter 5 is devoted to a martian field of conical mounds to propose a plausible solution to their fluids circulation, even by comparison with the Moroccan mounds.

1.1. MOROCCAN CARBONATE MOUNDS

The main topic of this study is the genesis of the Early Devonian Kess Kess conical mounds cropping out in the Tafilalt region (Fig. 1.1) in the Eastern Anti-Atlas of Morocco. In this region the Devonian limestones were exhumed along kilometer long ridges with a East-West orientation. The study area is one of these ridges, the Hamar Laghdad Ridge, located 20 km East of the city of Erfoud.

The long debate on the origin of the Kess Kess conical mounds includes hypotheses centred on simple biogenic accumulation up to hydrothermal venting. Convincing, more recent investigations on the origin and development of these mounds, however, consolidated the hypothesis that processes triggered by hydrothermal fluids influenced their development, and significantly contributed to their early lithification (Belka, 1998; Mounji et al., 1998). New insights coming from field survey and intense analysis (both presented in this thesis) have emphasized the role of an Early Devonian volcanic body which acted as source for the late magmatic fluids that influenced the Kess Kess growth. Indeed, the Kess Kess limestones set on the top of a volcanic rise composed of *in situ* basaltic breccia partially affected by neomorphic replacements. Minero-petrographic analyses and stable isotope investigations, associated with detailed geological and paleobiological field observations, suggest that during the micrite deposition, which is an important component of these mounds, a fluid mixing, dominated by low-temperature hydrothermal fluids and sea-water, occurred. The deposition of neomorphic minerals, including different phases of silica and

goethite, idiotopic to hypidiotopic dolomite, and particular faunal associations could also be related to fluids mixing during the mounds development. To find a solution to the question of the genesis of the Kess Kess mounds needs a multidisciplinary approach to solve several unsolved problems. With this aim, in samples collected during a detailed field survey, performed in order to produce a comprehensive geological picture, paleontological, mineralogical and stable isotope (carbon and oxygen) analyses were used to determine if the facies identified on the field could be put in relation with geochemical signatures and/or paleontological associations (Chapter 2).

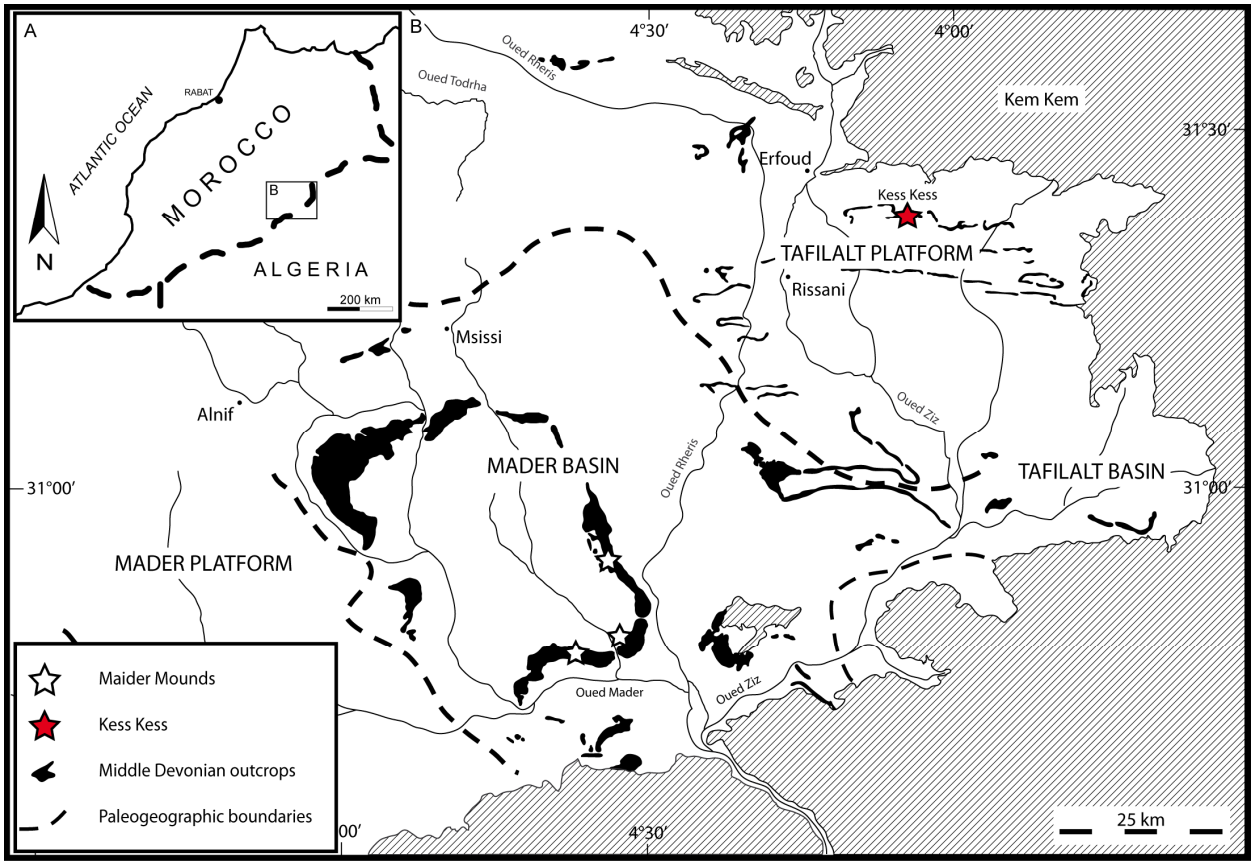

Figure 1.1. A) Map of north-western Africa showing the study area (box) detailed in B. B) Distribution of the Middle Devonian outcrops in the Tafilalt and Mader palaeogeograpy systems. The Kess Kess mounds cropping out at the Hamar Laghdad ridge (red star) are hosted in the Tafilalt platform whereas the Maïder mounds are hosted in the Maïder basin (white stars). Modified from Michard, 1976; Kaufmann, 1997.

In a second phase of the research, the Middle Devonian carbonate mounds of the Maïder Basin (Fig. 1.1) were compared with the Kess Kess mounds (Chapter 3). Hollard (1974) was the first to mention the three mound occurrences of Aferdou el Mrakib, Guelb el Maharch, and Jebel el Oftal in the Maïder Basin (Fig. 1.1), with shape, size, and facies that are fairly similar to the carbonate mounds of the Hamar Laghdad. Previous investigations (Wendt, 1993; Kaufmann et al., 1997; 1998a, b) recognized the mud mound nature of the Maïder buildups, which consist essentially

of microspar. Even for these buildups, however, genetic and early lithification factors are still a matter of debate. In Chapter 3 is discussed the general setting of the mounds in the Maïder Basin with a close examination of Aferdou el Mrakib mound, which is mostly interpreted as an organic reef. A paleontological and geochemical characterization of this mound allowed a comparison with the Kess Kess faunal association and geochemical fingerprints.

A number of representative samples from those facies suspected to be influenced by fluids circulation, from both Kess Kess and Maïder mounds, were analyzed using advanced analytical techniques. This process provided a detailed geochemical and petrographic data set for each of the selected facies (Chapter 4).

As previously stated, despite the broad literature on these two groups of Devonian mounds, the question of their genesis and the paleoecological reconstruction of the Hamar Laghdad were still waiting for a convincing solution. Despite fluid inclusions (Belka, 1998) and the isotopic composition of the micrite (Mounji et al., 1998) endorsed a hydrothermally-related origin, several problems are still unsolved and centred on: i) biotic vs abiotic control of carbonate precipitation; ii) origin of the thermal flux; iii) nature of the plumbing system. During my PhD I have tried to address to these scientific problems. Summarising, the puzzle of the Kess Kess genesis has also been addressed through the aid of analytical instruments looking for hydrothermally-related minerals, anomalous elements and describing the ecological niches that existed during the mounds development.

1.2. MOROCCAN CONICAL MOUNDS: POTENTIAL TERRESTRIAL ANALOGUES FOR MOUNDS OBSERVED ON MARS

Since the first man looked at the stars with a scientific eye the main questions were: could have life existed outside our planet? Are we alone in the Universe? Despite these atavic questions only recently the scientific community started to investigate the problem of extraterrestrial life with proper scientific tools. The new science of astrobiology encompasses wide interests spanning from detection of exobiological life to the study of early life on Earth, both considered the end-members for the understanding of the life phenomena to a extraterrestrial scale. Indeed, if the knowledge of extraterrestrial environments (and, perhaps, of life) is a scientific challenge of our generation, the increase in knowledge of the terrestrial extreme environments can help significantly in this effort and, also, to determine the possibility of planetary habitability.

Planetary habitability is the measure of a planet potential to develop and sustain life. As the existence of life beyond Earth is currently uncertain, planetary habitability is largely an extrapolation of conditions similar to those of early Earth and the characteristics that appear

favorable to life flourishing. NASA has defined the principal habitability criteria as "*extended regions of liquid water, conditions favorable for the assembly of complex organic molecules, and energy sources to sustain metabolism*". According to the Earth experience these three conditions are always present in the so-called extreme environments. Providing nutrients, energy and suitable substrates for microbial life the extreme environments could resemble the early Earth conditions and should be suitable for detecting life signature. Environments in the early Earth, such as seeps, black smokers, hydrothermal vents, etc., gave probably rise to the first primordial life. For these reasons some of the astrobiological scientific community addressed their attention to the geological products of ancient systems that may have had a relationships with extreme environmental conditions.

Nowadays it is known that Mars was a dynamic planet with lots of volcanic activity, tectonic displacements and hydrothermalism. These dynamic conditions gave rise to different geological conditions comparable with some the extreme environments of the early Earth, with abundant water (and other fluids) circulation. It is, therefore, useful a comparative approach between certain terrestrial environments and those, on Mars, which approximate at least some features because: ”*In the absence of field-based data, terrestrial analogs provide the basis for deciphering the geologic history of extraterrestrial surfaces and inferring the conditions through which they form*” (Skinner and Mazzini, 2009).

Especially in the last decade the efficiency of the satellites and rovers on Mars allowed the production of impressive imaging and compositional databases which made possible the preparation of a detailed geological cartography. From these databases suitable morphologies and compositional data have made possible a comparison with some terrestrial geological bodies. This body of information from the planetary research has enabled to take into account of new extraordinary details on morphology, stratigraphy, and soil and atmosphere composition, giving rise to questions such as for example: i) is it reasonable that similar morphologies correspond to a similar genesis?; ii) how rocks could preserve life signatures on Mars?; and, ultimately, iii) how Earth analogues could help us to define Mars habitability?

Although it is possible infer a large amount of information from imaging and spectroscopy databases, the geological fundamental information from the field survey is still lacking. A possible alternative can then be represented by the terrestrial geological record. Through them hypotheses can be imagined to fill at least some of the gap on Martian knowledge. Thanks to comparative analyses between terrestrial and martian bodies environments that could preserve life signatures can properly be described with a substantial improvement in the use of the most suitale abalytica tools.

1.3. CHAPTERS SUMMARIES

Chapter 2. This chapter is part of the paper in preparation "How hydrothermal phenomena have influenced the development and preservation of the Kess Kess Devonian mounds (Anti-Atlas, Morocco)". The purpose of this chapter is to discuss the mechanisms that allowed the mounds to originate and develop, to keep their peculiar morphology, and to address the still open questions about the biotic control on carbonate deposition and the fluids provenience. These goals were achieved through the integration of detailed stratigraphic and sedimentologic data collected during field surveys with the different sets of analytical data produced.

Chapter 3. The data reported in this chapter derived from a field survey in the Maïder Basin. In the Maïder Basin a family of Middle Devonian mounds that resemble the Kess Kess for their shape, lithology and faunal assemblage has been investigated. For comparative purposes with the Kess Kess mounds, the faunal association of the Aferdou el Mrakib mound has been reported. Part of this work was published in the paper:

Franchi, F., Shemm-Gregory, M., Klug, C., 2012. A new species *Ivdelinia* Andronov, 1961 from the Moroccan Givetian and its palaeoecological and palaeobiogeographical implications. Bulletin of Geosciences 87 (1), 1-11.

Chapter 4. The analytical work carried at the Department of Geology of the University of Johannesburg is reported in this chapter with emphasis on the geochemical composition of the limestones and element abundances. The mais purpose was to elucidate the type of water circulation through the sediments. For this purpose, XRD, XRF, EMPA, SEM-EDS and ICP-MS analyses on 21 selected samples from the Kess Kess mounds and 4 samples from the Maïder mounds (for comparative purposes) have been carried out.

Chapter 5. This chapter reports the part of planetary geology performed during my PhD and is part of the paper in preparation "Water related morphologies within layered deposits in Crommelin crater area (Arabia Terra, Mars)". Morphological and stratigraphic correlations were carried out on the deposits of the Crommelin and Firsoff Craters (Arabia Terra) where flow structures and conical mound settled on top of Equatorial Layered Deposits (ELDs) have been described. The morphologies described within the ELDs were compared with similar morphologies occurring elsewhere on Mars lowlands within a groundwater flow upwelling scenario. The Firsoff conical mounds were then compared with the Kess Kess mounds, interpreted as their potential terrestrial analogues. The assumed affinity between the water upwelling and the Firsoff landforms, and the derived astrobiological significance, are discussed in this chapter.

REFERENCES:

Belka, Z., 1998. Early Devonian Kess-Kess carbonate mud mounds of the eastern Anti-Atlas (Morocco), and their relation to submarine hydrothermal venting. Journal of Sedimentary Research 68, 368-377.

Hollard, H., 1974, Recherches sur la stratigraphie des formations du Dévonien moyen, de l'Emsien supérieur au Frasnien, dans le Sud du Tafilalt et dans le Maïder (Anti-Atlas oriental): Notes du Service Géologique du Maroc 264, 7–68.

Kaufmann, B. 1997. Diagenesis of Middle Devonian carbonate mud buildups of the Maïder Basin (eastern Anti-Atlas). Journal of Sedimentary Research A67, 945–956.

Kaufmann, B. 1998a. Middle Devonian reef and mud mounds on a carbonate ramp: Maïder Basin (eastern Anti-Atlas, Morocco), 417–435. In WRIGHT, V.P. & BURCHETTE, T.P. (eds) Carbonate Ramps. Geological Society of London, Special Publications 149.

Kaufmann, B. 1998b. Facies, stratigraphy and diagenesis of Middle Devonian reef- and mud-mounds in the Maïder (eastern Anti-Atlas, Morocco). Acta Geologica Polonica 48, 43–106.

Mounji, D., Bourque, P.A., Savard, M.M., 1998. Hydrothermal origin of Devonian conical mounds (kess-kess) of Hamar Lakhdad Ridge, Anti- Atlas, Morocco. Geology 26, 1123-1126.

Riding, R., 2002. Structure and composition of organic reefs and carbonate mud mounds; concepts and categories. Earth-Sciences Reviews 58, 163–231.

Skinner, Jr., J. A., Mazzini, A., 2009. Martian mud volcanism: Terrestrial analogs and implications for formational scenarios. Marine and Petroleum Geology 26 (2009) 1866–1878.

Toomey, D.F., Finks, R.M., 1969. Middle Ordovician (Chazyan) mounds, southern Quebec, Canada: a summary report. New York State Geological Association, 41st Annual Meeting, Guidebook to Field Excursions. Plattsburgh, New York, 121– 134.

Wendt, J., 1993, Steep-sided carbonate mud mounds in the Middle Devonian of the eastern Anti-Atlas, Morocco: Geological Magazine, 130, 69–83.

2. INFLUENCE OF HYDROTHERMAL PROCESSES IN THE DEVELOPMENT AND PRESERVATION OF THE DEVONIAN KESS KESS MOUNDS (ANTI-ATLAS, MOROCCO) *

2.1. INTRODUCTION

Carbonate mounds known in the geological record from Proterozoic to Present (Wilson, 1975; Flajs et al., 1995; Monty et al., 1995; Foubert and Henriet, 2009) consist of "bioherms that lack frameworks" (*sensu* Kopaska-Merkel and Haywick, 2001), and are "mud-dominated deposits with topographic relief and few or no stromatolites, thrombolites or in place skeletons" (Riding, 2002). They represent unique organo-sedimentary bodies found in different environmental settings from freshwater lakes to continental margins or intra-platform environments, from shallow- to deep-water marine slopes (Monty et al., 1995; Kopaska-Merkel and Haywick, 2001; Flügel, 2004). Despite their fine-grained composition and the absence of a rigid framework of invertebrate skeletons, mounds can develop into large structures with a high angle of accumulation (e.g., Riding, 2002; De Mol et al., 2005; Teichert et al., 2005; Foubert and Henriet, 2009). Size and shape of carbonate mounds range from less than one meter to few kilometres across (giant mounds) relief features with an ovoid to circular base (e.g., Monty et al. 1995; Foubert and Henriet 2009). Veins and fractures, stromatactoid (Bathurst, 1980), zebra (Fischer, 1964), biodetrital and fenestral fabrics, clotted and peloidal (microbial) microfabrics are among the most commonly observed features associated to carbonate mounds (e.g., Monty et al., 1995). Since Proterozoic mounds were essentially produced by microbes and benthic invertebrates; biodetrital and microbial-induced processes dominated Phanerozoic and Cenozoic mound constructions. Therefore, microbes are an important bio-component of the mounds and may also represent a primary contribution to the deep-water mound formation (Pratt, 1995), especially when they are associated to chemosynthetic-based *in situ* production of (mound) carbonates around hydrothermal vents or cold seeps at the sea floor (e.g., Campbell, 2006).

Carbonate mounds are well known in north-western Africa (Fig. 2.1) where Paleozoic successions outcrop in Morocco and Algeria (e.g., Wendt et al., 1993; Aitken et al., 2002; Barbieri et al., 2004). Among the most spectacularly exposed carbonate mounds are the conical clusters,

* This chapter consists of a paper by Fulvio Franchi, Barbara Cavalazzi, Catherine Pierre, Roberto Barbieri, "Influence of hydrothermal processes in the genesis and development of the Devonian Kess Kess mounds (Anti-Atlas, Morocco)" submitted to Sedimentary Geology in January 2013.

informally called Kess Kess, cropping out at the Hamar Laghdad Ridge, 16 Km south east of the town of Erfoud, in the Tafilalt region, Eastern Anti-Atlas, Morocco (Figs. 2.1 and 2.2). According to their conodont contents (Brachert et al., 1992; Aitken et al., 2002), these carbonates mounds are Early Devonian (Emsian) in age (Fig. 2.2C). However, the isolated Hollard Mound (Peckmann et al., 1999) and few other smaller mounds (Olempska and Bełka, 2010) located in the eastern part of the Hamar Laghdad ridge, have a more recent age, being dated to the Middle Devonian (Eifelian and Givetian-Frasnian, respectively) (Fig. 2.2B).

In contrast to the origin proposed for the Hollard Mound that is interpreted as a seafloor paleo-cold seep active in Eifelian age (Peckmann et al., 1999; 2005; Cavalazzi, 2007; Cavalazzi et al., 2007, 2012), the controversy surrounds the hypothesis proposed of the origin of the Emsian Kess Kess mounds. Since carbonate Kess Kess conical mounds were first described in the geological record (Mechinkoff in Roch, 1934), their genesis has been tentatively attributed to tectonic (folding) processes (Menchikoff in Roch, 1934), a biogenic origin by comparison with the modern South Pacific atolls (e.g., Alem et al., 1968; Gendrot, 1973), or coupled hydrodynamic accumulation-early lithification processes (Brachert et al., 1992). The discovery of the first chemosynthetic carbon fixation-based communities discovery (Lonsdale, 1977) suggested another explanation for mound formation and growth. Based on the temperature values obtained from the fluid inclusions, the rare earth elements (REEs) and stable isotopes compositions, and the presence of thermophilic faunas, an origin related to hydrothermal processes was more recently suggested to explain the formation of the Emsian mound micrite (Bełka, 1998; Mounji et al., 1998; Aitken et al., 2002; Berkowski, 2004, 2006, 2008; Bełka and Berkowski, 2005; Olempska and Bełka, 2010; Berkowski and Klug, 2012). Therefore, the muddy (authigenic carbonate) sediments of the mounds were supposed to be locally produced and lithified during an early stage of the hydrothermal activity driven by late-magmatic fluids related to the Early Devonian submarine calc-alkaline volcanic activity (Bełka, 1998; Mounji et al., 1998). Apparently, owing to the lack of unambiguous geochemical and sedimentological evidences, to date the origin of the Moroccan Emsian mounds (related to fluids venting?)is still debated.

The new data set discussed in this work will provide new evidences about the extant processes during the deposition of the whole Hamar Laghdad succession allowing to clarify the role of hydrothermal fluids in the Kess Kess growth. Considering the model proposed by Belka (1998) for the Kess Kess development, hydrothermal fluids seepage driven by volcanic rocks, we studied the whole succession focusing on the mineralogy of the volcanic rocks and the terminal part of the Seheb el Rhassel Group where the Kess Kess mound are exhumed. During these study

sedimentological and geochemical evidences of warm water circulation throughout the Hamar Laghdad were found in agreement with the proposed model.

2.2. GEOLOGICAL SETTING

2.2.1. Regional geology

Paleozoic deposits in the eastern Anti-Atlas of Morocco were part of the continental shelf sequence that developed in the north-western margin of Gondwana during Late Precambrian to Early Carboniferous (Piqué and Michard, 1989). These deposits were tentatively placed at approximatively 50° to 60°-70° south palaeolatitude on the southern margin of the Paleo-Tethys (Tait et al., 1995; Stampfli and Borel, 2002). The closure of the western Paleo-Tethys and the consequent clockwise Gondwana rotation during the Devonian resulted in a gradual formation of several intra-cratonic, non-folded basins that include the Maïder and Tafilalt Platforms-Basins systems (Wendt, 1985) (Fig. 2.1).

After the deposition of the Early Devonian (Lochkovian) *Scyphocrinites* beds, due to tectonic and volcanic events, the Early Devonian paleo-morphology of the Tafilalt Platform changed. A submarine calc-alkaline volcanic activity has created the topographic rise leading to the formation of a carbonate succession on top of which the Kess Kess mounds (Fig. 2.2D) developed during the Early Devonian (Bełka, 1998). Hollard (1981 a, b) has divided the Devonian deposits of the Hamar Laghdad Ridge in the following groups (from the base to the top): Merzane, Seheb el Rhassel, Amerboh, Bou Tchrafine and Achguig Groups (Figs. 2.2B-C and E). The Kess Kess mounds are located in the upper part of the Seheb el Rhassel Group (Figs. 2.2D-E).

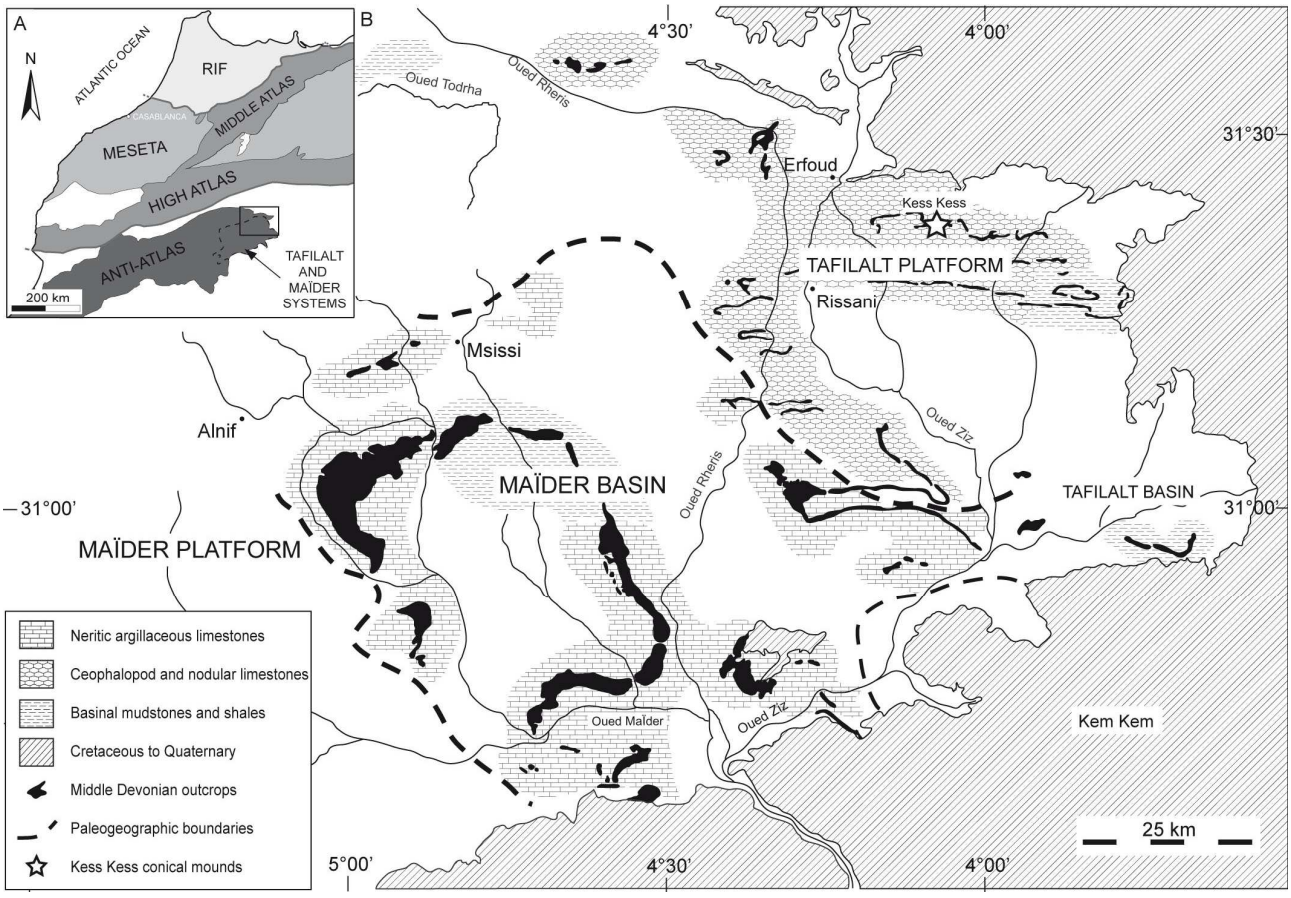

Figure 2. 1. Simplified geological map of north-western Africa. A) **Rif, Meseta and Atlas structural domains dominate the physiography of north-western Africa. The eastern part of Anti-Atlas domain includes the Devonain Tafilalt and Maïder palaeogeographic units (broken line). The study area (box) is detailed in B.** B) **Distribution of the Tafilalt and Maïder platform-basin system. The Kess Kess mounds cropping out at the Hamar Laghdad ridge (star) are hosted in the Tafilalt platform. Modified from Michard (1976), Kaufmann (1997).**

2.2.2. Stratigraphy of the Hamar Laghdad

The Lochkovian part of Merzane Group at the Hamar Laghdad Ridge is dominated by a partially exposed dome-shaped belt (Fig. 2.3A) of volcanic rocks (maximum exposed thickness of approximately 35 m) overlying reddish, crudely layered *Scyphocrinites* beds with abundant crinoids lying in life position, locally showing gypsum crusts. These volcanic rocks consist of volcanic breccias that occur in decimeter to meter thick beds of mm-sized pyroclasts (more details in paragraph 4.2). A Late Lochkovian-Early Pragian hiatus (Fig. 2.2C) characterizes the Merzane Group-Seheb el Rhassel Group unconformity.

The maximum thickness of the Seheb el Rhassel Group (approx. 100 m) occurs in the central area of Hamar Laghdad Ridge where the underlying volcanic deposits of the Merzane Group

are thicker. The Seheb el Rhassel Group mostly consists of wackestone with different amounts of auloporid, trilobite and crinoid remains with locally abundant tentaculites (refer to representatives of the Class Tentaculita, Bouček, 1964). However, the Seheb el Rhassel Group bottom strata are shallow marine carbonates with episodic brachiopod *lumachella* beds and meter thick strata of crinoidal packstone, whereas lenses of crinoidal packstone become more common in its middle-upper part. The Emsian mounds only occur to the last ten meters of the unit (Figs. 2.2C, E). Limestones of the infra-mounds deposits show a horizontal parallel stratification that is locally truncated by characteristic reddish clastic layers (centimeters to decimeters thick) typified by pisolites, cm-sized carbonate pebbles, and an high percentage of well-rounded clasts and pebbles of quartz.

At the Hamar Laghdad ridge the contact between Seheb el Rhassel Group and the Amerboh Group is marked by a substantial decrease in lithification upward. The grey limestones of the Seheb el Rhassel Group pass up into marlstone of the Amerboh Group, nodular limestones and bituminous limestone of the Bou Tchrafine and Achguig Groups (Figs. 2.2B-C, E). The dark, bituminous limestones represent the lower Kellwasser member (late Frasnian-early Fammenian) (Fig. 2.2C).

These regional framework is the result of an intensive field surveys and field observations, integrated with the broad literature the on both paleontological and geological aspects of Hamar Laghdad (for review see Alberti, 1981; Wendt et al., 1984; Brachert et al., 1992; Bełka, 1998; Aitken et al., 2002).

Figure 2. 2. (Next page) Schematic geological map and stratigraphy of the Hamar Laghdad ridge area, north-eastern Anti-Atlas, Morocco. A) Hamar Laghdad ridge (boxed area) is part of the Devonian outcrop in the Tafilat platform palaeogeographic unit (modified from Aitken et al. 2002). B) Satellite image showing the distribution of the described lithostratigraphic units cropping out at the Hamar Laghdad ridge. Colors in the map correspond to the lithostratigraphic units in C. C) Lithotratigraphic subdivision of the Hamar Laghdad ridge showing the stratigraphic position of the Kess Kess mounds (arrow) within the Seheb el Rhassel Group (modified from Bełka 1998; Aitken et al. 2002). D) Panoramic view of the Hamar Laghdad ridge (seen from west) showing several Kess Kess mounds. E) Panoramic view of few mounds (arrows) at the top of the Seheb el Rhassel Group at the Hamar Laghdad ridge (seen from west).

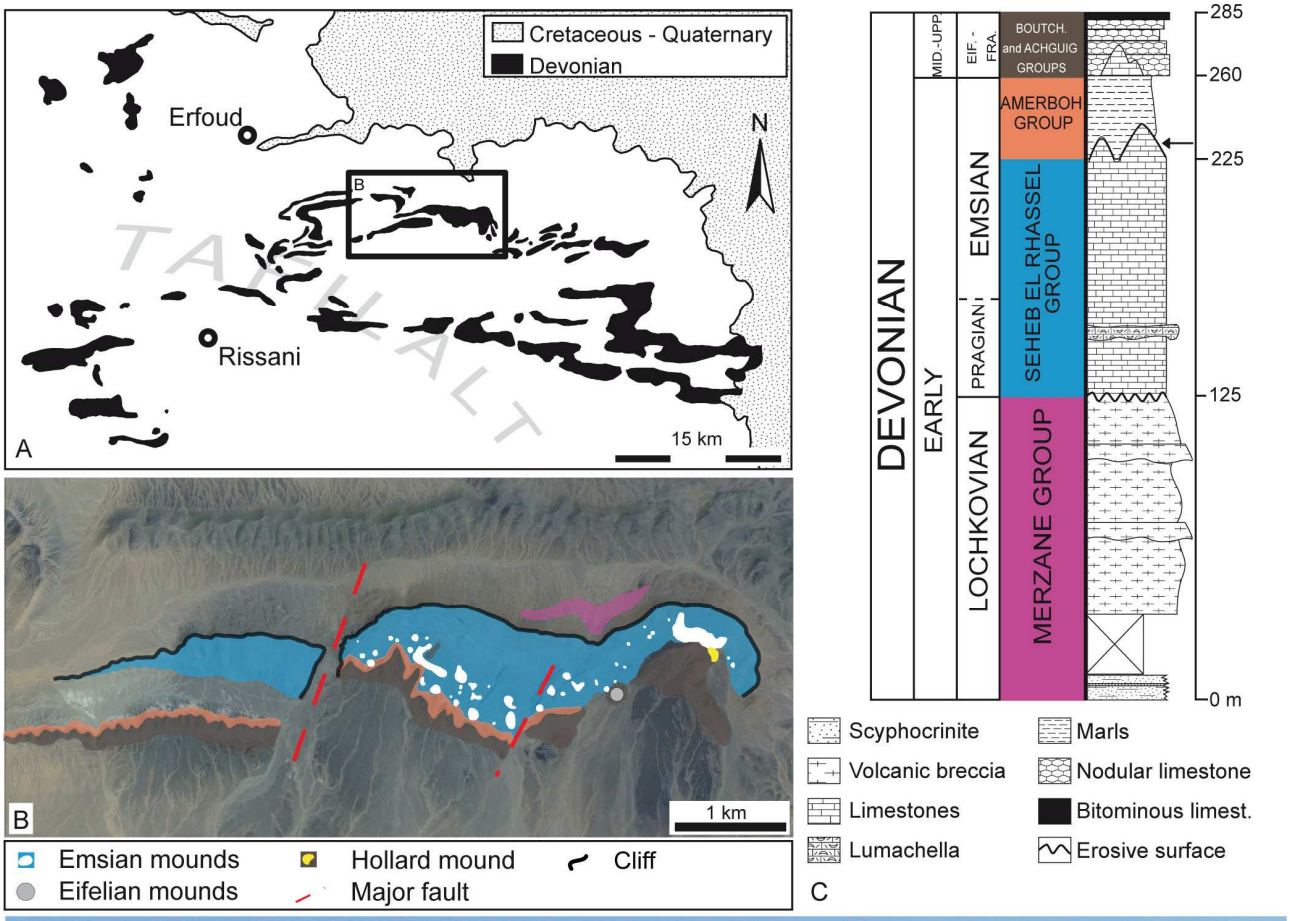
Cretaceous - Quaternary
Devonian
Erfoud
Rissani
N
B
TAFILALT
15 km
A
B
1 km
Emsian mounds
Eifelian mounds
Hollard mound
Major fault
Cliff
DEVONIAN
EARLY
MID.-UPP.
LOCHKOVIAN
PRAGIAN
EMSIAN
EIF. - FRA.
BOUTCH. and ACHGUIG GROUPS
AMERBOH GROUP
SEHEB EL RHASSEL GROUP
MERZANE GROUP
285
260
225
125
0 m
Scyphocrinite
Volcanic breccia
Limestones
Lumachella
Marls
Nodular limestone
Bitominous limest.
Erosive surface
C

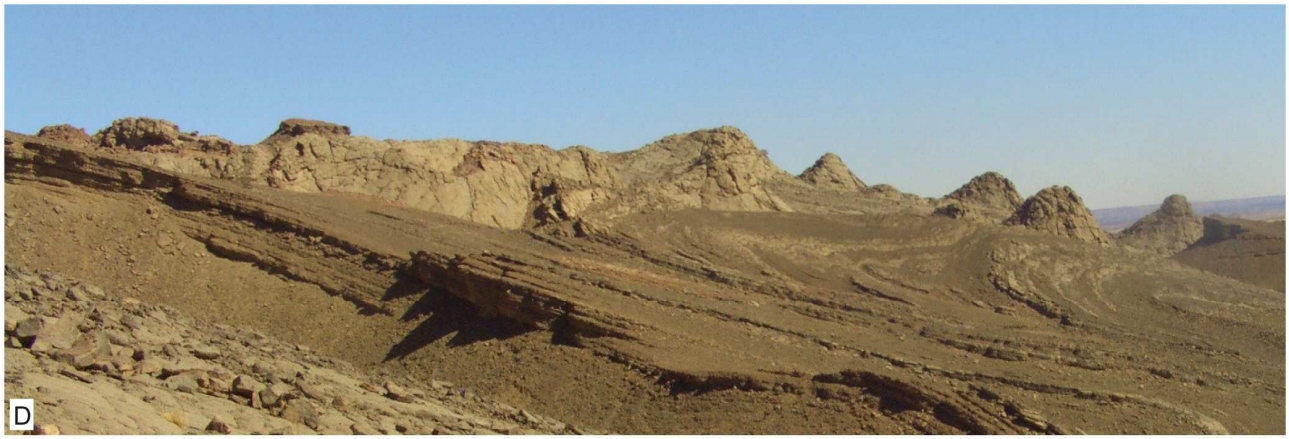
D

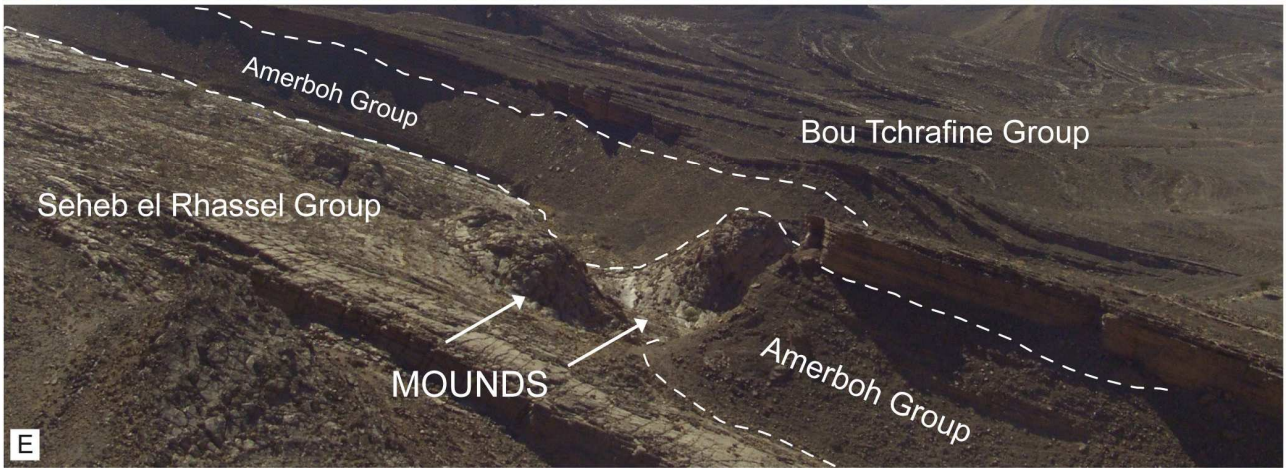
Amerboh Group
Bou Tchrafine Group
Seheb el Rhassel Group
MOUNDS
Amerboh Group
E

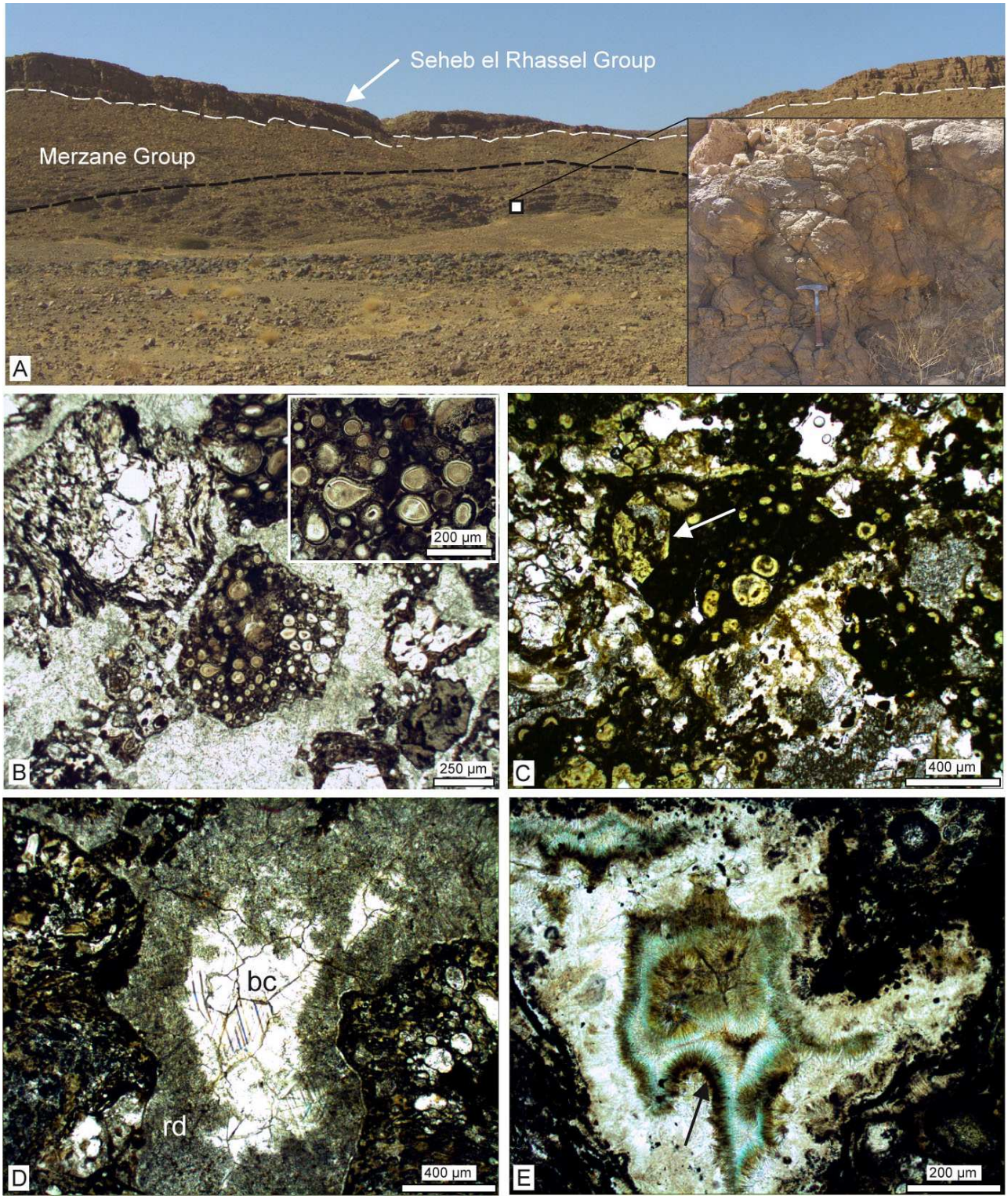

Figure 2. 3. Outcrop view and photomicrographs of the basaltic breccias of the Merzane Group below the Seheb el Rhassel Group (broken white line). A) **Dome-shaped outcrop of volcanic breccias (black broken line). In the boxed area a closer view of the volcanic breccias.** B) **Rounded pyroclasts cemented by calcite. In the boxed area a closer view of the vesicular pyroclasts. Vesicles are filled by phyllosislicates.** C) **Pyroclasts of the volcanic breccias cemented by isopachous radiaxial calcite (rd) and blocky calcite (bc).** D) **Detail of a vesicular pyroclast and euhedral olivine crystal (white arrow).** E) **Acicular clinochlore (arrow) and quartz cements.**

2.3. MATERIAL AND METHODS

Field observations and sample collections were conducted on May 2010 and February 2011 at the Hamar Lahgdad Ridge, eastern Anti-Atlas, Morocco (Figs. 2.1 and 2.2). Forty-seven Early Devonian, Emsian mounds and related infra-mound deposits were observed, described and more than 250 samples were collected from different stratigraphic levels. Samples were processed for mineralogical, petrographic and geochemical analyses, and paleontological and microfacies observations. The petrographic- and microfacies-based analyses were performed through 130 uncovered thin sections (45x60 mm^2 surface area, 30 μm foil thickness) with transmitted- and reflected-light microscopy at Dipartimento di Scienze Biologiche, Geologiche e Ambientali of the Università di Bologna (Italy). *In situ*, non-destructive analyses were performed with the use of a WITec alpha300R Confocal Raman microscope (Department of Geology and SPECTRAU facilities of the University of Johannesburg, South Africa) to identify the distribution of mineral phases and carbonaceous materials within the samples. Raman analyses were recorded and treated using WITecProject2.06® software, and compared with reference spectra from the RRUFF Data-Base using the Crystal Sleuth free software (Laetsch and Downs, 2006; White, 2009; Cavalazzi et al., 2012). Cathodoluminescence petrography was conducted using a CITL 8220 MK3 optical equipment (operating conditions: 17 kV beam voltage and 400 μÅ beam current) at Dipartimento di Scienze della Terra of the Università di Torino (Italy).

45 representative samples powdered and analyzed by using a Philips PW 1480, CuK_1, X-ray and a PANanalytical X-PetPro X-ray diffractometer, and an PANanalytical Magix PRO X-ray Fluorescent Spectrometer for mineralogical and elements distributions analyses, respectively (Dipartimento di Scienze Biologiche, Geologiche e Ambientali of the Università di Bologna; Department of Geology and SPECTRAU facilities of the University of Johannesburg, South Africa).

Morphological description and chemical (elemental) composition of microscopic features were obtained by scanning electron microscope (SEM) observations and energy dispersive X-ray spectrometer (EDS) analyses. SEM-EDS investigations were performed on etched (60 seconds in aqueous solutions with 1% HCl concentration) and non-etched freshly broken samples and thin sections by using a Jeol 5600 SEM-EDS (operating conditions: 15 and 25 kV accelerating voltage, and 15 and 20 mm working distance) equipped with an electron back-scattering CENTAURUS system at Department of Geology and SPECTRAU facilities of the University of Johannesburg (South Africa).

Preliminary $\delta^{13}C$ and $\delta^{18}O$ stable isotopes analyses were performed at the IsoAnalytical Limited laboratories (Crewe, UK) on bulk carbonates. Micro-drilled and micro-milled (drill tip size: 2 mm and 200-100 µm, respectively) specific carbonate phases from polished slab surfaces and thin sections were then analyses at the LOCEAN laboratory, Université Pierre et Marie Curie (Paris). The CO_2 gas extracted from the carbonates by attack with 100% phosphoric acid at 90°C was analyzed with a Dual Inlet –Isotopic Ratio Mass Spectrometer (Isoprime-GV Instruments). The analytical precision of carbon and oxygen data was 0.01‰, and referred to the VPDB standard (Vienna Pee Dee Belemnite). The oxygen stable isotopic values were computed referred to VSMOW (Vienna Standard Mean Ocean Water) in accordance with O'Neil et al. (1969) and Friedmann and O'Neill (1977), and the paleo-temperatures reported in °C.

Figure 2. 4. (Next page) Transmitted light photomicrographs of Merzane Group volcanic breccia. Numbers correspond to spectra in B. B) Representative Raman spectra of the volcanic breccia characterized by clinochlore bands (200, 551, 581 cm^{-1}) within the vesicles filling (1) and olivine replacements, quartz bands (128, 208, 466 cm^{-1}) within the cements (2), calcite bands (283, 712, 1088 cm^{-1}) within bright cements (3) and anatase bands (14, 398, 514, 638 cm^{-1}) around the vesicles and within the non-pleochroic glass (4).

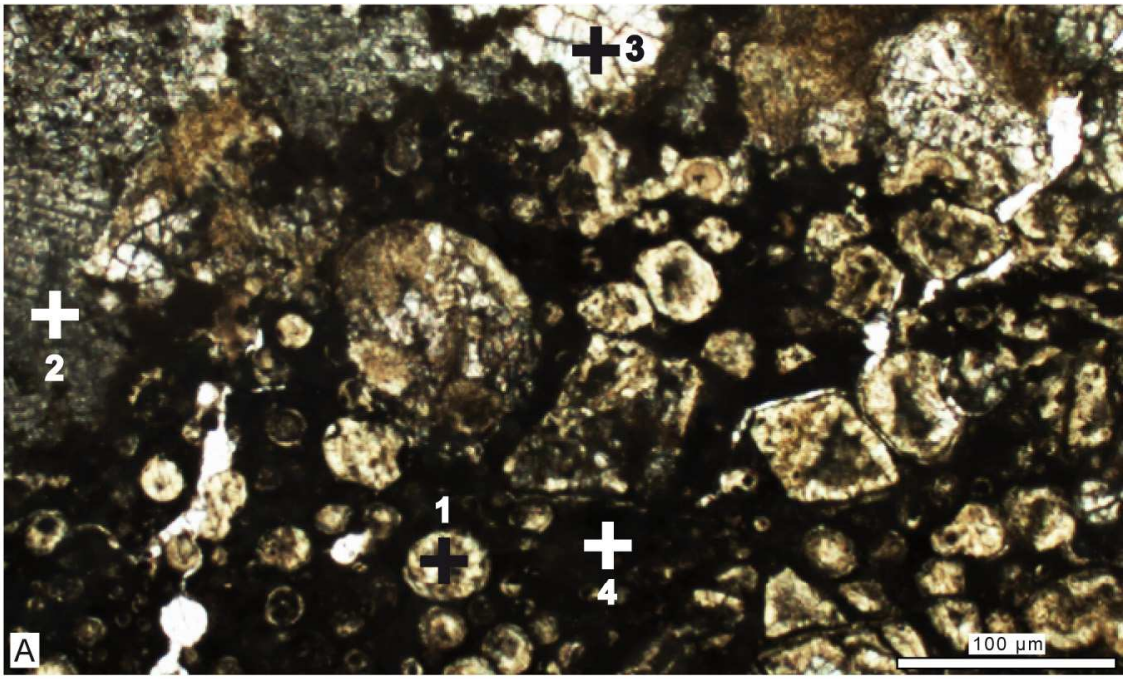
3
2
1
4
A
100 µm

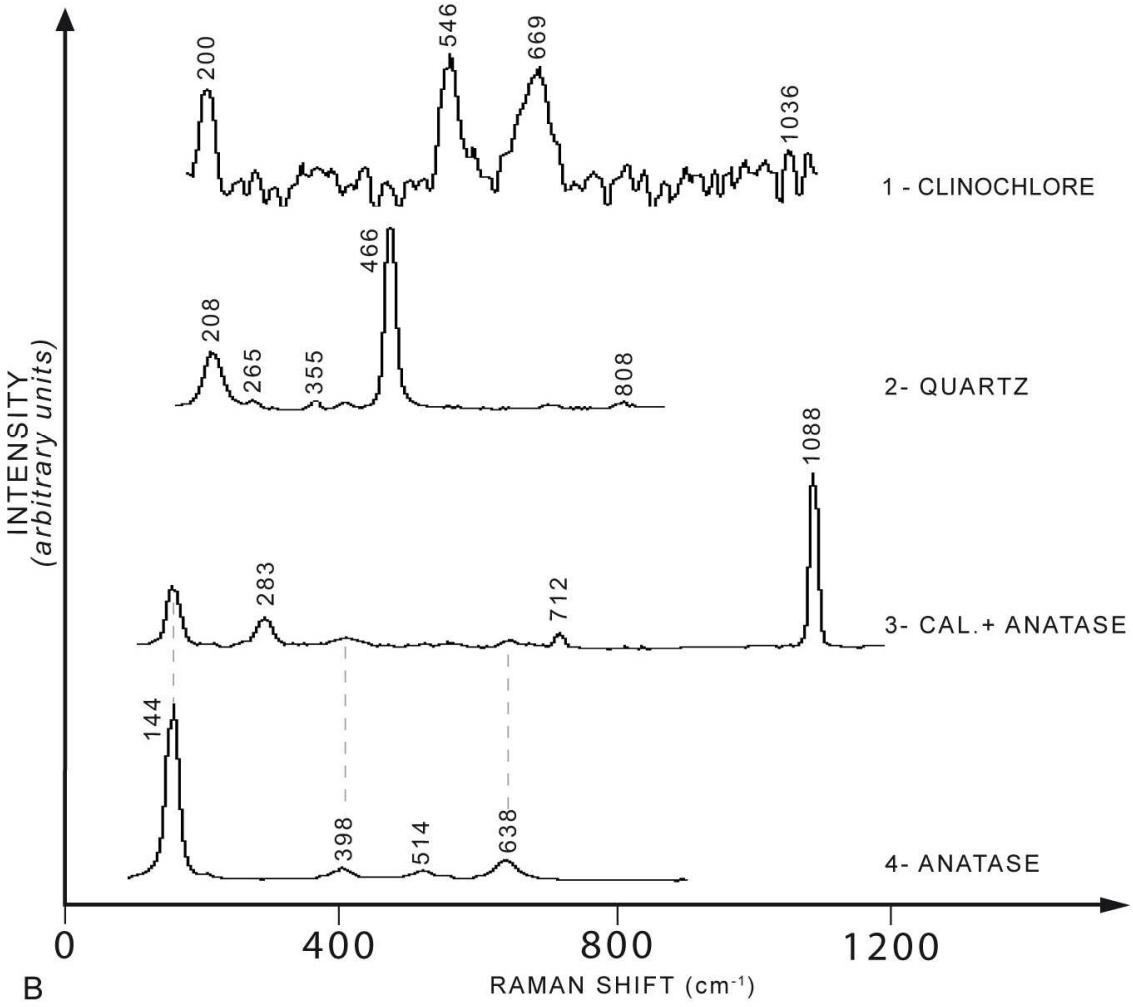
INTENSITY
(arbitrary units)
200
546
669
1036
1 - CLINOCHLORE
208
265
355
466
808
2- QUARTZ
283
712
1088
3- CAL.+ ANATASE
144
398
514
638
4- ANATASE
0
400
800
1200
RAMAN SHIFT (cm-1)
B

2.4. RESULTS

2.4.1. Merzane Group

Volcanic dome-shaped deposits have been observed in the central-eastern part (31° 22' 51.73"N; 4° 2' 29.22"W) of the Hamar Laghdad ridge (Figs. 2.2B and 2.3). They occur as layered meter-thick breccia of well-rounded millimetric volcanic fragments (Fig. 2.3B). These fragments, pyroclasts, consist of devitrified primary glass with spread euhedral olivine phenocrysts (Fig. 2.3C) and vesicles (former amygdales) (Figs. 2.3B-C) replaced and filled by neomorphic fibrous phyllosilicate, clinochlore ($(Mg_5Al)(AlSi_3)O_{10}(OH)_8$) (Figs. 2.3B-C,E and 2.4). Titanium dioxides, anatase (Ti_2O), with fibrous radiaxial calcite and blocky calcite (Fig. 2.3D), locally dissolved and replaced by quartz, cement the pyroclasts (Figs. 2.3B-D and 2.4). This volcanic rocks are thus ascribed to low-Si olivine-rich basalt breccia.

A system of decimeter-wide fractures filled by calcite cements and debris crosscut the basaltic breccia belt. The veins continue beyond the Merzan-Seheb el Rhassel Group boundary increasing their thickness.

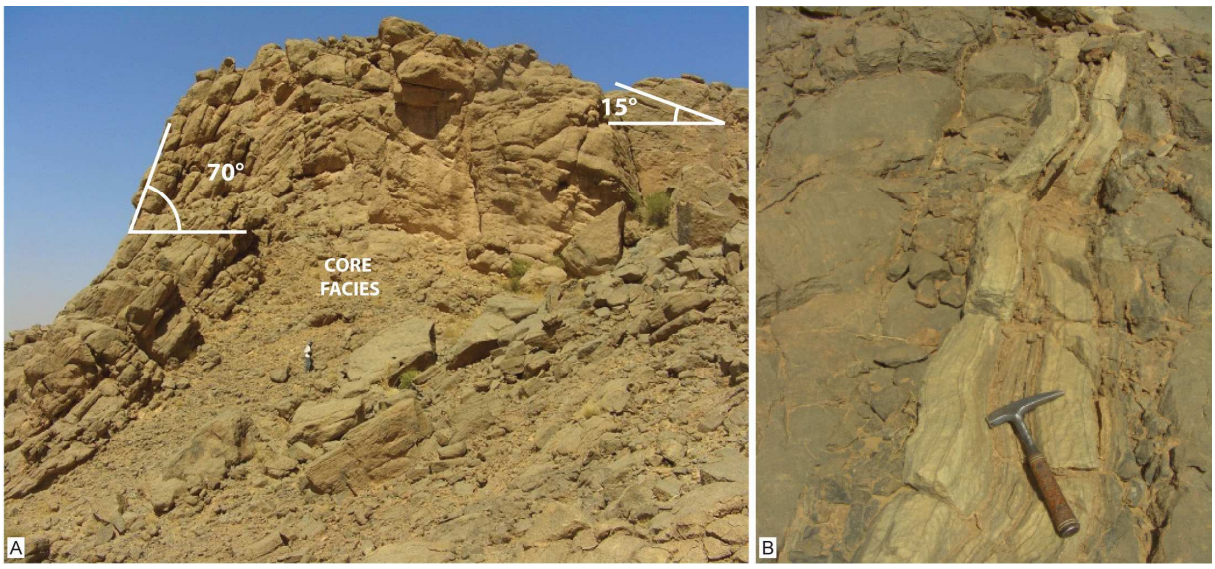

Figure 2. 5. Field views of the Emsian Kess Kess carbonate mounds. A) Cross section of a mound (31° 22' 37.29"N, 4°2' 35.91"W) showing the strong asymmetry of the flanks (slopes angles in white) and a crude internal stratification truncated in the core facies (man for scale). B) The black and white banded limestones filling a vein (hammer for scale) cross cutting the the Emsian mound.

2.4.2. Seheb el Rhassel Group

2.4.2.1. Conical mounds

The Emsian Kess Kess mounds are typically 20-30 meters high with a 40-55 meters circular to sub-elliptical base (Fig. 2.5A). All mounds show a well-defined conical shape characterized by steep flanks with exception of two elongated mounds located in the center (31° 22' 48.71”N-4° 3' 29.91”W; 31° 22' 41.07”N-4° 3' 21.97”W) and in the eastern part (31° 22' 55.51”N-4° 2' 3.15”W; 31° 22' 50.33”N-4° 1' 53.62”W) of the Hamar Laghdad (Fig. 2.2B), respectively. A common feature of the Emsian mounds is a distinct asymmetry of their flanks (Fig. 2.5A): the basin-ward flanks of the mounds constantly reach an angle (up to 70°) higher than the opposite up-slope flanks (up to 35°) (Fig. 2.5A). The mounds are commonly well exposed in outcrop, however, only few dissected mounds reveal their (internal) three-dimensional pattern (Fig. 2.5A). Their internal coarse stratification with meter-sized strata follows the mound shape (Fig. 2.5A). Massive stromatactis-bearing limestones with mono-specific macro-invertebrate guilds of trilobites (*Scutellum* sp.) and brachiopods, and metric zebra structures also typify the rarely exposed core facies of the mounds. Stromatactis and zebra structures as observed in the field, may represent more than the 50% of the whole rock of the Kess Kess Emsian mounds (**cf.** 4.1.3, Fig. 2.9A).

The Kess Kess mounds and the infra-mound deposits are cross-cutted by a system of veins (Fig. 2.5B) and neptunian dikes (*sensu* Bates and Jackson, 1980). The veins attain an average thickness of 50 centimeters, and are filled by generations of black and white isopachous radiaxial marine calcite cements and carbonate debris (Fig. 2.5B). The veins are thinner (5 cm) in the lower part of the Seheb el Rhassel Group close to the Merzane Group, whereas they seem to disappear few meters after the transition to the Amerboh Groups. The neptunian dikes, formerly fissures filled with submarine sediments, are filled by marine carbonates debris with the same or younger age, of their host rocks.

2.4.2.2. Mineralogy and Petrography

Carbonates from Seheb el Rhassel Group including the mounds investigated by using optical and Raman microscopy, XRF and XRD diffraction, SEM-EDS analysis resulted characterized by low-Mg calcite, dolomite, trace of terrigenous materials, Fe-rich minerals such as pyrite, goethite and small amounts of carbonaceous material. However, dark red sediments were observed associated to meter sized chimney-like structures (Fig. 2.6A) outcropping in the upper part of the

Seheb el Rhassel Group closed to the cliff of the Hamar Laghdad. The chimney-like structures are characterized in their inner part by massive deposit of goethite, α-Fe^{3+}O(OH), and quartz pebbles, whereas the edge is made of Fe-rich carbonates (Fig. 2.6A). Under optical microscope, goethite occurs in acicular, botryoidal and rod-shaped crystals (Figs. 2.6B-D). Fe-rich carbonates are characterized by zoned euhedral dolomite crystals with inequigranular idiotopic to hypidiotopic fabric (Fig. 2.6E), whereas late blocky and syntaxial calcite cements fill the pore spaces (Fig. 2.6F), whereas fibrous radiaxial calcite and fine-grained matrix are lacking (Fig. 2.6E). The dolomite crystals are typified by Fe enrichment along the accretion surfaces. These Fe-rich carbonates result cross cutted by millimetric veins filled with authigenic quartz cements (Fig. 2.6F).

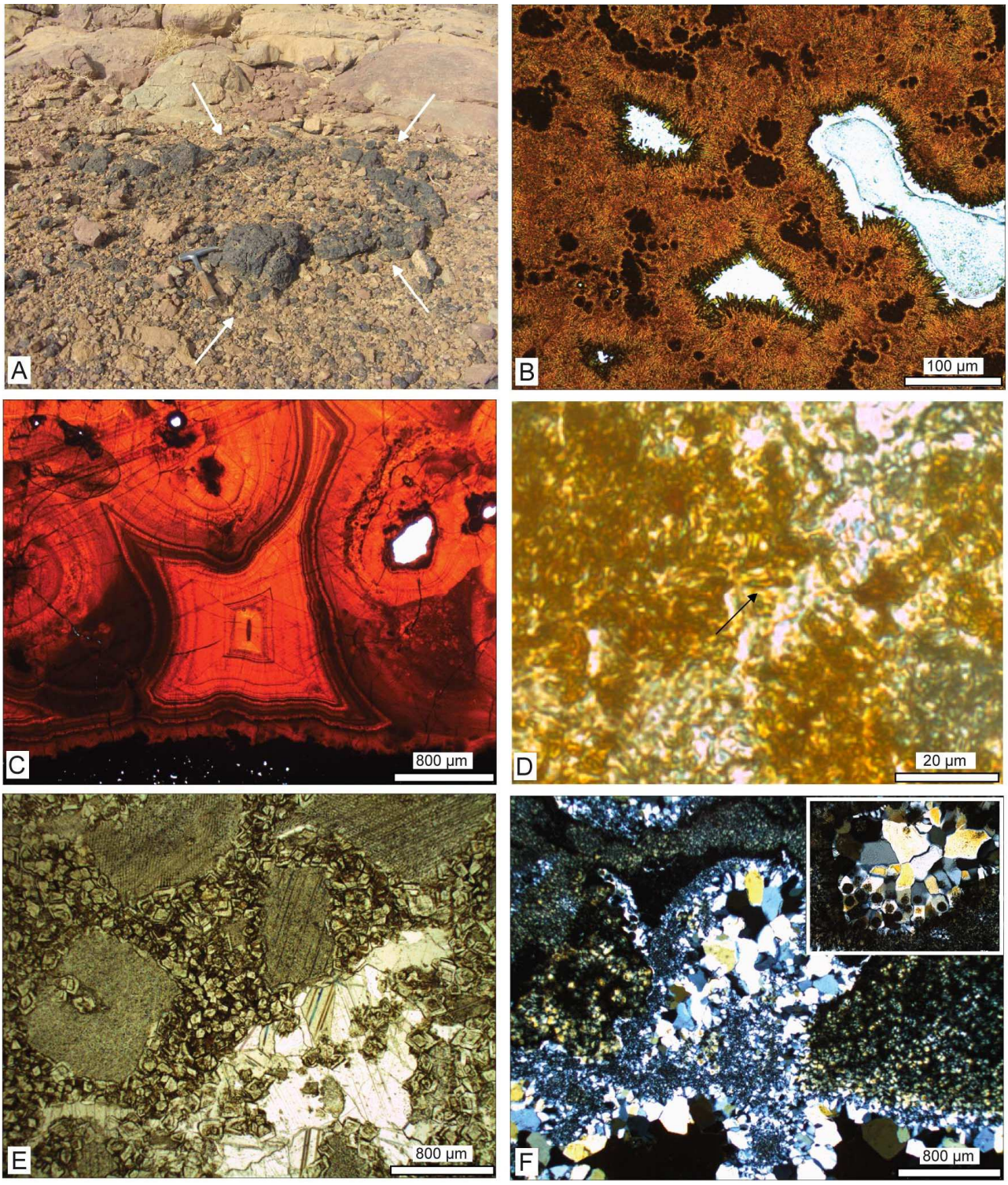

Figure 2. 6. Field view and photomicrographs of the topmost part of the Seheb el Rhassel Group in correspondence of a chimney-like structure (A) filled by dark red rocks (arrows). B-D) Acicular crystals, botryoids and rodshaped goethite (arrow) of goethite deposits, respectively. E) Crinoidal grainstone cemented by hypidiotopic inequigranular dolomite. F) Net of millimetric veins and cavities filled by mega- and micro-quartz showing turbid peloid-like fabric (box).

2.4.2.3. Facies descriptions

Appreciable variation in lithofacies exists throughout the Seheb el Rhassel Group, which consists mostly of fossiliferous limestones, composed of mottled micrite/microsparite with variable amounts of skeletal debris and carbonate cements. Particularly crinoidal packstone/grainstone and brachiopods *lumachella* strata occur in the lower part of the Group, whereas the upper part of the Group, characterized by mounds occurrences, is dominated by fossiliferous wackestone and coral floatstone. Despite the whole Seheb el Rhassel Group is composed of limestones with high amount of bioclasts the mounds lack a rigid biogenic framework and are matrix supported.

Fenestral fabrics (Fig. 2.7) are widespread throughout the Seheb el Rhassel Group, especially in absence of skeletal remains within the Kess Kess mounds. Based on the shape of the spar-filled voids, two different types of laminoid-fenestral fabrics can be recognized: LF-A type (Fig. 2.7A) and LF-B1 type (Fig. 2.7B) (*sensu* Tebbutt et al., 1965; Müller-Jungbluth and Toshek, 1969).

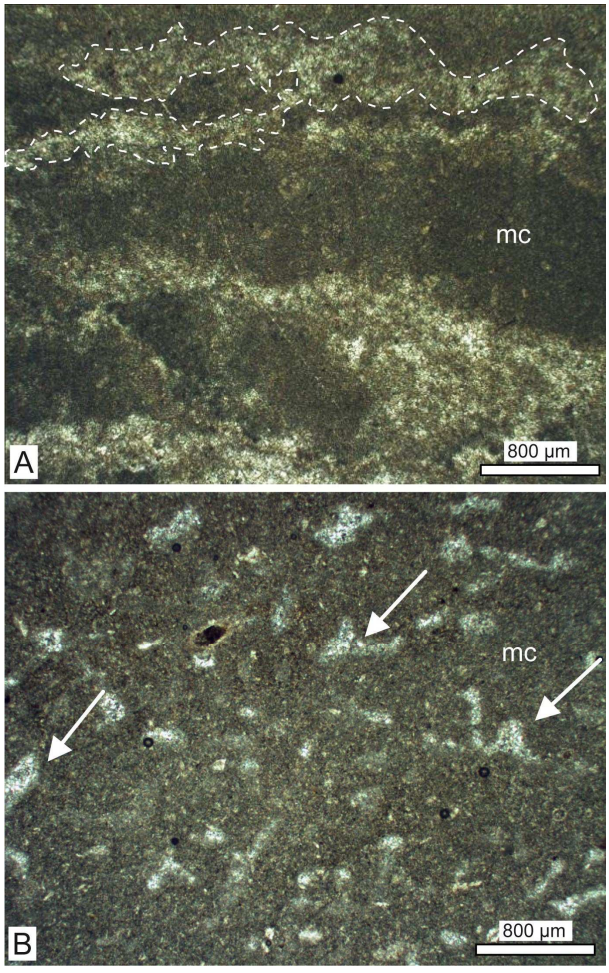

Figure 2. 7. Photomicrographs of the fenestral fabrics within the Seheb el Rhassel micrite (mc). A) LF-A type fenestrae (broken line). B) LF-B1 type fenestrae

Clotted micrite (Fig. 2.8) is also a common feature throughout the Seheb el Rhassel limestone, often within dark micrite and near the veins.

The stromatactis cavities of the Seheb el Rhassel are common features within the micrite and wackestone of the Kess Kess mud mounds (Fig. 2.9A). Stromatactis infill consists of several generations of isopachous, radiaxial, fibrous calcite and blocky calcite toward the center of the cavities (Figs. 2.9B, C). The floor of these cavities usually consists of laminated, fine-grained carbonates with peloidal micrite and silt-sized carbonate particles; sometimes the floor is made up of laminated micrite with densely packed trilobite remains (Fig. 2.10). The stromatactis cavities of the Kess Kess mound limestones are commonly few centimeters wide (Figs. 2.9A-C),

however, meter-sized cavities are also observed (Fig. 2.10A). Stromatactis and, near fractures, layered micrite often occurs as the product of the interbedding between black organic matter-rich levels and grey micrite.

Zebra-like fabrics is another common feature of the Kess Kess mounds (Fig. 2.9D). The zebra-like structures are generated by several meters length thin layers of dark to grey micrite (average thickness: 1-2 cm) and white calcite cement (average thickness: 0.5-1 cm) (Fig. 2.9D) where biota remains rarely occur. They are observed in the inner core of the Kess Kess mounds (where erosion removed the external strata of the mounds).

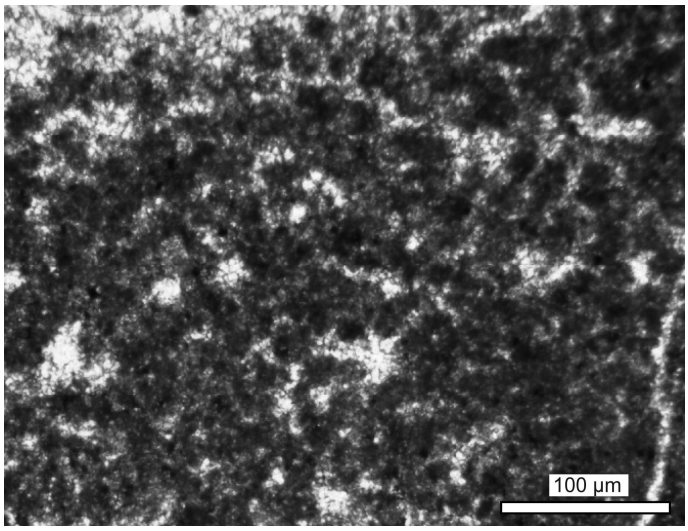

Figure 2. 8. Photomicrograph of clotted micrite from the upper part of the Seheb el Rhassel Group.

A number of microfacies have been recognized and described in the Seheb el Rhassel Group from bottom to top (Figs. 2.10-2.15):

- *crinoidal packstone-grainstone* microfacies is organized in decimeter-sized normally graded horizons (Fig. 2.11A) of micrite and fragments of poorly preserved crinoids ossicles (e.g., dissolution effects, microborings) (Fig. 2.11B). Pore spaces result filled with late diagenetic sparry calcite and syntaxial calcite overgrowing the crinoid plates (Figs. 2.11B-C). This facies is observed to the lower part of the Seheb el Rhassel Group, whereas is less representative of the upper part of the Group where crinoidal packstone occurs in discontinuous meters-sized lens.

- *brachiopod lumachella* microfacies include shells and shell-fragments of spiriferids (*Apousiniella* sp., *Spinella* sp., *Spirinella* sp.), atrypids (*Atrypa* sp., *Desquamatia* sp.), orthids (*Schizophoria* sp., *Isorthis* sp.), athyrids (*Athyris* sp.), and the widespread rhynchonellids (*Camarotoechia marocanensis*) (Fig. 2.12). Brachiopods occur at the bottom and central part of the Seheb el Rhassel Group, and are observed in the core facies of the mounds. In the lower part of the Group brachiopods are arranged in densely packed *lumachella*-like strata of *Schizophoria* sp, *Atrypa* sp. (*Desquamatia*), *Spinella* sp. disarticulated shells. Articulated shells of *Isorthis* sp. and *Chamarotoechia marocanensis* are observed to the upper part of the Seheb el Rhassel Group. They are organized in densely packed lens (Fig. 2.13A), few meters long and normally several decimeters

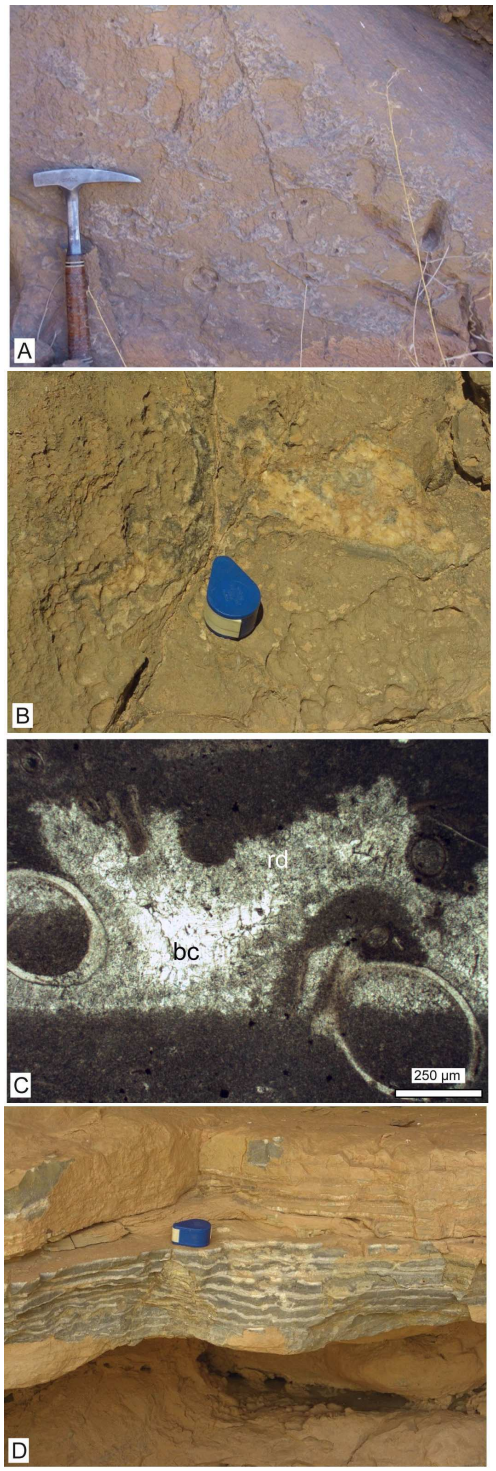

thick, or scattered in the core facies of the mounds. *Chamarotoechia marocanensis* is the most common brachiopod species at the Seheb el Rhassel Group.

- *fossiliferous wackestone* microfacies (Fig. 2.14A) is the most common at the Kess Kess mounds, and result characterized by mottled micrite and microsparite with variable amount of bioclasts of especially auloporids (e.g. *Bairnbridgia* sp.), crinoid plates, trilobites fragments, rare brachiopod and (articulated and disarticulated) ostracod valves, whereas tentaculites are concentrated in their upper part. Sparry calcite cements are observed in association of aulopord remains (Fig. 2.14B), whereas syntaxial calcite cements overgrow the crinoid ossicles (Fig. 2.11C), Fenestral fabric and clotted micrite is also a common feature of this microfacies, and are abundant where the bioclasts are rare.

- *coral floatstone* microfacies are easily recognizable in outcrops and thin sections (Figs. 2.13B and 2.14B). The coral assemblages of the Seheb el Rhassel Group include tabulate corals such as auloporids (e.g. *Cladochonus, Aulocystis* and *Bairnbridgia*), thamnoporids and favositids, and rugose solitary corals (e.g. *Hamarophyllum* and *Laccophyllum*). Corals are commonly scattered in the limestone as bioclasts, and when in life position they form meter-size circular colonies (**cf.** 5.1). However abundant corals were observed they do not generate any rigid framework.

Figure 2. 9. Stromatactis and zebra fabrics within the Emsian Kess Kess mounds. A) Stromatactis bearing limestone in the inner exposed part of a mound (31° 22' 31.72"N; 4° 2' 48.98"W). The flat base of the stromatactis cavities result parallel to the mound strata (deep direction on the right side of the figure). B) Typical stromatactis structure with a flat floor and an irregular roof. The filling material result of organic matter-rich radiaxial fibrous calcite (thin black layer) and blocky calcite (white part). C) Photomicrographs of a stromatactis structure filled by marine radiaxial calcite (rd) and blocky calcite (bc) late cement. D) Non fossiliferous zebra (banded) fabric in the core facies of a Emsian Kess Kess mound (31° 22' 27.80"N; 4° 2'

- *scutellid trilobites floatstone-rudstone* microfacies (Fig. 2.10) is uniquely observed associated to core facies of the mounds, and easily recognizable due to characteristic weathered and eroded pattern (Fig. 2.10A). These microfacies consists of a densely packed assemblage of trilobite remains (*Scutellum* sp., Pusch 1833) organized in small lenses or meter dome-shaped deposits (Fig. 2.10A). The scutellid remains usually consist of mm- to a few cm-sized pygidia. Rarely, complete exuviae are observed. The scutellid-reach limestone show a bimodal fabric (Fig. 2.10B): the lower part consists of floatstone to rudstone with less than 10% of cement, and the upper part consists of a highly washed rudstone with less than 10% of micrite. The elongated trilobite remains are preferentially oriented approx. parallel to the cavities base and the concavities of the bioclasts, in the cement-rich rudstone, present eroded and discordant geopetal filling (Fig. 2.10C). In both these facies, cements are fibrous radiaxial marine calcite. Blocky calcite cements fill in the major voids. XRF, SEM-EDX and Raman analyses of this facies (Fig. 2.15) revealed the presence of

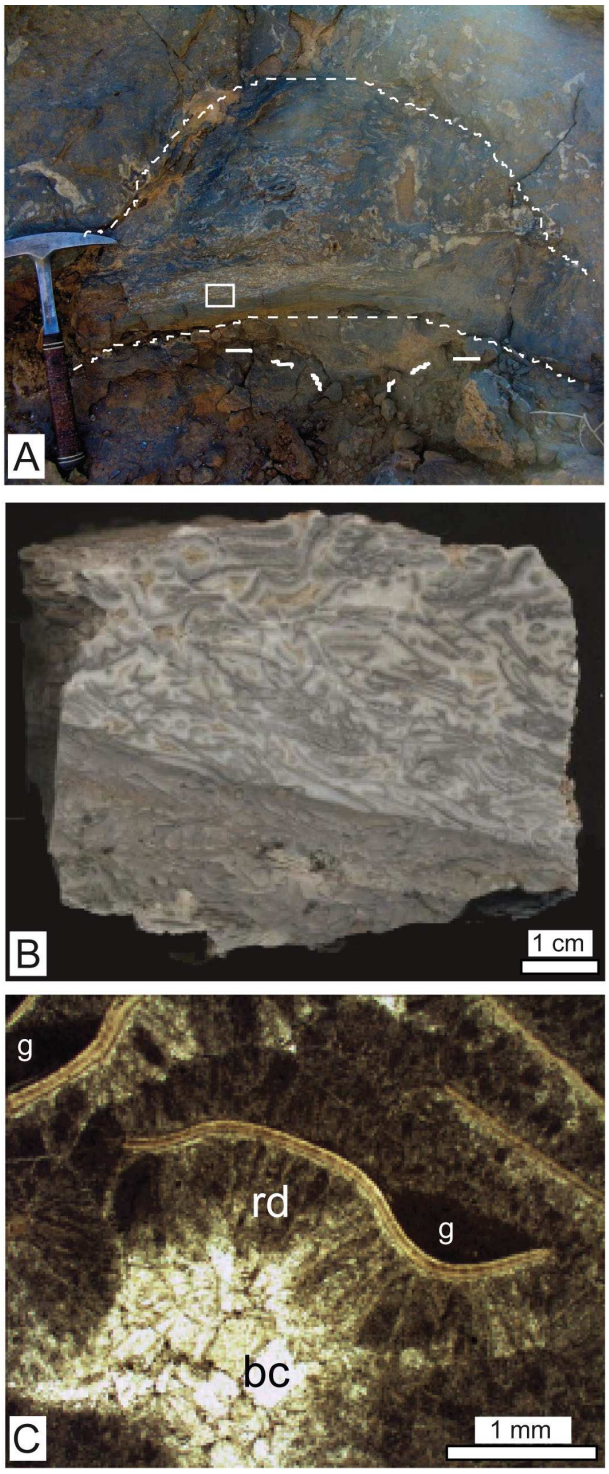

Figure 2. 10. Scutellum sp. within the scutellid trilobites floatstone-rudstone microfacies within the Emsian Kess Kess mounds. A) Outcrop view of a stromatactoid cavity (thin broken line) linked with a vertical conduit/vein (heavy broken line) and filled by bimodal limestone. B) Polished slab of a sample from the stromatactoid filling (box in A). The bottom part of the sample (grey) is a trilobite floatstone, in the topmost part (white) micrite is lacking (rudstone). C) Trilobite rudstone (locally cementstone) with geopetal micrite (g) cemented by fibrous radiaxial calcite (rd) and blocky calcite (bc).

patchy microcrystalline quartz replacement of trilobite's cuticles (Figs. 2.15B-D). Particularly Raman analyses of the trilobites hosting carbonates revealed the presence of carbonaceous matter within the fibrous radiaxial calcite (Fig. 2.15D) and goethite coupled with quartz within the micrite that fills in the shell (Fig. 2.15D).

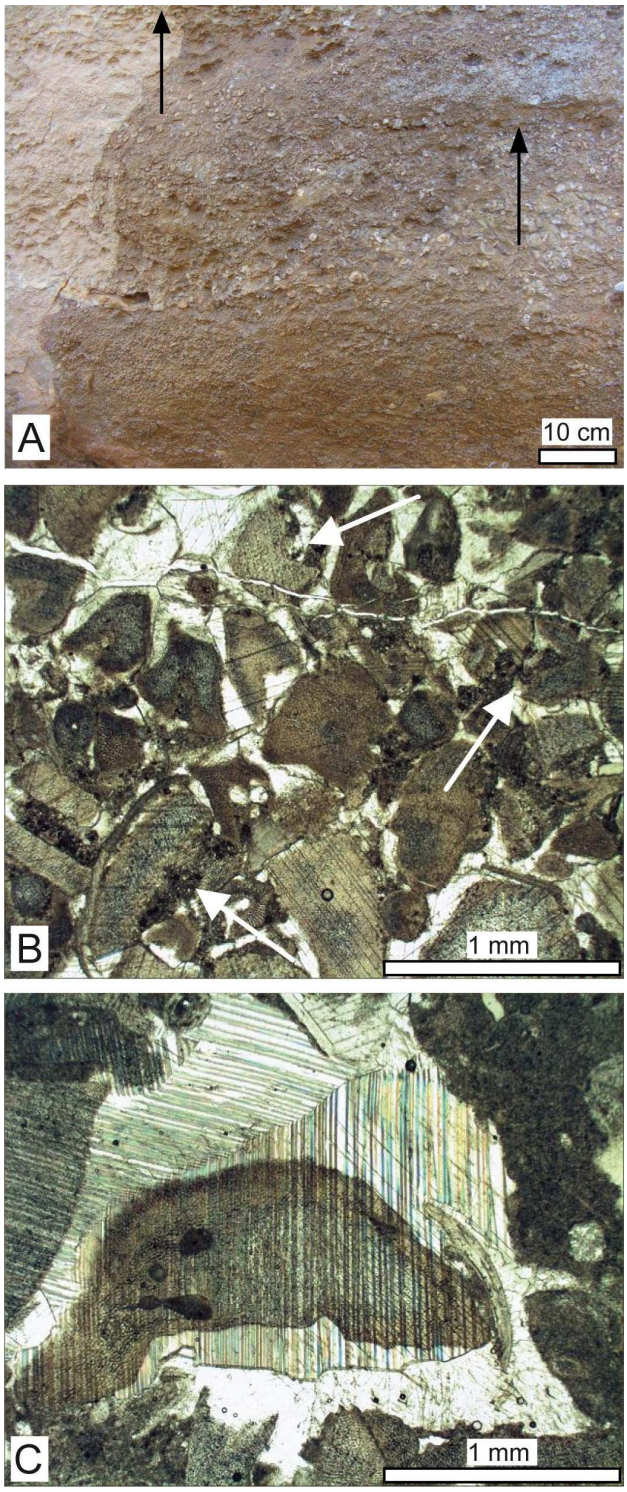

- *tentaculites packstone* microfacies (Fig. 2.14C) is characterized by dense accumulation of well-preserved tentaculites with subordinate trilobite fragments and crinoid ossicles. Although thin and elongated tentaculites usually do not show any orientation, a slightly oriented pattern can be locally observed (Fig. 2.14C). This facies is mud dominated and cements are rare. Tentaculites become abundant toward the top of the Seheb el Rhassel Group and tentaculites packstone facies represent the upper part of the Group succession, and result in meter-thick, weathered layers draping the mud buildups. These layers are thinner in the infra-mounds facies.

- *ostracod packstone* microfacies consists of densely packed, large and disarticulated ostracod valves and crinoid plates, with less than 50% of micrite. This microfacies is observed fill in some neptunian dikes cutting mud mounds and associated to their apical part. Olempska and Bełka (2010) assigned the ostracod

Figure 2. 11. Outcrop view and photomicrographs of the crinoidal grainstone microfacies within the Emsian Kess Kess mounds. A) Outcrop view of the crinoidal packstone organized in normally graded (fining-upward) layers (black arrows) in the western part of theHamar Laghdad ridge (31° 22' 42.23"; 4° 4' 4.63" W). B) Crinoidal grainstone cemented by syntaxial calcite. The crinoidal ossicles showing microborings and dissolution effects (arrows). C) Syntaxial calcite cements overgrownin poorly preserved (fragmented) crinoid

mass occurrence to a new taxon, *Hamaroconcha kornickeri* and limit this ostracod-bearing facies to the Eifelian (Middle Devonian) time postdating the Kess Kess mounds.

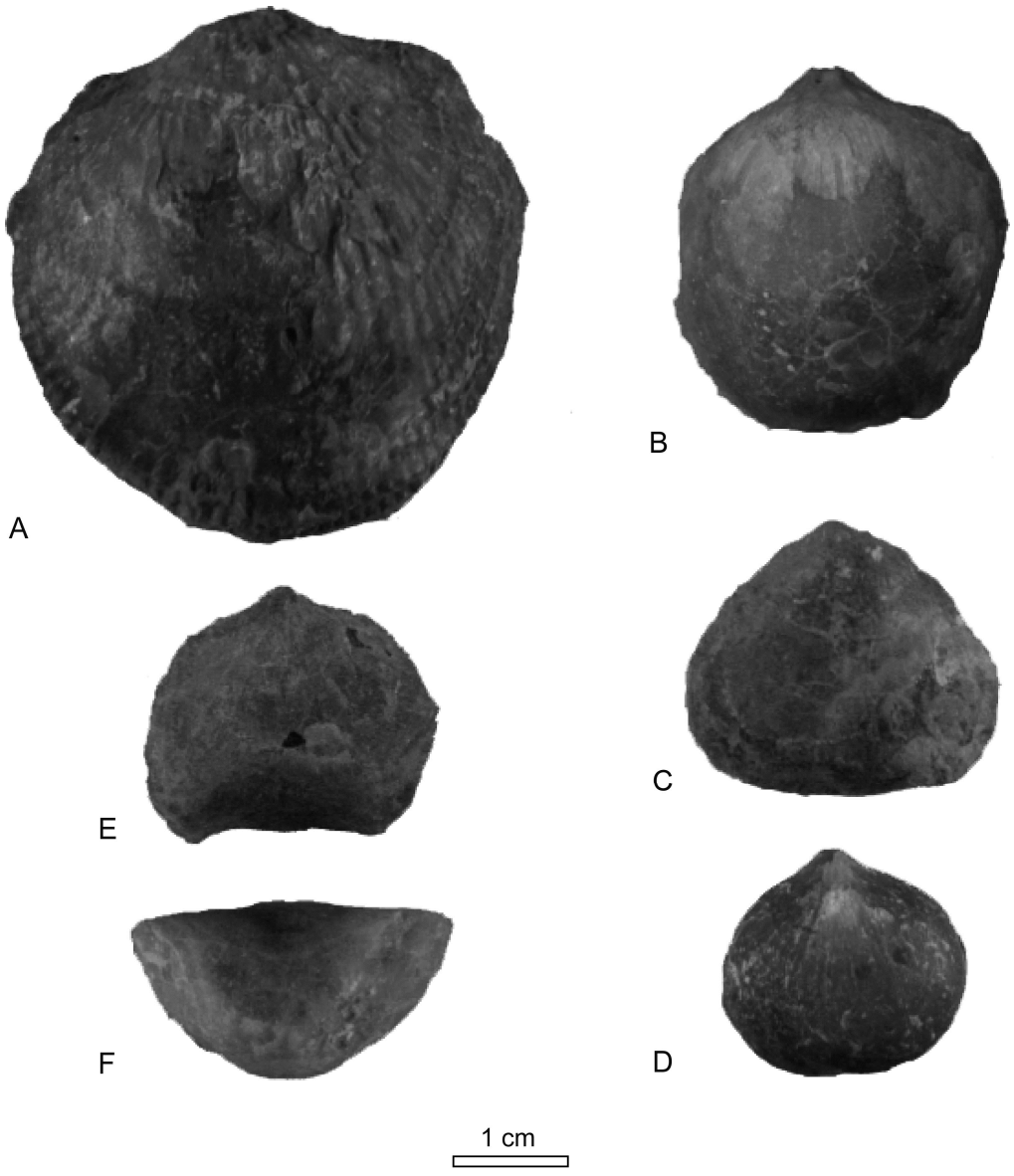

Figure 2. 12. Brachiopods, Lower Devonian, Seheb el Rhassel Group. A) Desquamatia sp. ventral view from the lumachella strata at the bottom of the Group. B) Atrypa sp. dorsal view from the lumachella strata at the bottom of the Group. C) Athyris sp. ventral view from a lumachella lens in the upper part of the Group. D) Isorthis sp. ventral view from the upper part of the Group scattered in the limestones near a mound. E-F) Camarotoecha marocanensis dorsal and anterior views, ripsectively, from a lumachella lens in the upper part of the Group.

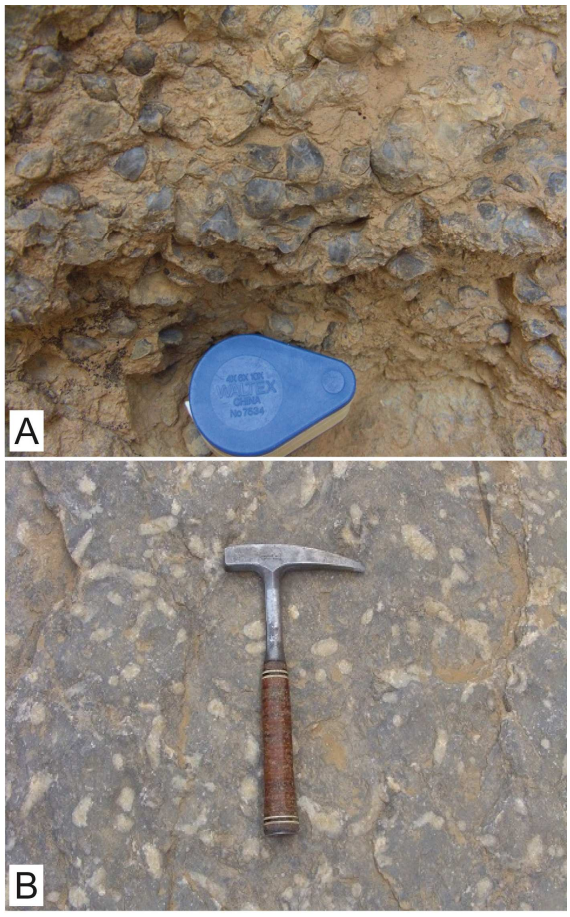

Figure 2. 13. Outcrop views of macro-invertebrates facies of Seheb el Rhassel Group. A) Close up of a densely-packed brachiopod (Chamarotoechia marocanensis) lens in the middle and upper part of the Seheb el Rhassel Group within the brachiopod lumachella microfacies. B) Dense accumulation of centimeter-size solitary rugose corals cropping out in the coral floatstone microfacies of the upper part of the Seheb el Rhassel Group characterized.

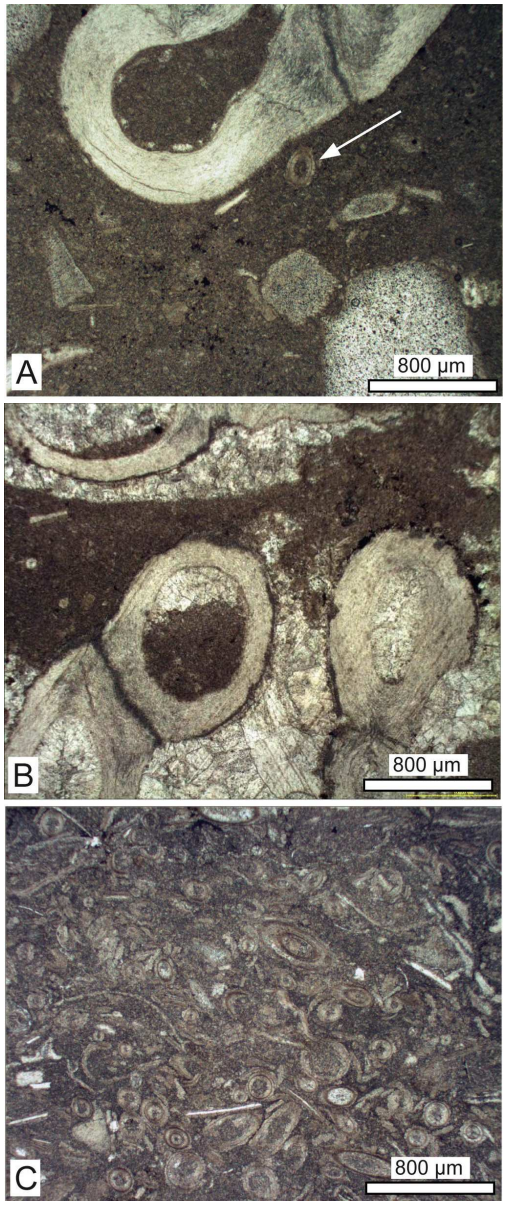

Figure 2. 14. Photomicrographs of the different Seheb el Rhassel Group microfacies. Fossiliferous wackestone microfacies with (A) auloporid corals (top of the figure), crinodal ossicles (bottom right) and transversal section of tentaculitoid (arrow), and (B) blocky calcite cement around the auloporids remains. C) Tentaculites packstone microfacies dominated by equatorial shells sections.

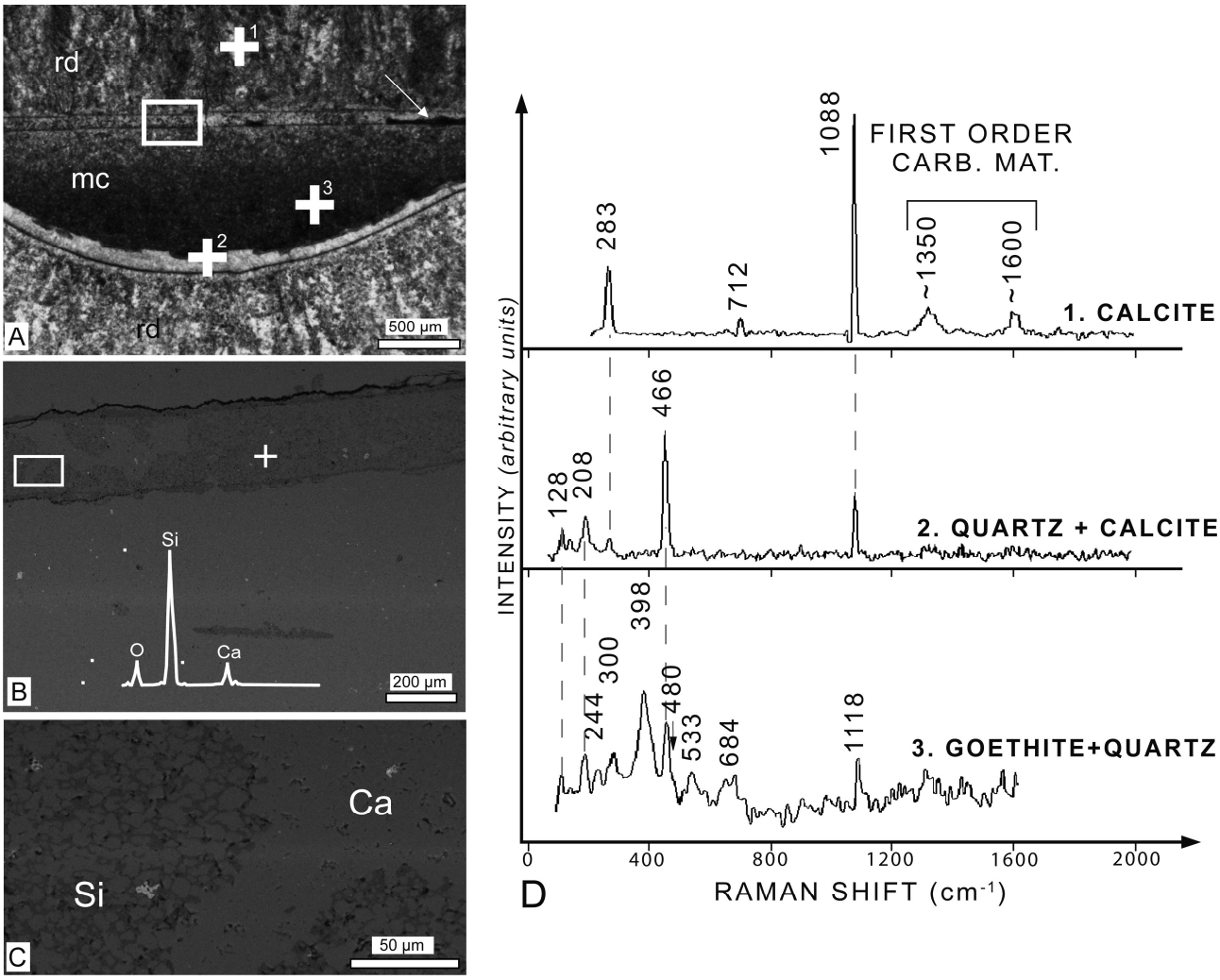

Figure 2. 15 Photomicrographs, SEM/EDS analyses and Raman spectra of the trilobites rudstone facies (same as figure 10). A) Transmitted light -photomicrograph of a trilobite shell filled by micrite (mc) and cemented by radiaxial isopachous calcite (rd). The arrow points to a thin mineral crusts. B) Back scattered electron (BEI) micrograph of the inner part of the trilobite shell (box in A) and EDS spectra of the trilobite shell (white cross) showing the presence of Si. C) Particular of the trilobite carbonate (Ca) shell (box in B) showing the patchy distribution of the silica (Si). D) Representative Raman spectra of the fossiliferous host rock and the mineral phases detected in the sample (referred to numbers in A). The (1) fibrous radiaxial calcite (Raman bands: 283, 712, 1088 cm^{-1}) is characterized by D1 (~1350 cm^{-1}) and G2 (~1600 cm^{-1}) bands of first order carbonaceous matter. The spectra in correspondence of the trilobite shell (2) is characterized calcite (broken grey line) and quartz bands (128, 208, 466 cm^{-1}). The dark material filling the shell cavity (3) is characterized by quartz (broken grey line) and goethite bands (244, 300, 398, 480, 533, 684, 1118 cm^{-1}). Raman spectra were compared with reference spectra from RRUFF DataBase by Mazzetti and Thistlethwaite (2002), Laetsch and Downs (2006), White (2009) Demoulin et al. (2010).

2.4.2.4. Carbonate cements

Several paragenetic cement phases were observed filling the voids and cavities of the Kess Kess mounds that include (Fig. 2.16) radiaxial fibrous calcite, luminescent and non-luminescent scalenohedral calcite, non-ferroan moderately-luminescent blocky calcite, and ferroan non-luminescent blocky calcite. In addition, a sparry syntaxial calcite has been reported associated to the major cavities and overgrowing crinoid ossicles (**cf.** crinoidal packstone/grainstone).

Radiaxial fibrous calcite cement was observed to form an isopachous crust distributed around bioclasts (Fig. 2.10C), walls of primary cavities and stromatactis (often showing a botryoidal fabric) and filling the veins. Multiple generations of black and white radiaxial calcite cements fill the veins generating a characteristic banded pattern (Fig. 2.5B). Because the high number of the micro-inclusions of dolomite microcrystal and fluids, radiaxial cements under transmitted light microscope appear turbid (Fig. 2.16A) and exhibits a typical undulose extinction (cross nicols). Cathodoluminescence observations of these radiaxial fibrous calcite cements show a dull- to mottled-luminescence (Fig. 2.16B).

Scalenohedral calcite cements under cathodoluminescence microscopy show sharp and well-preserved dog tooth-shaped crystals (Fig. 2.16B). Cathodoluminescence observations allow to discern two generations of scalenohedral cements. The first generation of scalenohedral cement forms a non-luminescent and discontinuous, but persistent, thin layer at the top of dull-luminescent radiaxial calcite cements (Fig. 2.16B). Locally, this non-luminescent layer shows poikilitic inclusions (Fig. 2.16B). The second generation of scalenohedral calcite cements is characterized by banded-luminescent calcite developed in optical continuity on top of an isopachous crusts represented by the first generation of scalenohedral cement (Fig. 2.16B). A fine-banded fabric due to the alternation of bright- and dull-luminescent, fluid inclusion-free, cements characterizes this second generation of scalenohedral cement.

Blocky calcite with radiaxial fibrous and subordinate scalenohedral calcite cements, fill most of the pore spaces (with the exception of the vein infilling) of the carbonate of the Sehebel Rhassel Group. The crystal size of the blocky calcite usually increases toward the center of the voids in association with syntaxial overgrowths (Fig. 2.16A). Two generations of blocky calcite were recognized (Fig. 2.16B). The first generation of the blocky calcite is in continuity with the bright-luminescent scalenohedral banded calcite, and consists of non-ferroan, bright-luminescent (blocky) crystals (Fig. 2.16B). The second generation that represent the youngest carbonate cement phase in the Emsian Kess Kess mounds, consists of ferroan, non-luminescent blocky crystals.

Syntaxial calcite cement is exclusively observed around the crinoidal plates within the crinoids grainstone where they also represents more than 50% of the carbonate cements (Figs. 2.11B-C), and occluding the central parts of the largest voids (Fig. 2.16A). Commonly syntaxial calcite is observed to cement the washed grainstone (>50% of cements), and potentially represents an end product of the fluid circulation during the diagenesis.

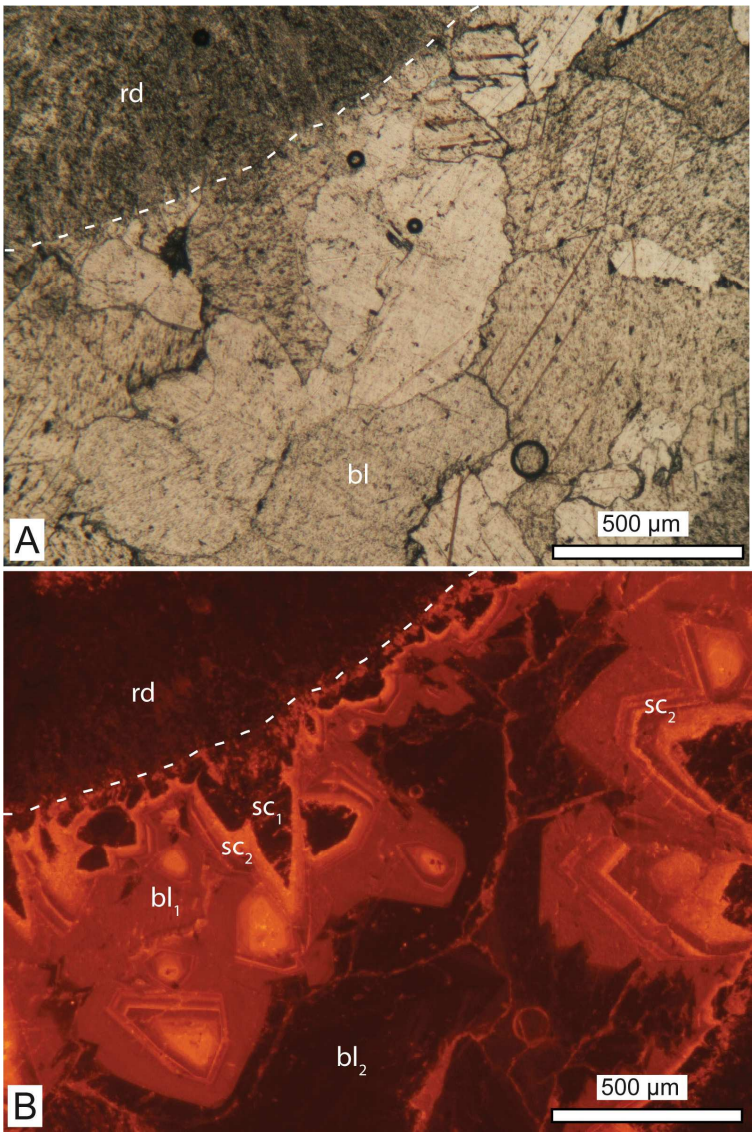

Figure 2. 16. Seheb el Rhassel limestone cements stratigraphy. A) Transmitted light photomicrographs of an isopachous level of fibrous radiaxial calcite (rd) followed by coarse-grained blocky calcite (bl). B) Cathodoluminescence photomicrographs of the same cements in A showing detailed cements sequence: dull- to mottled-luminescent radiaxial calcite (rd), non- luminescent scalenohedral cement (sc_1), bright- to banded-luminescent scalenohedral calcite (sc_2), moderately-luminescent blocky cement (bl_1) and non-luminescent blocky cement (bl_2).

2.4.2.5. Stable isotopes composition

C and O stable isotope compositions were obtained from 1) bulk analyses of selected carbonate facies, and 2) specific carbonate phases and cements including micrite, euhedral dolomite, radiaxial and blocky calcite of the most representative microfacies of the Seheb el Rhassel Group including the Emsian Kess Kess mounds (Fig. 2.17).

The $\delta^{13}C$ and $\delta^{18}O$ values of bulk carbonates were obtained from samples of the following facies (described above): brachiopod *lumachella*, micrite mound core facies and infra-mound area, reddish pisolites facies, scutellid floatstone, carbonate filling the veins, and Fe-rich carbonate from the chimney-like structures. Samples from brachiopod *lumachella* facies of the lenses within the mound core facies and *lumachella*-like strata are characterized by very low $\delta^{18}O$ values (-8.28‰ VPDB and -5.17‰ VPDB) , and $\delta^{13}C$ values of -3.84 ‰ and -2.86‰ VPDB, respectively. Micrite from the mound core facies displays a highly depleted $\delta^{18}O$ value (-10.33‰ VPDB), whereas micrite from the infra-mounds facies presents $\delta^{18}O$ values of -2.81‰ and -9.91‰ VPDB. Micrite from mound and infra-mound facies have average $\delta^{13}C$ value of 0.00 ± 1‰ VPDB (Fig. 2.17B). Pisolites laminae and fine grained matrix from the reddish pisolites facies show a different isotopic compositional trend compared to the other infra-mounds lithologies with low $\delta^{18}O$ values (down to -9.06‰ VPDB) and an average $\delta^{13}C$ value of -6.00‰V PDB (Fig. 2.17A). Micrite from the scutellid floatstone displays $\delta^{18}O$ values ranging between -9.85 ‰ and -4.92 ‰ VPDB, and $\delta^{13}C$ values ranging between -1.18 ‰ and +1.10 ‰ VPDB. The euhedral dolomite crystals from the Fe-rich facies near the chimney-like structures show $\delta^{18}O$ value of -9.4 ‰ PDB and average $\delta^{13}C$ value of -3.4 ‰ VPDB.

C and O stable isotope analyses obtained from specific carbonate phases and cements such as micrite, radiaxial fibrous calcite, blocky calcite and dolomite idiomorphic cements from mounds and infra-mounds limestones, scutellid floatstone and veins filling show that micrite has lower $\delta^{18}O$ values than the cement phases, whereas their average $\delta^{13}C$ value is 0 ‰ VPDB, and the $\delta^{13}C$ values of the dark carbonates filling veins are commonly negative.

The $\delta^{18}O$ values of micrite range between -11.34‰ and -1.45‰, VPDB (Fig. 2.17B); the $\delta^{13}C$ values are negative (down to -16.74‰ PDB) but, the average value of micrite was -7.00‰ VPDB, and the lowest values were obtained from the dark micrite near the vein structures (Fig. 2.17A). Radiaxial fibrous calcite cements have an $\delta^{18}O$ value of -3.50‰ VPDB, and a large range of $\delta^{13}C$ values (-16.53‰ to +1.47‰ VPDB) where the most depleted values come from the cements within the veins filling (Fig. 2.17A). Excluding the outsiders from the veins filling the average radiaxial calcite cements $\delta^{13}C$ value in the Seheb el Rhassel Group is near 0‰. $\delta^{18}O$ values

of the blocky calcite cements range between -6.77‰ and -0.64‰ VPDB, whereas their $\delta^{13}C$ values range between -12.53‰ and +2.10‰ VPDB, with an average value of -2.05‰ VPBD. The most negative blocky calcite value (-12.53‰ VPDB) was detected in dark limestone near the veins structures (Fig. 2.17A). The euhedral dolomite crystals are characterized by low $\delta^{18}O$ values (down to -9.41‰) and $\delta^{13}C$ depleted as -3.4‰ VPDB (Fig. 2.17B).

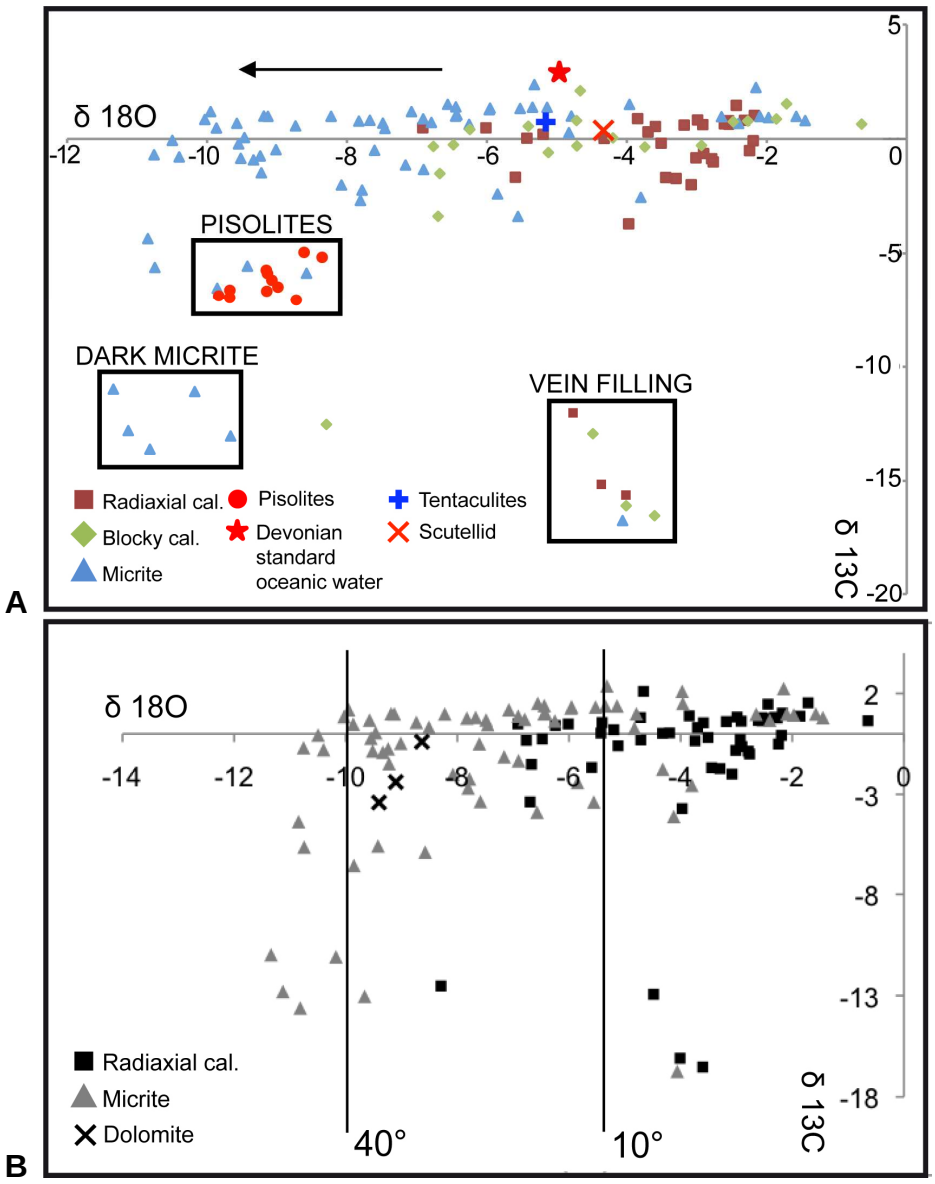

Figure 2. 17. Seheb el Rhassel Group limestone isotopic composition ($\delta^{13}C$ and $\delta^{18}O$) compared with mean oceanic Devonian water isotopic composition (star in A). A) Isotopic values of several carbonate phases and facies. The black arrow is the normal trend of the isotopic composition during the increasing of burial condition characterized by a shift of the oxygen to lower values (Hurley and Lohmann, 1989). B) Micrite, calcite cements and dolomite isotopic compositions. Vertical lines correspond to the temperatures (from 10° to 40°C) from the equation proposed by Friedman and O'Neil (1977) for $\delta^{18}O$ normalized to SMOW.

2.5. INTERPRETATIONS AND DISCUSSIONS

The set of data collected in this study support an hydrothermal fluid origin fro the Emsian Kess Kess mounds at the Hamar Laghdad ridge, and report new information showing how the hydrothermal fluids could have acted as a genetic factor and influenced their preservation. The new analytical results are here combined with field observation and previous researches to define a more consistent framework, and bring new insight of current knowledge of the Emsian Kess Kess mounds.

Detailed facies and microfacies analyses reveal that despite the diverse and abundant biogenic remains, frame-building organisms for instance observed in morphologically similar Aferdou el Mrakib Devonian mound (Franchi et al., 2012) located in the Maïder basin (Fig. 2.1), are here absent. According to Fagerstrom's (1991) theory about the "reef-building guilds" taxonomic composition, the fauna observed at the Seheb el Rhassel Group including the Emsian Kess Kess mounds do not include constructor such as binder or baffler organisms (e.g., stromatoporoids, sponges). For instance, Bełka and Berkowski (2005) report the only occurrence of well preserved macro-invertebrates in life position documented at the Emsian Kess Kess mounds around vent source-like structures. However, these macro-invertebrates, thermophilic rugosae corals were observed do not generate any rigid framework. Despite, brachiopods *lumachella* and crinoidal packstone-grainstone facies (below the mounds) at the bottom of the Seheb el Rhassel Group have been observed, no evidence of diffuse mass transport or other high-energy sedimentary processes related to the mounds have been documented during field observations. Also, the big amount of bioclastic components of the Seheb el Rhassel limestones show no current or wave-driven sedimentary structures, and/or physical evidences that would explain the abrupt shape of the Kess Kess mounds and their preservation (Mounji et al., 1998). Therefore an origin related to mechanical or hydrodynamic (biodetrital) accumulation of the limestones (Brachert et al., 1992) it does not explain the preservation of Kess Kess steep morphologies under such hydrodynamic pressure (e.g. Mounji et al., 1998), hence it cannot be taken into account. Therefore, a hydrothermal activity, with consequent fluid-mixing scenario, driving the mud early lithification could explains the Kess Kess mound steep geometry (Aitken, 1995; Bełka, 1998; Mounji et al., 1998). The hydrothermal fluids migrated through fractures and fissures of rocks (Mounji et al., 1998) and pore of sediments to the sediment-water interface and disperse into submarine capping sediments drastically changing their chemical composition and temperature as consequence of the mixing with the cold seawater in the pore space of the shallow buried sediments (Marumo and Hattori, 1999; Nakaseama et al., 2008; Brand et al., 2010). Thorough this migration quartz cements, goethite and a hydrothermal vent-

related secondary minerals, clinochlore (e.g. Seyfried et al., 2011; Dekov et al., 2008) and anatase (Dekov et al., 2009), were deposed in the facies where the flow circulated (Figs. 2.4 and 2.15). Clinochlore was reported associated to hydrothermal mounds as secondary product of diffuse fluid discharge through the sediment at low temperature (150–200 °C) around the conduits (Dekov et al. 2008). Anatase was reported as secondary product of hydrothermal venting from the Eolo Seamount in the Tyrrhenian sea associated to irregular grained quartz (Dekov et al. 2009). Hence, presence of such pervasive hydrothermal fluids in the muddy sediments may catalyzed the diagenesis resulting in fast and extensive diagenetic processes with consequent good preservation of the morphologies and geochemical signatures (Walter et al., 2007). Similar mechanisms could explain the Emsian Kess Kess mounds morphologies and the reasonable proposed hydrothermal origin of the genesis of the Emsian Kess Kess mounds can be also supported by the described stratigraphic setting of the Hamar Laghdad ridge. The platform on which the deposition of the Seheb el Rhassel limestones occurred is the likely result of the positive morphology generated by a submarine alkaline basaltic event with emplacement of low-Si olivine-rich basalt breccia. The shape of the pyroclasts (Fig. 2.3) suggests any transport and/or burial compression processes, thus they are an *in-situ* basaltic breccia supporting the early Devonian volcanism and the consequent heat source (Mounji et al., 1998).

Hence, a late magmatic fluid circulation considered the engine of the hydrotermalism that make in place the Emsian Kess Kess mounds replaced primary volcanic glass and olivine crystals with secondary hydrothermal minerals such as anatase and clinochlore (Fig. 2.4) and cemented the pyroclasts with neomorphic quartz, marine fibrous radiaxial calcite and blocky calcite (Fig. 2.3). Then through the upward migration the fluids silicified the trilobites cuticles within the mounds and formed chimney-like structures near the Hamar Laghdad cliff.

2.5.1. Facies analyses of the Seheb el Rhassel Group

From the facies analysis of the Seheb el Rhassel group limestones emerged a deepening-upward trend of the sedimentations. At the bottom of the Seheb el Rhassel Group were observed horizons characterized by normal gradation (fining upward) that may be referred to a significant currents regime or storm events with mass transport (near the lower storm wave base). These facies, characterized by densely packed, coarse and reworked bioclasts (crinoidal packstone/grainstone and brachiopods *lumachella*), gradually disappear toward the top of the Group. At the upper part of the Seheb el Rhassel Group the facies became mud-dominated (fossiliferous wackestone) and in the last tenth of meters, where the Kess Kess mounds occur, tentaculites abundances within the fossil record

increased substantially (tentaculites packstone) revealing a deepening-upward trend (see Aitken et al., 2002 for a review). Indeed the Kess Kess developed in deep-water setting below the photic zone as suggested by lack of calcareous algae (Bełka et al., 1998) and abundance of stromatactis structures within the Kess Kess mounds associated to a quite-water environment below the fair-weather wave base (Bourque et al., 1986) or near the storm wave base (Kaufmann, 1996).

Within the mounds, in the upper part of the Seheb el Rhassel Group, occurrences of densely packed scutellid trilobites (trilobites floatstone/rudstone) were described. These anomalous facies, condensed inside meter-sized stromatactoid cavities, suggested a relation between the development of Kess Kess and the bloom of these macro-invertebrates (*Scutellum* sp.) that elsewhere in the Seheb el Rhassel Group represent a small amount of the bioclasts scattered in the sediments. Presence of dikes and veins branching off the walls off these stromatactoid cavities also suggested a synsedimentary fluids circulation that gave rise to a peculiar paleo-niche and probably washed over the micrite from the trilobites grainstone (Figs. 2.10B-C). The irregular pattern of geopetal structures and the float-like fabric (Fig. 2.10B) could be due to circulation of fluids through the lose sediments suddenly followed by early lithification via fibrous radiaxial cements (Flügel, 2004). During these reworking process: goethite was deposed within the geopetal micrite, the bioclasts were encrusted by quartz and the LMC of the trilobites shells was partially replaced by patchy quartz (Figs. 2.15).

The Seheb el Rhassel Group cement stratigraphy reflects a progressive, marine-phreatic to shallow-burial process because the cement sequence does not exhibit any break or corrosion surface, which might be expected under the influence of meteoric water during early diagenesis. Analogue preserved cements succession revealing a progressive marine-to- burial transition was described in the Maïder basin Middle Devonian mounds (Kaufmann, 1997). The transition between the pristine radiaxial calcite and the scalenohedral banded-luminescent calcite (through the non-luminescent scalenohedral calcite) seems related to burial progression and the consequent change (instability) of pore water chemical parameters leading to the alternation of bright- and dull-luminescent calcite (banded pattern). Dull-luminescence represents intermediate Mn and Fe contents and moderate diagenesis, and pristine cements are supposed to be non luminescent with low Mn and Fe contents (Brand et al., 2010) preserving pristine geochemistry. The non-luminescent Fe-rich blocky calcite, as the latest diagenetic product, suggests a precipitation under strongly negative redox conditions in the presence of ferrous ions, which acted as luminescence inhibitors (Aitken et al., 2002 and references therein). The presence of thick crusts of pristine radiaxial fibrous cement in all the primary cavities (including stromatactis) is a consequence of the early lithification due to early marine cementation, and the preservation of this phase excludes dissolution and

diagenetic overprinting (e.g., Mounji et al., 1998). However, low recrystallization grade was observed associated to specific facies, formally the Fe-rich carbonates associated to the chimney-like structures, characterized by zoned euhedral dolomite crystals. Contrary to the described paragenetic sequence this facies lacks micrite and radiaxial fibrous calcite cements and idiotopic to hypidiotopic dolomite cements the bioclasts. However the bioclasts were not affected by dolomitization or pressure-solution(Fig. 2.6E). Toward the center of the major voids the sequence continues the normal marine-to-burial trend with blocky calcite cements and locally syntaxial calcite.

2.5.2. Goethite and quartz of the Seheb el Rhassel Group as an evidence of hydrothermalism

Raman, XRD and XRF analyses reveal a homogeneous composition of the carbonates of the Seheb el Rhassel Group including the Emsian mounds, that result made of low-Mg calcite. However, Fe-rich facies dominated by goethite, quartz and dolomite mineral phases have been described associated to chimney-like structures (Fig. 2.6). Whereas goethite and quartz have been also observed associated to the trilobites floatstone-packstone facies within the mounds (Figs. 2.15).

Iron (Fe) and Fe-minerals including goethite are abundant in marine sedimentary systems (Taylor and Konhauser, 2011). Presence of Fe in marine system can be related to different geological processes including submarine volcanic exhalations, and accumulate in (Phanerozoic) ocean seafloor sediments in its ferric form (FeIII). Goethite at the ocean sea-floor is known to directly precipitate from low-temperature hydrothermal exhalation (Puteanus et al., 1991). The iron in the hydrothermal fluids can precipitates due to the oxic nature of Earth's (Phanerozoic) ocean, and form ferric oxhydroxide that transform in goethite as ageing process (Iizasa et al., 1998). Subaerial and marine chimney structures are peculiar of hydrothermal systems and have been described from active systems (e.g., Dekov et al., 2008) and in the geological record (e.g., Chen et al., 2009). Therefore, the goethitic chimney-like structures of the Seheb el Rhassel Group could represent together with the Emsian Kess Kess mounds, an evidence of the submarine hydrothermal venting related to the Merzane Group volcanic activity. Additionally, goethite deposits within the Kess Kess carbonate mounds have been commonly observed associated to *Scutellum* sp. shells of the trilobite floatstone/rudstone facies (Fig. 2.15). Deposition of goethite within this facies is probably due to local chemical (oxic) micro-condition driven by fluid injection along the fractures that characterize the stromatactoid cavities where the trilobites floatstone/rudstone was described.

Stability of goethite is constrained to particular chemo-physical conditions depending from temperature and pressure (Garrels and Christ, 1967; Reyes et al. 2003). Despite goethite (α-$Fe^{3+}O(OH)$) minerals are commonly instable under burial conditions, and convert in hematite (Fe_2O_3) at 80°-100°C (e.g., Lowe and Byerly, 2003), occurrences of stable goethite have been reported from hydrothermal systems with temperature up to ~130°C at 1bar and ~175°C at 1kbar (Garrels and Christ, 1967; Reyes et al. 2003).

Within the Seheb el Rhassel limestones goethite precipitation may be associated to the late stage of mound growth and/or before the burial diagenesis, or related to post-diagenetic processes. Indeed the presence of ferroan non-luminescent blocky cements in the Seheb el Rhassel limestones as end product of the diagenesis, suggests reducing conditions for pore waters of mound limestones, therefore adverse condition for goethite precipitation during the diagenesis. Thus the goethite deposits associated to chimney-like structures could be formed in a hydrothermally-dominated environment as also suggested by their peculiar rod-shaped morphologies (Fig. 2.6D). These goethite rod-shaped morphologies are similar to the ones interpreted as microbial morphologies (Iizasa et al., 1998, pag. 9, Fig. 5), described from the Coriolis Troughs (southwestern Pacific) hydrothermal sulfide-bearing deposits. Iizasa et al. (1998) consider the goethite rods at Coriolis Troughs a primary hydrothermal signature. Bacterial mediation is considered as a primary factor of ferrous mineral precipitation (see Southam, 2012 for a recent review) that could have catalyzed the formation of goethite in hydrothermal systems as documented in the Coriolis Troughs (Iisaza et al., 1998), and in the Teahitia-Mehitia and Macdonald hot spot areas (Puteanus et al., 1991).

Discrete occurrences of Si-minerals have been observed within the lower part of the Hamar Laghdad ridge in the Merzane Group (Lochkovian *Scyphocrinites* and low-Si basaltic breccia), and in the Seheb el Rhassel Group (Figs. 2.3, 2.4 and 2.15). Pyroclasts of the volcanic breccia of the Merzane Group are locally cemented by turbid coarse-grained quartz (Figs. 2.3 and 2.4), anatase and clinochlore (Fig. 2.4). Whereas the Si-mineral phase in the Seheb el Rhassel Group was neomorphic quartz associated to the chimney-like structures (Fig. 2.6F), and small amount of neomorphic quartz associated to scutellids of the trilobites floatstone/rudstone of the mound core facies (Figs. 2.10 and 2.15). Here, quartz phase encrusts and locally replaces the low-Mg calcite of trilobite cuticles (Fig. 2.15). Fossilized trilobite typically shown a mineralized exoskeleton composed by calcium carbonate, specifically low-Mg calcite (LMC) (Wilmot and Fallik, 1989; Lee et al., 2012). Although the LMC of trilobite cuticles is a stable carbonate phase (Richter and Füchtbauer, 1978), alteration processes can be induced by highly reactive pore fluids (Wilmot and Fallik, 1989) such as hydrothermal fluids. Recently, quartz replacing trilobite eyes from the Bou Tchrafine Group at the Hamar Laghdad ridge have been also described (Klug et al., 2009; Lee et al.,

2012). Klug et al. (2009) reported the presence of partially silicified trilobite exoskeleton within a Givetian *red cliff* among the Kess Kess mounds, and propose for them a diagenetic in origin. Although the authors mentioned a possible relation within silicified trilobite and the pervasive Devonian hydrothermal activity at the Hamar Laghdad ridge, an hydrothermal-related origin of these Si-minerals was not considered due to the limited occurrence of silicified trilobites.

Silica deposits and silicification are the most common processes associated to hydrothermal alteration of volcanic rock (Ellis and McMahon, 1977). Therefore, the presence of partially silicified trilobites and neomorphic quartz associated to the Kess Kess mounds and chimney-like structures could be probably explained by a pervasive Devonian hydrothermal activity at the Hamar Laghdad Ridge driven by alkaline basaltic volcanism. Circulation of Si-rich fluids related to volcanism of the Merzane Group replaced LMC of the trilobites of the triblobite floatstone/rudstone facies and then deposed the sediments related to the chimney-like structures.

2.5.3. Carbon and oxygen Stable isotope composition

Although the late magmatic fluids circulation in the Hamar Laghdad appears to be a prime candidate for the Kess Kess genesis, according to some authors (Joachimski and Buggisch, 1999) there are several discrepancy of the geochemical data (i.e. C and O stable isotopes) reported in literature (e.g. Belka, 1998; Mounji et al., 1998) and the proposed hydrothermal venting. For a better understanding of the Kess Kess relation with hydrothermal fluids the carbon and oxygen stable isotope compositions obtained from the described different carbonate and cement phases of the Seheb el Rhassel Group were discussed and compared with the data from literature from the same area (Belka, 1998; Mounji et al., 1998; Joachimski and Buggisch, 1999; Aitken et al., 2002).

Paleotemperature reconstruction of the studied Emsian limestones were referred to the standard values of the Devonian oceanic water at the middle latitudes (Fig. 2.17). The $\delta^{13}C$ and $\delta^{18}O$ standard values of the Devonian oceanic water at the middle latitudes were ≈ +2,5 (±1) ‰ and ≈ -5,0 (±1) ‰ PDB, respectively (Hurley and Lohmann, 1989). Assuming that 1) the oxygen isotopic composition of ocean water similar to the above standard values, and 2) the temperature increase during burial diagenesis with consequent depletion of primary $\delta^{18}O$ values ($\delta^{13}C$ constant) (Hurley and Lohman, 1989):

1) The average $\delta^{18}O$ values of micrite result negative compare to signal obtained from calcitic cements (Fig. 2.17) and the progressive depletion of $\delta^{18}O$ values due the increase of temperatures during the burial was inverted in the Seheb el Rhassel limestones. Indeed the cements

$\delta^{18}O$ composition is closer to the marine standard than the micrite $\delta^{18}O$ composition (Fig. 2.17). During a normal marine diagenesis, the standard composition (Devonian oceanic water at the middle latitudes) affected by a burial diagenesis comprised between 0 and 2 km, that however is far deeper than the burial reached by the Seheb el Rhassel Group (Guido et al., 2012), shows values of $\delta^{18}O$ = -5,7 ‰ and $\delta^{13}C$ = 0,5 ‰ (Ali, 1995).

2) The $\delta^{18}O$ micrite values negative as -10‰ PDB suggest precipitation from fluids with temperatures higher than ambient seawater. Expected temperature (Friedmann and O'Neil, 1977) for fluids flowing through the Seheb el Rhassel Group included the Emsian Kess Kess mounds are constrained in a slightly precise range of 40-45°C compatible with 36-56°C proposed by Mounji et al. (1998). Although the temperatures obtained are conservative compared to 120°C obtained by Bełka (1998) from fluid inclusions coming from the mound buildups, they can easily suggest a low-hydrothermal fluids circulation. Probably, temperature of 120°C should correspond to a approximate $\delta^{18}O$ value of -24 ‰ PDB (Friedmann and O'Neil, 1977). This discrepancy may be due to the fast mixing of the hot fluids with cold oceanic water with consequent reducing of temperature registered in the sediments.

3) A $\delta^{18}O$ negative trend can be observed through the Seheb el Rhassel Group micrite with the more negative values in correspondence of the Kess Kess mounds and less depleted values from the infra-mounds micrite and from the samples collected at the bottom of the Group. Particularly the micrite within the brachiopods *lumachella* lens near the mounds core facies (upper part of the Group) is slightly depleted respect to the brachiopods *lumachella* at the bottom of the Group.

4) Slightly depleted $\delta^{18}O$ stable isotope data that document the presence of methane-rich fluids in the Hamar Laghdad mounds were reported from the Middle Devonian Hollard Mound and from veins filling in the Emsian limestone of the Seheb el Rhassel Group (Mounji et al., 1998; Peckmann et al., 1999, 2005; Buggish and Krumm, 2005; Cavalazzi et al., 2007; this study). The moderate depletion reported in this work from the veins filling could be due to mixing of different fluids during the seepage and/or microbial selective consumption of the methane in the deeper strata in correspondence of the sulfate reduction surface (Reeburgh, 1980; Devol et al., 1984) before the formation of the authigenic carbonates. Otherwise the CO_2 source may not be attributable directly to the methane but resulting from the oxidation of sedimentary organic material by sulfate reducing bacteria with a $\delta^{13}C$ of approx. -20 ‰ (Ritger et al., 1987) which are probably responsible of the general low depleted values in the Kess Kess limestones. Moreover the $\delta^{13}C$ values could be influenced by the water temperature, in fact, as suggested by Canet et al. (2005), under hot water seepage the CO_2 degassing cause a ^{13}C enrichment and consequent increase of $\delta^{13}C$ values with loss

of methane and/or organic geochemical signatures. The gradual increase of temperature and loss of CO_2 may have been fed by the cyclic warm fluid circulation during deposition of the limestones.

The $\delta^{18}O$ values of micrite sampled from the Kess Kess mounds is more depleted than those from underlying strata and thus probably depends from direct precipitation of the micrite from heated fluids that reached the surface during mounds development. However, at the stratigraphic level of the mounds, there is a pronounced excursion to less negative $\delta^{18}O$ values moving from the mounds to the infra-mounds area that localized the fluid advection in the mounds occurrence.

2.6. CONCLUSIONS

The Emsian Kess Kess mounds developed at the top of the Seheb el Rhassel Group that is a ~100 meter thick succession of fossiliferous limestones developed above the basaltic breccia dome-shaped belt generated during the Lochkovian submarine volcanic activity in an epicontinetal sea associated to the Tafilat Platform/Basin system (Figs. 2.1 and 2.2). The effect of the late volcanism (late magmatic fluid circulation) in this area influenced the mineralogy and morphologies of Hamar Laghdad stratigraphic succession including the Kess Kess mounds catalyzing their early lithification.

The described *in situ* volcanic rocks (basaltic breccia) fuelled a cyclic heating flux and low-temperature hydrothermal fluids circulation. The hydrothermal (vent-related) secondary minerals observed at different stratigraphic levels of the Seheb el Rhassel Group are new evidence of a low-temperature hydrothermal fluids circulation at the Hamar Laghdad ridge. These fluids flowing through the Hamar Laghdad succession i) alter the volcanic breccia where pyroclasts occur cemented by quartz and in association with clinochlore and anatase, ii) induce a discrete silicification supported by the presence of silicified trilobite cuticles within stromatactis, additionally, trace of goethite were observed within these silicified trilobite, and iii) gave rise to chimney-like structures dominated by goethite dark red deposits associated with neomorphic quartz and Fe-rich limestone.

In this frame, our stable isotopic data, especially the remarkable shift of the micrite $\delta^{18}O$ composition toward negative values, support the hydrothermal (vent-related) hypothesis for the origin of the Emsian Kess Kess mounds. In fact, geological constrains of the Hamar Laghdad ridge, such as the shallow burial reached, suggest to exclude the deep burial diagenesis in order to justify

the low $\delta^{18}O$. Therefore, the low $\delta^{18}O$ values of micrite of the Emsian Kess Kess mounds can be explained as evidence of to precipitation from low-temperature hydrothermal fluids.

The distribution of the temperature values extrapolated from the Seheb el Rhassel Group $\delta^{18}O$ values indicates that during the deposition of the primary micrite the water temperature was far above the mean oceanic temperature at these latitude and depth (40°-45°C). There is no burial diagenesis trend (increment of the temperature with the burial) and the calcite cement presents $\delta^{18}O$ values compatible with equilibrium with the Devonian mean oceanic water.

The plumbing system varied during the geological history of Hamar Laghdad; it resulted in fractures and veins connected with large cavities filled by trilobites floatstone/rudstone within the Kess Kess mounds, to meter-sized rounded chimneys-like structures in the upper part of the Group, to the veins and neptunian dikes system that probably postdate the Kess Kess development. These evidences delineate a scenario of intermittent hydrothermalism during the Early and middle Devonian.

The occurrence in different stratigraphic levels of secondary hydrothermal products such as low-Si olivine-rich basaltic breccia cemented by quartz and associated to clinochlore and anatase, levels in the Seheb el Rhassel Group (Emsian) and Bou Tchrafine Group (Eifelian) of silicified trilobite locally associated to small amount of goethite, several generations of mounds in the Emsian (the Kess Kess) up to the Frasnian (vents) with faunal associations adapted to particular environmental conditions (scutellid trilobites, vents ostracods and thermophilic corals), goethite dominated chimney-like structures with quartz and euhedral dolomite, point out to an evolving low-temperature hydrothermalism connected to the mound’s formation.

REFERENCES

Aitken, S.A., Collom, C.J., Henderson, C.M., Johnston, P.A., 2002. Stratigraphy, paleoecology, and origin of Lower Devonian (Emsian) carbonate mud buildups, Hamar Laghdad, eastern Anti-Atlas, Morocco, Africa. Bull. Can. Pet. Geol. 50, 217-243.

Alberti, G.K.B., 1981. Scutelluidae (Trilobita) aus dem Unter-Devon des Hamar Laghdad (Tafilalt, SE-Morocco) und das Alter der "mud mounds" (Oberes Zlichovium bis tiefstes Dalejum). Senckenbergiana lethaea 62, 193-204.

Alem, A., Gendrot, C., Koch, B., Negroni, P., Rabate, J., 1968. Étude sur l'Hamar Laghdad (Tafilalt). Bureau de Recherches et de Participations Minères, Morocco, pp 64.

Ali, M.Y., 1995. Carbonate cement stratigraphy and timing of diagenesis in a Miocene mixed carbonate-clastic sequence, offshore Sabah, Malaysia: constraints from cathodo-luminescence, geochemistry, and isotope studies. Sediment. Geol. 99, 191-214.

Barbieri, R., Ori, G.G., Cavalazzi, B., 2004. A Silurian cold-seep ecosystem from the Middle Atlas, Morocco. Palaios 19, 527-542.

Bates, R.L., Jackson, J.A., 1980. Glossary of Geology. American Geological Institute, Falls Church, VA, pp 749 .

Bathurst, R.G.C., 1980. Stromatactis-origin related to submarine-cemented crusts in Paleozoic mud mounds. Geology 8, 131-134.

Bełka, Z., 1998. Early Devonian Kess-Kess carbonate mud mounds of the eastern Anti-Atlas (Morocco), and their relation to submarine hydrothermal venting. J. Sediment. Res. 68, 368-377.

Bełka, Z., Berkowski, B., 2005. Discovery of thermophilic corals in an ancient hydrothermal vent community, Devonian, Morocco. Acta Geol. Pol. 55, 1-7.

Berkowski, B., 2004. Monospecific rugosan assemblage from the Emsian hydrothermal vents of Morocco. Acta Geol. Pol. 49,75-84.

Berkowski, B., 2006. Vent and mound rugose coral associations from the Middle Devonian of Hamar Laghdad (Anti-Atlas, Morocco). Geobios 39, 155-170.

Berkowski, B., 2008. Emsian deep-water Rugosa assemblages of Hamar Laghdad (Devonian, Anti-Atlas, Morocco). Palaeontogr. Abt. A284, 17-68.

Berkowski, B., Klug, C., 2012. Lucky rugose corals on crinoid stems: unusual examples of subepidermal epizoans from the Devonian of Morocco. Lethaia 45, 24-33.

Bouček, B., 1964. The Tentaculites of Bohemia: Their Morphology, Taxonomy, Phylogeny and Biostratigraphy. Publishing House of the Czechoslovaki Academy of Sciences, Prague, pp 215.

Bourque, P.A., Amyot, G., Desrochers, A., Gignac, H., Gosselin, C., Lachambre, G., Laliberte, J.Y., 1986, Silurian and Lower Devonian reef and carbonates complexes of the Gaspé Basin, Québec- a summary. Bull. Can. Pet. Geol. 34, 452-489.

Brachert, T.C., Buggisch, W., Flügel, E., Hüssner, H.M., Joachimski, M.M., Tourneur, F., Walliser, O.H., 1992. Controls of mud mound formation: the Early Devonian Kess-Kess carbonates of the Hamar Laghdad, Antiatlas, Morocco. Geol. Rundsch. 81, 11-44.

Brand, U., Azmy, K., Tazawa, J., Sano, H., Buhl, D., 2010. Hydrothermal diagenesis of Paleozoic seamount carbonate components. Chem. Geol. 278, 173-185.

Buggisch, W., Krumm, S., 2005. Paleozoic cold seep carbonates from Europe and North Africa: an integrated isotopic and geochemical approach. Facies 51, 566-583.

Canet, C., Prol-Ledesma, R.M., Torres-Alvarado, I., Gilg, H.A., Villanueva, R.E., Lozano-Santa Cruz, R., 2005. Silica-carbonate stromatolites related to coastal hydrothermal venting in Bahía Concepción, Baja California Sur, Mexico. Sediment. Geol. 174, 97-113.

Campbell, K.A., 2006. Hydrocarbon seep and hydrothermal vent palaeoenvironments and paleontology: past developments and future research directions. Palaeogeogr. Palaeoclimatol. Palaeoecol. 232, 362-407.

Cavalazzi, B., 2007. Chemotrophic filamentous microfossils from the Hollard Mound (Devonian, Morocco) as investigated by focus ion beam. Astrobiology 7, 402-415.

Cavalazzi, B., Barbieri, R., Ori, G.G., 2007. Chemosynthetic microbialites in the Devonian carbonate mounds of Hamar Laghdad (Anti-Atlas, Morocco). Sediment. Geol. 200, 73-88.

Cavalazzi, B., Barbieri, R., Cady, S.L., George, A.D., Gennaro, S., Lui, A., Westall, F., Rossi, A.P., Ori, G.G., Taj-Heddine, K., 2012. Iron-framboids in the hydrocarbon-related Middle Devonian Hollard Mound of the Anti-Atlas mountain range in Morocco: evidence of potential microbial biosignatures. Sediment. Geol. 263-264, 183-193.

Chen, D., Wang, J., Qing, H., Yan, D., Li, R., 2009. Hydrothermal venting activities in the Early Cambrian, South China: Petrological, geochronological and stable isotopic constraints. Chem. Geol. 258, 168-181.

Dekov V.M., Cuadros J., Shanks W.C., Koski R.A., 2008. Deposition of talc – kerolite-smectite - smectite at seafloor hydrothermal vent fields: Evidence from mineralogical, geochemical and oxygen isotope studies. Chemical Geology 247 (2008) 171–194.

Dekov V.M., Kamenov G.D., Savelli C., Stummeyer J., Thiry M., Shanks W.C., Willingham A.L., Boycheva T.B., Rochette P., Kuzmann E., Fortin D., Vértes A., 2009. Metalliferous sediments from Eolo Seamount (Tyrrhenian Sea): Hydrothermal deposition and re-deposition in a zone of oxygen depletion. Chemical Geology 264 (2009) 347–363

Demoulin, A., Trigance, C., Neff, D., Foy, E., Dillmann, P., L'Hostis, V., 2010. The evolution of the corrosion of iron in hydraulic binders analysed from 46-and 260-year-old buildings. Corrosion Science 52, 3168–3179.

De Mol, B., Henriet, J.-P., Canals, M., 2005. Development of coral banks in Porcupine Seabight: do they have Mediterranean ancestors? In: Freiwald A, Roberts JM (ed) Cold-Water Corals and Ecosystems. Springer, pp 515-533.

Devol, A.H., Anderson, J.J., Kuivila, K., Murray, J.W., 1984. A model for coupled sulfate reduction and methane oxidation in the sediments of Saanich inlet. Geochim. Cosmochim. Acta 48, 993-1004.

Ellis, E.J., McMahon, W.A.J., 1977. Chemistry and Geothermal System. Academic Press, New York, pp. 392.

Fagerstrom, J.A., 1991. Reef-building guilds and a checklist for determining guild membership. Coral Reefs 10, 47-52.

Fischer AG (1964) The Lofer cyclothems of the Alpine Triassic. Kansas Geol Surv Bull 169:107-149

Flajs, G., Vigener, M., Keupp, H., Meischner, D., Neuweiler, F., Paul, J., Reitner, J., Warnke, K., Weller, H., Dingle, P., Hensen, C., Schäfer, P., Gautrer, P., Leinfelder, R., Hüssner, H., Kaufmann B., 1995. Mud mounds: A polygenetic spectrum of fine-grained carbonate buildups. Facies 32, 1-69.

Flügel, E., 2004. Microfacies of Carbonate Rocks-Analysis, Interpretation and Application. Springer-Verlag, Heidelberg, pp 976

Foubert, A., Henriet, J.-P., 2009. Nature and significance of the recent carbonate mound record: The Mound Challenger code. Lect Notes Earth Sci 126. Springer, Dordrecht, pp. 298.

Franchi, F., Shemm-Gregory, M., Klug, C., 2012. A new species *Ivdelinia* Andronov, 1961 from the Moroccan Givetian and its palaeoecological and palaeobiogeographical implications. Bulletin of Geosci. 87, 1-11.

Franchi, F., 2012. Carbonate conical mounds of the eastern Anti-Atlas (Morocco) and their relation with potential analogues on Marsv. Universityof Bologna, Italy, Unpublished PhD thesys.

Friedman I., O'Neil J.R., 1977. Compilation of stable isotope fractionation factors of geochemical interest. In: Fleisher M. (Ed.), Data of geochemistry, 6th edn. USGS Prof Pap, 440KK, 12 pp.

Garrels, R.M., Christ, C.L., 1967. Solutions, minerals and equilibria. New York, Harper and Row Publishing Co, 450 pp.

Gendrot C (1973) Environments du Dévonian récifal du Marocco. Notes Serv Géol Maroc 34:55-86

Guido, A., Mastandrea, A., Demasi, F., Tosti, F., Russo, F., 2012. Organic matter remains in the laminated microfabrics of the Kess-Kess mounds (Hamar Laghdad, Lower Devonian, Morocco). Sediment. Geol. 263-264, 194-201.

Hollard, H., 1981a. Principaux caractères des formations dévoniennes de l'Anti-Atlas. Notes Mém. Serv. Géol. Maroc. 42, 15-22.

Hollard, H., 1981b. Tableaux de corrélations du Silurien et du Dévonien de l'Anti-Atlas. Notes Mém. Serv. Géol. Maroc. 42, 23.

Hurley, N.F., Lohmann, K., 1989. Diagenesis of Devonian reefal carbonates in the Oscar Range, Canning Basin, Western Australia. J. Sediment. Petrol. 59, 127-146.

Iizasa, K., Kawasaki, K., Maeda, K., Matsumoto, T., Saito, N., Hirai, K., 1998. Hydrothermal sulfide-bearing Fe-Si oxyhydroxide deposits from the Coriolis Troughs, Vanuatu backarc, southern-eastern Pacific. Marine Geol. 145, 1-21.

Joachimski, M.M., Buggisch, W., 1999. Hydrothermal origin of Devonian conical mounds (kess-kess) of Hamar Lakhdad Ridge, Anti-Atlas, Morocco: Comment and Reply. Geology 28, 893-894.

Kaufmann, B., 1996. Facies, stratigraphy and diagenesis of Middle Devonian reef and mud-mounds in the Maïder (eastern Anti-Atlas, Morocco). PhD thesis, University of Tübingen.

Kaufmann, B., 1997. Diagenesis of Middle Devonian carbonate mud buildups of the Maïder Basin (eastern Anti-Atlas). J. Sediment. Res. A67, 945-956.

Klug, C., Schulz, H., De Baets, K., 2009. Red trilobites with green eyes from the Early Devonian of the Tafilalt (Morocco). Acta Palaeontol. Pol. 54:117-123.

Kopaska-Merkel, D.C., Haywick, D.W.A., 2001. A lone biodetrital mound in the Chesterian (Carboniferous) of Alabama? Sediment. Geol. 145, 253-268.

Laetsch, T.A., Downs, R.T., 2006. Software for identification and refinement of cell parameters from powder diffraction data of minerals using the RRUFF Project and American Mineralogist Crystal Structure Databases. Program and Abstracts of the 19th General Meeting of the International Mineralogical Association in Kobe, Japan, pp P08-25 http://rruff.info/.

Lee, M.R., Torney, C., Owen, A.W., 2012. Biomineralisation in the Palaeozoic oceans: Evidence for simultaneous crystallisation of high and low magnesium calcite by phacopine trilobites. Chem. Geol. 314-317, 33-44.

Lonsdale P., 1977. Clustering of Suspension-Feeding Macrobenthos Near Abyssal Hydrothermal Vents at Oceanic Spreading Centers. Deep-Sea Research 24, 857-863.

Lowe, D.R., Byerly, G.R., 2003. Ironstone pods in the Archean Barberton greenstone belt, South Africa: Earth's oldest seafloor hydrothermal vents reinterpreted as Quaternary subaerial springs. Geology 31, 909-912.

Marumo, K., Hattori, K.H., 1999. Seafloor hydrothermal clay alteration at Jade in the back-arc Okinawa Trough: mineralogy, geochemistry and isotope characteristics. Geochim. Cosmochim. Acta 63, 2785-2804.

Mazzetti, L., Thistlethwaite, P.J., 2002. Raman spectra and thermal transformations of ferrihydrite and schwertmannite. Journal of Raman Specroscopy 33, 104–111.

Michard, A., 1976. Elements de Géologie Marocaine. Notes Mém. Serv. Géol. Maroc. 252, 1-408

Monty, C.L.V., 1995. The rise and nature of carbonate mud-mounds. an introductory actualistic approach. In: Monty CLV et al. (ed) Carbonate Mud-Mounds Their Origin and Evolution. Spec Publs Int Ass Sediment 23, 11-48.

Mounji, D., Bourque, P.A., Savard, M.M., 1998. Hydrothermal origin of Devonian conical mounds (kess-kess) of Hamar Lakhdad Ridge, Anti- Atlas, Morocco. Geology 26, 1123-1126.

Müller-Jungbluth, W.V., Toshek, P.H., 1969. Karbonatsedimentol-ogische Arbeitsunterlagen. Veröffentlichungen der Universität Innsbruck, Alpenkundliche Studien 4, 32 pp.

Nakaseama M, Ishibashi J.-I., Ogawa K., Hamasaki H., Fumino K., Yamanaka T., 2008. Fluid-sediment interaction in a marine shallow-water hydrothermal system in the Wakamiko submarine crater, South Kyushu, Japan. Resource Geology 58, 289-300.

Olempska, E., Bełka, Z., 2010. Hydrothermal vent myodocopid ostracods from the Eifelian (Middle Devonian) of southern Morocco. Geobios 43, 519-529.

O'Neil, J.R., Clayton, R.N., Mayeda, T.K., 1969. Oxygen isotope fractionation in divalent metal carbonates. J. Chem. Phys. 51, 5547-5558.

Peckmann, J., Walliser, O.H., Riegel, W., Reitner, J., 1999. Signatures of hydrocarbon venting in a Middle Devonian carbonate mound (Hollard Mound) at the Hamar Laghdad (Antiatlas Morocco). Facies 40, 281-296.

Peckmann, J., Little, C.T.S., Gill, F., Reitner, J., 2005. Worm tube fossils from the Hollard Mound hydrocarbon-seep deposit, Middle Devonian, Morocco: Palaeozoic seep-related vestimentiferans? Palaeogeogr. Palaeoclimatol. Palaeoecol. 227, 242-257.

Piqué, A., Michard, A., 1989. Moroccan Hercynides: a synopsis. The Paleozoic sedimentary and tectonic evolution at the northern margin of west Africa. Am. J. Sci. 289, 286-330.

Pratt, B.R., 1995. The origin, biota and evolution of deep-water mudmounds. In: Monty CLV, Bosence DWJ, Bridges PH, Pratt BR (ed) Carbonate Mud-Mounds. Their Origin and Evolution. Spec. Publ. Int. Assoc. Sedimentol. 23, 49-123.

Puteanus, D., Glasby, G.P., Stoffers, P., Kunzendorf, H., 1991. Hydrothermal ion-rich deposits from the Teahitia-Mehitia and Macdonald hot spot areas, southwest Pacific. Mar. Geol. 98, 389-409.

Pusch, G.G., 1833. Geognostische Beschreibung von Polen sowie der übrigen Nordkarpaten-Länder, Teil 1. Stuttgart, 338 pp.

Reeburgh, W.S., 1980. Anaerobic methane oxidation: Rate depth distribution in Skan Bay sediments. Earth Planet. Sci. Lett. 47, 345-352.

Reyes, A.G., Grapes, R., Clemente, V.C., 2003. Fluid-rock interaction at the magmatic-hydrothermal interface of the Mount Cagua geothermal system, Philippines. In: Simmons SF, Graham I (ed) Volcanic, Geothermal, and ore-forming fluids: rulers and witnesses within the Earth. Geochem. Soc. Spec. Publ. 8, 197-222.

Richter, D.K., Füchtbauer, H., 1978. Ferroan calcite replacement indicates former high-magnesian calcite skeletons. Sedimentology 25, 843-860.

Riding, R., 2002. Structure and composition of organic reefs and carbonate mud mounds; concepts and categories. Earth-Sci Rev. 58, 163-231.

Ritger, S., Carson, B., Suess, E., 1987. Methane-derived authigenic carbonates forms by subduction-induced pore-water expulsion along the Oregon/Washinton margin. Geol. Soc. Am. Bull. 98, 147-156.

Roch, E., 1934. Sur des phénomènes remarquables observés dans la région d'Erfoud (confins Algero-Marocains de Sud). Ass. l'Étude Géol. Méditerr. Occident. 5, 1-10.

Schlager, W., 2003. Benthic carbonate factories of the Phanerozoic. Int. J. Earth Sci. 92, 445-464.

Seyfried W.E. Jr., Pester N.J., Ding K., Rough M., 2011. Vent fluid chemistry of the Rainbow hydrothermal system (36_N, MAR): Phase equilibria and in situ pH controls on subseafloor alteration processes. Geochimica et Cosmochimica Acta 75, 1574–1593.

Southam, G., 2012. Minerals as substrates for life: The prokaryotic view. Elements 8, 101-106.

Stampfli, G.M., Borel, G.D., 2002. A plate tectonic model for the Paleozoic and Mesozoic constrained by dynamic plate boundaries and restored synthetic oceanic isochrones. Earth Planet. Sci. Lett. 196, 17-33.

Tait, J.A., Bachtadse, V., Soffel, H., Franke, W., 1995. Paleozoic paleogeography of the circum Atlantic continente. Terra Nostra 8, 133.

Taylor, K.G., Konhauser, K.O., 2011. Iron in Earth Surface Systems. Elements 7, 83-120.

Tebbutt, G.E., Conley, C.D., Boyd, D.W., 1965. Lithogenesis of a distinctive carbonate rock fabric. University of Wyoming Contributions to Geology 4, 1-13.

Teichert, B.M.A., Bohrmann, G., Suess, E., 2005. Chemoherms on Hydrate Ridge — Unique microbially-mediated carbonate build-ups growing into the water column. Palaeogeogr. Palaeoclimatol. Palaeoecol. 227, 67-85.

Walter, L.M., Ku, T.C.W., Muehlenbachs, K., Patterson, W.P., Bonnell, L., 2007 Controls on the δ13C of dissolved inorganic carbon in marine pore waters: an integrated case study of isotope exchange during syndepositional recrystallization of biogenic carbonate sediments (South Florida, USA). Deep-Sea Res. II 54, 1163-1200.

White, S.N., 2009. Laser Raman spectroscopy as a technique for identification of seafloor hydrothermal and cold seep minerals. Chem. Geol. 259, 240-252/

Wendt, J., 1985. Disintegration of the continental margin of northwestern Gondwana: Late Devonian of the eastern Anti-Atlas (Morocco). Geology 13, 815-818.

Wendt, J., Aigner, T., Neugebauer, J., 1984. Cephalopod limestone deposition on a shallow pelagic ridge: the Tafilalt Platform (upper Devonian, eastern Anti-Atlas, Morocco). Sedimentology 31, 601-665.

Wendt, J., Bełka, Z., Moussine-Pouchkine, A., 1993. New architectures of deep-water carbonate buildups: Evolution of mud mounds into mud ridges (Middle Devonian, Algerian Sahara). Geology 21, 723-726.

Wilmot, N.V., Fallik, E., 1989. Original mineralogy of trilobite exoskeletons. Palaeontology 32, 297-304.

Wilson, J.L., 1975. Carbonate Facies in Geologic History. Springer Verlag, New York.

Wright, V.P., 1992. A revised classification of limestones. Sediment. Geol. 76, 177-185.

3. COMPARATIVE STUDY OF THE BRACHIOPOD FAUNAS OF MAÏDER MIDDLE DEVONIAN MOUNDS*

3.1. INTRODUCTION

The occurrence of many Devonian mounds in the Tindouf Basin (Dumestre & Illing 1967), in the Sebkha Azzel Matti (Wendt *et al*. 1997), and in the Moroccan eastern Anti-Atlas is well documented in literature, particularly the Anti-Atlas Tafilalt (see Tab. 2.1), and Maïder Basin (Wendt 1993; Kaufmann 1995, 1996, 1997, 1998a, b). In chapter 2 we faced the geological problem of the Kess Kess conical mounds; here we introduce the Maïder basin mounds to complete the outline of the Devonian conical mounds in the Anti-Atlas. This research, based mainly on field survey results and palaeontological studies, allowed to compare two conical clusters characterized by a controversial origin.

The Maïder Basin (Fig. 3.1) offers one of the most impressive outcrops of Devonian mounds. Hollard (1974) was the first who mentioned the 4 mud mounds at Jebel el Oftal, the solitary mud mound at Guelb el Maharch, and the reef mound named Aferdou el Mrakib in the Maïder Basin (Fig. 3.2). Because of their shape and lithology, these mounds are very similar to the Kess Kess mounds of Hamar Laghdad (Chapter 2). Even though they have been studied for decades, the origin of the carbonate buildups of the Maïder Basin is still under debate and detailed descriptions of strategic taxa, *e.g*. brachiopods, could provide new palaeoecological data useful for inferring their genesis and compare it with the Kess Kess genesis. The data discussed here came from a field survey in the Maïder basin aimed to collect limestone samples from the carbonate mounds buildups to make the comparison with the Kess Kess limestones. The field work gave new insights about the Maïder mounds structures allowed to compare sedimentological features occurring in both regions as neptunian dikes and veins. The micro facies described in chapter 2 were described even from the Maïder mounds.

During the field survey, aimed to collect samples of the Maïder basin faunal association, a new species of brachiopods was discovered. One of the main purposes of this work is to provide a detailed description of this taxon *Ivdelinia pulchra* sp. nov., which is part of the Aferdou el Mrakib reef guild. The other specimens collected during the field survey in February 2011 belong to the orders Spiriferida, Orthida, and Athyridida. Only a few strophomenids were found in another

* This chapter consists of a paper by Franchi, F., Shemm-Gregory, M., Klug, C., 2012. A new species *Ivdelinia* Andronov, 1961 from the Moroccan Givetian and its palaeoecological and palaeobiogeographical implications. Bulletin of Geosciences 87 (1), 1-11.

mound locality. *Ivdelinia pulchra* sp. nov. occurs in various situations: it can be found in monospecific shell beds (see Klug *et al*., 2009), locally, associated with abundant specimens of the gypidulid *Devonogypa* (which reaches almost 80 mm shell length) in low diversity associations together with some other brachiopods, and sometimes, it can be found in free association with the variable fauna of the Aferdou el Mrakib reef mound.

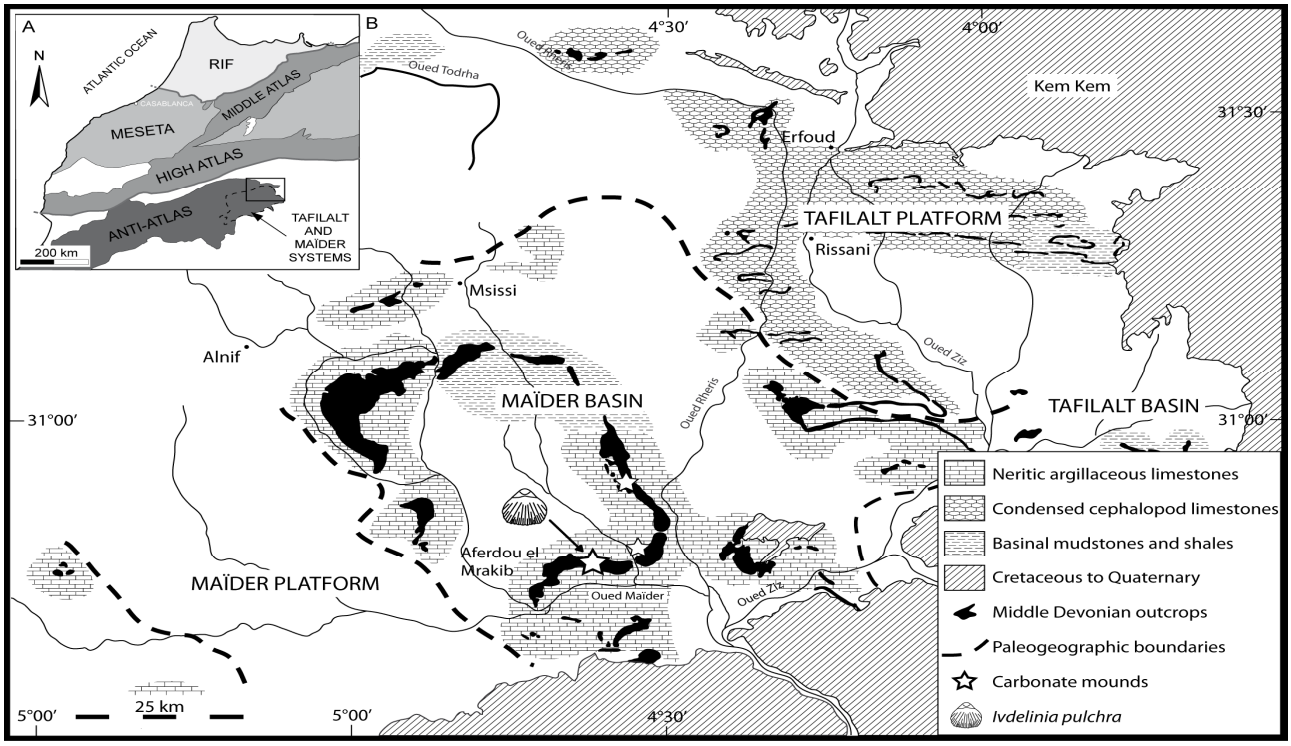

Figure 3. 1. Simplified geological map of north-western Africa. A) **Rif, Meseta and Atlas structural domains dominate the physiography of north-western Africa. The eastern part of Anti-Atlas domain includes the Devonain Tafilalt and Maïder palaeogeographic units (broken line). The study area (box) is detailed in B.** B) **Distribution of the Tafilalt and Maïder platform-basin system. The Kess Kess mounds cropping out at the Hamar Laghdad ridge (star) are hosted in the Tafilalt platform. Modified from Michard (1976), Kaufmann (1997).**

3.2. GEOLOGICAL SETTING

Maïder platform/basin system is one of the systems resulting from the clockwise Gondwana rotation (see paragraph 2.1.1) during the Devonian (Wendt, 1985). This platform/basin system was generated by early Variscan tensional stresses on the passive continental margin of northwest Gondwana (Wendt,1985; 1988).

The Maïder region is situated south of Msissi (Fig. 3.1), where the Devonian strata crop out in a 50 km wide amphitheater-like structure. The carbonate buildups lie on top of a 200–300 m thick Middle Devonian succession of argillaceous, fossiliferous limestones (Hollard, 1974; Wendt, 1993). During the Late Devonian, the Maïder Basin was filled by a succession of approx. 800 m of shales and sandstones, which correspond to just some tens of meters of cephalopod limestone in the Maïder Platform (Wendt, 1991). Afterwards, Upper Devonian/Lower Carboniferous marine siliciclastic deposits levelled both the platform and the basin.

3.3. CARBONATE BUILDUPS: previous works

The long lasting debate on the origin of the carbonate buildups of the Maïder Basin roots in two main problems: their genesis and the control of their stratigraphic position. Kaufmann (1998a) suggested a microbial origin for the carbonates of the Maïder Basin mud mounds, in spite of the microbial structures only being preserved in stromatactis fabrics as happened for the Kess Kess mounds, and concluded that changes of the physico-chemical parameters of the water would have allowed the microbial communities to fix the CaCO3 in their biofilms (Chafetz and Bucrynski, 1992; Monty, 1995) consolidating the steep flanks of the carbonates buildups. This hypothesis is also supported by high accumulation rates of the mound facies, greater than in the off-mound facies, purity of mound carbonates (95% CaCO3), and homogeneous calcite mineralogy (Kaufmann, 1996), which suggests an authigenic origin.

The scattered occurrence of the carbonate buildups can hardly be explained by the presence of cold seeps and/or hot vents on the sea floor (*e.g.*, Belka 1998). Geochemical data do not support this suggestion unequivocally. Methane seepages are not supported by the ^{13}C-values of the mound carbonates which suggest normal marine conditions, and the ^{18}O-values do not indicate a sufficiently elevated temperature to suggest any hydrothermal activity (Kaufmann, 1997). Nevertheless, Aferdou el Mrakib and Guelb el Maharch carbonate buildups appear to be aligned with a Precambrian E-W trending strike-slip fault system (Kaufmann 1998a) that could be a preferential way for deep fluids. It cannot be excluded, therefore, that the development of the carbonate buildups was initiated with a low temperature hydrothermal water seepage and subsequent benthic fauna colonization. Mixing with the normal sea water might also explain the near-normal isotopic values.

In literature Aferdou el Mrakib mound is the only one with a certain genesis related to biogenic accumulation (*e.g.* Kaufmann et al., 1997) and is interpreted as a reef mound, particularly in its last growing phase.

Kaufmann (1996, 1997) established the age of the Maïder carbonate buildups by the study of conodont faunal associations formerly described by Belka *et al*. (1997). The oldest build-ups described here are, according to the above mentioned authors, the mounds number 1 to 3 at Jebel el Otfal, which were dated as early *costatus costatus* zone (early Eifelian); mound number 4 is younger and spans throughout the *kockelianus* up to the lower *ensensis* zone (late Eifelian). The solitary mound at Guelb el Maharch was stratigraphically positioned in the early *varcus* conodont zone (early Givetian) and the reef mound at Aferdou el Mrakib ranges from the *hemiansatus* to the early *varcus* conodont zone (early Givetian).

3.3.1. Jebel el Oftal

The oldest carbonate buildups of the Maïder Basin are the 4 Eifelian mounds of Jebel el Oftal. Only one of these mounds (the number 2 in Kaufmann, 1998) reaches the dimension of Guelb el Maharch, with a diameter of 120-150 m and 40 m high (Fig. 3.2 A). Also this mound shows asymmetric flanks, with a steeper southwestern flank (ca. 40°) representing the closest analogue of the Kess Kess mounds in the Maïder basin. The other 3 mounds are smaller, not properly cone shaped and partially covered by Quaternary sediments. Less abundant corals and brachiopods specimens characterize these mounds. Instead in the Jebel el Oftal carbonate buildups appears trilobites assigned to the genus Phacops (rare occurrences in Aferdou el Mrakib buildups) and assembrages of scutellid trilobites analogues of the scutellid rudstone described in the Kess Kess. In this facies scutellid remains are less packed and the lithofacies is a wackestone. The carbonate buildups are composed by stromatactis bearing crinoidal wakestone. There are no evidences for the presence of dikes in the Jebel el Oftal buildups.

3.3.2. Guelb el Maharch

The early Givetian Guelb el Maharch buildup emerges from the southeastern margin of the plain for 45 m (Fig. 3.2 B). The exposed base has a diameter of approx. 120 m. The shape of this mound is asymmetric (the same characteristic of Kess Kess conical mound) with a steeper eastern flank (approx. 45°). The faunal assemblage of this smaller carbonate buildup is impoverished and dominated by echinoderms (crinoids) and tabulate corals (auloporid). Except for the absence of trilobites and for the less abundance of tentaculites, this association corresponds to Kess Kess fauna. This assemblage is attributable to deeper water environment (Wendt, 1993; Kaufmann, 1995). From a lithological point of view Guelb el Maharch is composed by a stromatactis bearing wakestone. Many dikes, filled by dark to violet micrite and cements with lithoclasts and iron

pebbles, cut the flanks of this solitary mound. Kaufmann (1997) suggests that this fractures system was opened during late Givetian and filled by the dark sediment overlaying the carbonate buildup.

Figure 3.2. The carbonate buildups. A) mound number 2 at the Jebel el Oftal, the largest in this locality, approx. 40 meters high. B) Guelb el Maharch solitary mound seen from W, approx. 40 meters high. C) Aferdou el Mrakib reef mound seen from NE, 100–120 meters high.

3.3.3. Aferdou el Mrakib

The Aferdou el Mrakib mound with its approx. 900 m diameter and 100–120 m altitude is the largest mound of the Anti-Atlas (Fig. 3.2C). The Aferdou el Mrakib fauna is enriched in macroscopic organismal remains compared to the other Maïder Basin carbonate buildups; a broad description of the faunal assemblage from this carbonate buildup was provided by Kaufmann (1998b).

The entire buildup is made up of stromatactis-bearing wackestones, floatstones, and rudstones. Bioclasts are mainly crinoids, corals and subordinate brachiopods. The concordance between the bottom of the stromatactis structures and the strata dip seem to suggest a synsedimentary origin for these cavities. Neptunian dikes filled by dark to violet micrite and a variety of cements cut across the Aferdou el Mrakib buildup. The topmost southeastern part of the buildup is pervasively dolomitized and fossils and structures, therefore, have been obliterated or at least were overprinted by dolomitization. Whereas at the Aferdou el Mrakib mound the fossil remains are more abundant than in other buildups of the Maïder Basin, the taxonomic composition seems to be the same in all the studied places. The predominance of stromatoporoids and rugose corals as well as the absence of calcareous green algae suggests a moderately shallow environment below the euphotic zone (Kaufmann, 1995; 1996).

3.4. MATERIALS AND METHODS

Samples of limestones were collected in the Maïder basin in February 2011. All studied brachiopods were collected in February and March 2011 from the Aferdou el Mrakib reef mound along the Maïder Basin (Fig. 3.1). Further informations on the localities are provided by Wendt (1993) and Kaufmann (1995, 1996, 1997, 1998a, b). The newbrachiopods specimens described here are deposited at the Museo Geologico Giovanni Capellini of the University of Bologna (Bologna, Italy) with the serial numbers MGGC 21835–21844. Specimens are preserved as shell material and coated with magnesium oxide prior to photographing. In the present paper the brachiopod taxonomy systematics follows the revised *Treatise on Invertebrate Paleontology* (Blodgett *et al*. 2002).

Petrographic and palaeontological investigations of the samples collected during the field survey were performed on 20 thin sections. XRD and XRF analyses on the bulk limestone were performed at the SPECTRAU facilities (University of Johannesburg). Further description of the geochemical composition of the sample collected in the Maïder basin will be reported in chapter 4.

3.5. RESULTS

In the next paragraphs will be reported the results of the field survey with particular emphasis for the Aferdou el Mrakib mound palaeontological association. This mound was chosen for its dissimilarity with the other mounds of the Maïder region and for its abundant reef fauna. The

mineralogical and geochemical consideration about the studied samples will be reported in chapter 4.

3.5.1. Faunal association

The Aferdou el Mrakib rocks are dominated by *in situ* and detrital crinoids, tentaculitids (tentaculites, styliolinids and rare nowakiids), tabulate corals such as auloporids (*Bainbridgia*, *Cladochonus, Remesia, Aulocystis*), striatoporoids (*Pachystriatopora*), thamnoporids (*Thamnopora*), favositids (*Platyaxum*), heliolitids (*Heliolites*, large mamelons up to almost one meter), rugose corals, both solitary (*Heliophyllum, Cystiphylloides, Acanthophyllum, Macgeea*) and colonial (*Hexagonaria*, *Phillipsastrea*). The Aferdou el Mrakib mound also yields one of the most abundant brachiopod guilds of the Maïder Basin which consists of pentamerids (*Ivdelinia*, *Devonogypa*), spiriferids (*Atrypa*, *Desquamatia*, *Planatrypa*, *Carinatina*), orthids (*Schizophoria*), athyrids, and leptaenid strophomenids.

Despite of the abundance of *in situ* frame builders (stromatoporoids, tabulate and rugose corals), framestones and boundstones (as described by Wright 1992) are lacking in this buildup. Several stromatoporoids (*Actinostroma*) only appear to locally bind other bioclasts. According to Fagerstrom's (1991) theory of reef guilds, the Aferdou el Mrakib fauna is compatible with a constructor guild and a baffler guild.

3.5.2. Systematic palaeontology of Ivdeliania

Andronov (1961) established the genus *Ivdelinia* with the type species *I. ivdelensis* (Khodalevich, 1951) from the Ural Mountains and included 4 European and 32 Russian species, most of which he established in this monograph. Biernat (1966), however, considered *Ivdelinia* only as a subgenus of *Gypidula* Hall, 1867 and argued that splitting of ribs is not a generic-level character because it is only recognizable in adult specimens. Jux (1969) followed Biernat (1966) in his study of the German Devonian gypidulids and Godefroid (1972) regarded *Ivdelinia* as a genus, redescribed the type species, and figured detailed serial sections. Malygina & Sapelnikov (1973) and Sapelnikov (1985) described further taxa from Lower Devonian and Eifelian strata of the Ural Mountains and Central Asia. Brice (1982) subdivided the genus into two subgenera with material from Arctic Canada based on the presence and absence of a ventral median septum. Blodgett & Boucot (1999) reported the first species from Alaska and proposed its relationship to *Ivdelinia* species from the Urals. Even though a lot of taxonomic work has been done so far on this genus, the systematic description of North African material, which was first mentioned in literature almost two decades ago is still lacking until now. Systematic information about the described taxon are summarized below.

Order Pentamerida Schuchert & Cooper, 1931

Suborder Pentameridina Schuchert & Cooper, 1931

Superfamily Gypiduloidea Schuchert & LeVene, 1929

Family Gypidulidae Schuchert & LeVene, 1929

Subfamily Ivdeliniinae Sapelnikov, 1985

Genus *Ivdelinia* Andronov, 1961

Subgenus *Ivdelinia* (*Ivdelinia*) Andronov, 1961

Type species. – *Gypidula ivdelensis* Khodalevich, 1951, p. 22.

Diagnosis. – *Ivdelinia* with strongly raised costae or plicae and with median septum. [After Blodgett *et al.* (2002), p. 1014.]

Stratigraphic and geographic occurrence. – Lochkovian to Givetian (lower Lower to upper Middle Devonian); Ural Mountains, Central Asia, Siberia, Uzbekistan, Alaska (USA), Arctic Canada, Europe (Germany, Belgium, Czech Republic), North Africa.

***Ivdelinia pulchra* sp. nov. (**Fig. 3.3)

1998b *Ivdelinia* sp. Kaufmann, pl. 13, fig. 11.

Derivation of name – From the Latin word *pulcher, pulchra, pulchrum* = beautiful.

Holotype – Articulated, but broken, specimen showing the spondylium stored in the Museo Geologico Giovanni Capellini, Bologna, Italy, under the inventory number MGGC 21842a.

Type horizon and locality – Lens of gray to dark gray crinoidal wackestone to floatstone with abundant organic matter. Lower Givetian, northeastern flank of Aferdou el Mrakib reef mound, Maïder Basin, Anti-Atlas, Morocco.

Material – 2 articulated specimens, 8 external ventral valves, 1 fragment of internal ventral valve (MGGC 21835–21844).

Stratigraphic and geographic distribution – Lower Givetian (probably *hemiansatus* conodont zone); Maïder Basin, Morocco.

Diagnosis – Large *Ivdelinia* with 3 to 5 plications on fold which show furrows in the anterior third of valve. Fold bordering plications almost parallel and higher than fold. Sulcus tongue clearly developed with straight anterior margin.

Description – Shells medium to large-size, strongly ventribiconvex to planoventriconvex. Hinge line strophic. Almost entire shell covered by plications which are diminishing on flanks toward the lateral ends. Plications split by furrows in the anterior third of valve. Sulcus moderately broad, sulcus bordering plications coarser than plications of fold and sulcus and usually higher elevated than fold. Fold flat to U-shaped in cross-section. Sulcus tongue clearly developed, box-like

in anterior view, and with straight anterior margin. Dorsal valve always wider than long. Ventral median septum clearly developed, high, and long, reaching to at least half of shell length. Spondylium gypiduloid (see Blodgett *et al*. 2002, fig. 621.12). Microornamentation not preserved.

Discussion. – A vast number of taxa of *Ivdelinia* are described, especially from the Ural Mountains (Russia), some of which can probably be rejected as already stated by Biernat (1966). It is beyond the scope of this work, to revise all species of *Ivdelinia*, especially because we could not study the type or topotype material of these taxa. Therefore, we discuss the new species only from literature data and external morphology of illustrated specimens. If no other indication is provided, the compared taxa are from Lower Devonian–Eifelian strata of the Ural Mountains. *Ivdelinia pulchra* sp. nov. differs from *I. ivdelensis* (Khodalevich, 1951) in wider forms, and fewer and broader ribs on flanks. *Ivdelinia acutolobata* (Sandberger and Sandberger, 1850–1856) including its cf.-forms from the Ural Mountains, the Holy Cross Mountains (Poland), and Germany has smooth flanks or flanks covered with one or two weak plications and only one plication in the sulcus and only 2 plications on the fold, which also represent its bordering plications. *Ivdelinia* sp. cf. *I. multiplicata* (Roemer, 1854) figured by Biernat (1966, pl. 2, figs. 2–4) has many more and finer plications than *I. pulchra*, while the specimens of *I. multiplicata* figured by Andronov (1961, pl. 3, figs. 11–17) show a smaller sulcus tongue and only very short furrows in the anterior part of the plications. *Ivdelinia pseudoivdelensis* (Khodalevich, 1951) is probably a juvenile form of another *Ivdelinia* species, but the specimen figured in Andronov (1961, pl. 4, figs. 24–27) shows very short furrows in the plications and coarser sulcus bordering plications than *I. pulchra*. *Ivdelinia geniculatis* Andronov, 1961 is wider, smaller, and has more plications on the fold than our new species. *Ivdelinia menneri* Andronov, 1961 has many more and finer plications, *I. archangalskii* Andronov, 1961 also has finer plications and a more transverse outline than *I. pulchra*. *Ivdelinia krestovnikovi* Andronov, 1961 has fewer and coarser ribs than *I. pulchra* and broader fold and sulcus bordering plications. *Ivdelinia milradowitchi* Andronov, 1961 has a posteriorly smooth shell, its fold is almost inconspicuous, but shows a coarse median furrow, whereas the complete external surface in *I. pulchra* is covered by plications with furrows of equal size. *Ivdelinia uralensis* Andronov, 1961 has in general plications of the same size as *I. pulchra*, however, the median costa of the sulcus is remarkably coarse, but specimens are smaller than in the new species. Flanks in *I. egorovi* Andronov, 1961 are smooth and its fold is not U-shaped in cross-section. Furthermore, specimens are smaller than in *I. pulchra. Ivdelinia savtschencoi* Andronov, 1961 differs from the new species in having smaller and more transverse specimens with fewer plications. The representatives of *I. petropavlowskiensis* Andronov, 1961 show coarser plications on the fold and larger furrows on the plications than in *I. pulchra*. *Ivdelinia antiqua* Andronov, 1961 has smaller

forms with a less distinct sulcus tongue and coarser plications than the new species. *Ivdelinia motovilichaensis* Andronov, 1961 has a higher elevated fold and higher plications than *I. pulchra*. *Ivdelinia intima* Andronov, 1961 and *I. pulchra* show plications of the same size. Nevertheless, *I. intima* has a subcircular, rather than transverse outline and larger furrows on its plications than the new species. *Ivdelinia planosella* Andronov, 1961 is questionably regarded as a species of *Ivdelinia* because the furrows on the plications are not visible on the figured specimen (Andronov, 1961, pl. 7, figs. 16–18). This taxon has finer plications than *I. pulchra*. *Ivdelinia apera* Andronov, 1961 has coarser plications than the new species and an inconspicuous fold. The dorsal valves of *I. planosella* and *I. aspera* are not illustrated. The plications of *I. crassicosta* Andronov, 1961 are more distinct and coarser than in *I. pulchra*. *Ivdelinia rossica* Andronov, 1961 differs from *I. pulchra* in having finer costae and a more transverse and smaller specimens. In contrast to *I. pulchra*, *I. moldawanzewi* Andronov, 1961 is smaller with a thinner fold and fewer plications on the flanks. *Ivdelinia moldawanzewi* form alpha Khodalevich & Breivel, 1959, differs from the new species also in smaller intercalated plications on the fold and in the sulcus. The plications in *I. soswaensis* Andronov, 1961 are sharper and specimens of this taxon are smaller and show a broader sulcus than *I. pulchra*. Representatives of *I. trivialis* Andronov, 1961, *I. pulchellis* Andronov, 1961, and *I. kelleri* Andronov, 1961 are very similar to each other and all are forms smaller than *I. pulchra*, with fewer plications on the fold and mostly possess a very pronounced median plication in the sulcus. *Ivdelinia sarytchevi* Andronov, 1961 is smaller and has a broader sulcus and a broader fold than *I. pulchra*. *Ivdelinia ataevi* Andronov, 1961 is quite similar to *I. pulchra*, but differs from the new species in being smaller, having a deeper sulcus, and larger furrows on the plications. *Ivdelinia sphaerica* Andronov, 1961 is subcircular instead of transverse, smaller, and shows a less elevated fold, and larger furrows on the plications than *I. pulchra*. *Ivdelinia simplex* Andronov, 1961, *I. maslovi* Andronov, 1961, and *I. karjavini* Andronov, 1961 are all smaller and have coarser plications with no or shorter furrows than *I. pulchra*. *Ivdelinia procerula* (Barrande, 1879) from the Barrandian region (Czech Republic) and the Holy Cross Mountains is much smaller, has a circular outline, and fewer but overall coarser costae with clearly preserved furrows. The flanks are smooth or covered anteriorly by very weak and broad costae with fine, short, but well developed furrows. *Ivdelinia madmonica* Sapelnikov & Kartaschova, 2003 is more compact and with more ribs in the sulcus, furthermore, the furrows on the ribs are shorter than in *I. pulchra*. *Ivdelinia praeivdelensis* Sapelnikov *in* Sapelnikov and Mizens, 2005 shows smaller and more compact forms with a coarser median furrow on the fold than the new species. *Ivdelinia lahuseni* (Tschernyschew, 1885) shows smaller forms with higher and angular plications than in *I. pulchra*. *Ivdelinia dissecta* Malygina &

Sapelnikov, 1973, has a smooth fold with an angular and deep median furrow, a high and angular median plication in the fold and finer plications on its flanks than the bordering plications of the fold and sulcus, whereas in *I. pulchra*, the fold and sulcus show numerous plications, which are less deep and elevated. Furthermore, the plications on the fold, sulcus, and flanks are of equal size. Brice (1982) described *I. grennellensis* Brice, 1982 from the Arctic Canadian Islands. This species has a shorter ventral median septum, a more compact form, and 4 ribs on the fold. The furrows on the costae are almost invisible in her monograph, and the illustrated representatives of Li & Jones (2002) show more costae on flanks, a shorter sulcus tongue, and weaker furrows on the costae. *Ivdelinia pseudoivdelensis* (Khodaievich, 1951) has smaller and more transverse shells with costae of unequal size, whereas *I. pulchra* has less transverse shells, larger specimens, and costae of equal size. The subspecies *I. rectangularis quadruplicata* (Torley, 1934) from Germany shows most similarities to *I. pulchra*, but this subspecies is smaller and has a more strongly transverse ornament than the new species. Besides the morphological differences described herein, no taxon of *Ivdelinia* has been reported from Givetian strata so far.

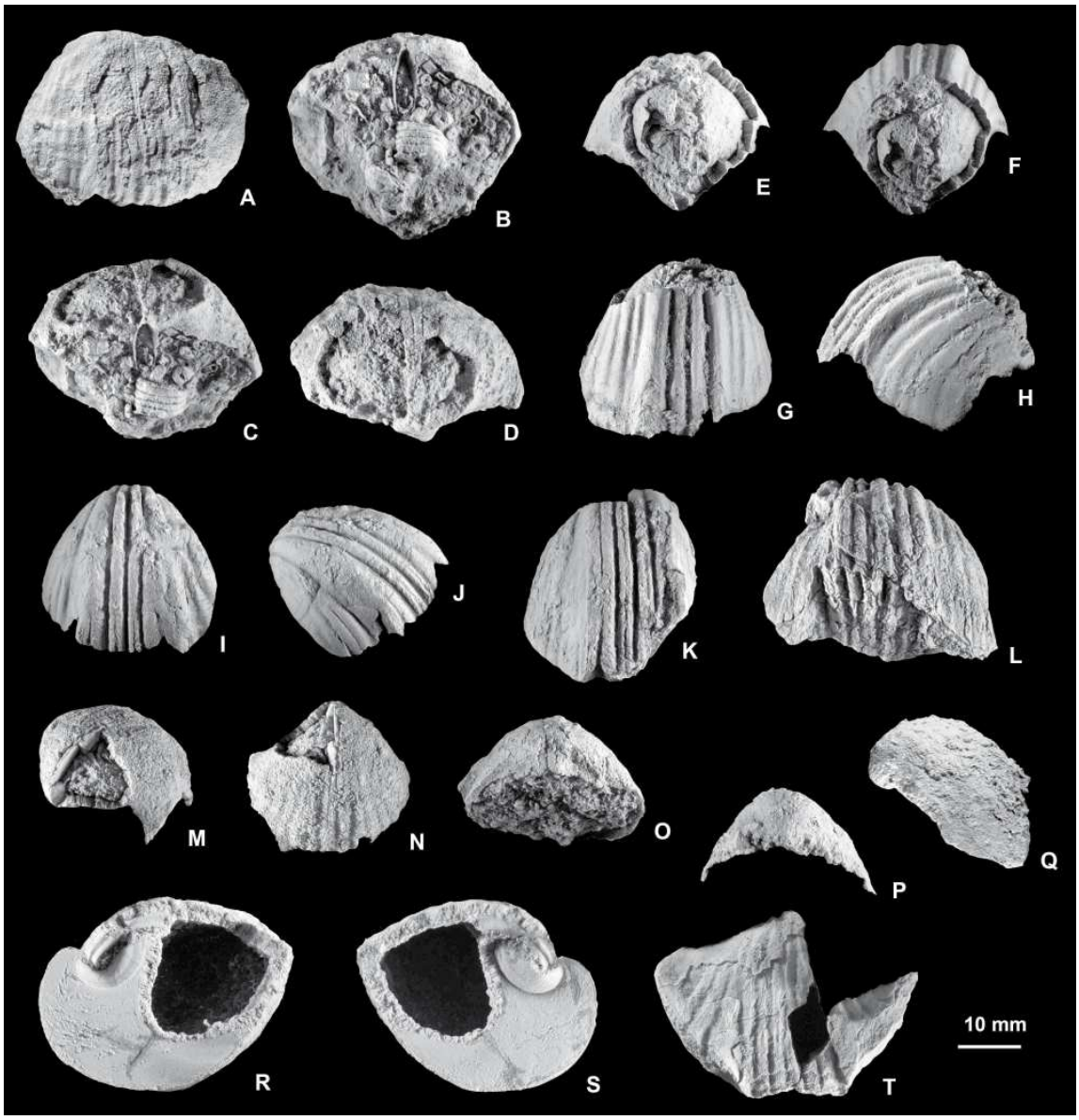

Figure 3. 3. Ivdelinia pulchra sp. nov. A-D) MGGC 21837. Ventral (A), dorsal (B), oblique posterodorsal (C), and oblique posterior (D) views of ventral valve; note the spondylium (B) and the ventral median septum (C). E-H) MGGC 21838. Posterior (E), oblique posterior (F), ventral (G), and oblique anterolateral (H) views of ventral external valve. I, J) MGGC21843. Ventral (I) and oblique anterolateral (F) views of ventral external valve. K) MGGC 21839. Ventral view of ventral external valve; note furrows on ribs. L) MGGC28144. Anterior view of articulated shell; note furrows on ribs and margin of sulcus tongue. M, N) MGGC21840. Oblique posterolateral (M) and ventral (N) views of ventral external valve; note ventral median septum. O) MGGC 21835. Oblique posterior view of ventral external valve. P, Q) MGGC 21836. Posterior (P) and lateral (Q) views of ventral external valve. R, T) MGGC 21842a, b. Holotype. Lateral (R, S) and dorsal views of articulated specimen; note spondylium, ventral median septum, and outline of dorsal valve. A–Q from Aferdou el Mrakib, north-eastern flank, southern Maïder Basin, Anti-Atlas, Morocco, leg. F. Franchi, February 2011. R–T from Aferdou El Mrakib, northwestern flank, southern Maïder, Anti-Atlas, Morocco, leg. C. Klug, March 2011. All specimens are Early Givetian age and original size (1.0x).

3.6. PALAEOBIOGEOGRAPHICAL AND PALAEOECOLOGICAL IMPLICATIONS

The origin of *Ivdelinia* lies without doubt in the Ural Mountains, where their highest diversity has been described from Eifelian strata. Outside Central Asia and the Ural Mountains, the first *Ivdelinia* appeared during the Emsian, and this agrees with a step-by-step loss of the Early Devonian endemism with a faunal migration pathways from Asia to Central Europe and North Africa (*e.g.*, Schemm-Gregory and Jansen, 2008; Schemm-Gregory, 2009a, b). Within the phylogenetic relationships of taxa of *Ivdelinia* shown by morphological similarities of the *Ivdelinia* faunas, a geographical relationship between Europe and North Africa can be confirmed. Additionally, as already proposed by Blodgett & Boucot (1999) and Blodgett *et al*. (2002), a closer relationship of SW Alaska to the Urals than to the Canadian Arctic Islands appears plausible. Even though a single species of *Ivdelinia* occurs in the Canadian Arctic Islands, suggesting a faunal migration, the subgenus *Ivdelinella* Brice, 1982 seems to be endemic for this region. The species *Ivdelinia* (*Ivdelinella*) *salairica* Gratsianova, 1998 would be the first taxon within this subgenus from Emsian strata; due to the lack of plications or only faint plications on the dorsal valve and the lack of the median septum we attribute this taxon to *Carinagypa* Johnson and Ludvigsen (1972) (personal communication R.B. Blodgett, 2011).

Gypidulid brachiopods are restricted to distinct environmental palaeohabitats. Jux (1969) reported that gypidulids are abundant in the turbiditic and fine grained sandstone and marly limestone facies, gypidulid coquinas were also found in near shore plattenkalk facies. With a faunal assemblage made up of tabulate and rugose corals, atrypids, and rhynchonellids, the studied mud mounds of the Maïder Basin seem to represent a suitable palaeoenvironment for *Ivdelinia*. During ontogeny, ivdelinids probably reduced their pedicle and were dependent on a fine-grained substrate in which they were partly embedded umbonally in a stable position. Furthermore, living in clusters also guarantees shelter from being transported by currents.

On Aferdou el Mrakib, mass-occurrences are remarkable (Fig. 3.4), where *Ivdelinia* co-occur with large *Devonogypa*, which apparently shared the same palaeoecological requirements. The patchy distribution across the bottom strata of Aferdou el Mrakib indicates a more or less allochthonous state of these occurrences. Apparently, they formed little forest-like or colony-like aggregations during the early stage of the reef growth. These brachiopod mass-occurrences, as well as the crinoid remains, acted as a substrate for the colonization by the reef builder communities. The abundance of bioclastic remains, especially crinoids, within the embedding dark rock, was already described elsewhere in the shallow platform facies in Tafilalt Basin and Maïder Basin, suggesting that the

colonies bloomed in a quite turbulent environment (compatible with Gypidulid ecology) characterized by currents and not properly in the reef buildups. Conversely in the other Anti-Atlas analogue basins, where no reef buildups were described, *I. pulchra* does not occur, which shows that this taxon is strongly related with reef development. Furthermore, we must consider that during Givetian age the Maïder Basin was situated at middle-high latitude (Tait et al., 1995; Stampfli & Borel 2002) and water temperature must have been lower than in present day tropical platforms. Anyway the high latitude is comparable with the Urals latitudes throughout the Devonian, where *Ivdelinia* first occurred.

Figure 3. 4. Mass-occurrence of *Ivdelinia pulchra* sp. nov. and *Devonogypa* sp. on Aferdou el Mrakib, northeastern flank.

3.7. CONCLUSION

From a petrographic, sedimentological and palaeontological point of view Mider mounds are analogues of the Kess Kess, anyway this work outlined several differences between the two mounds families.

Despite we described almost the same faunal assemblage there are different abundance of framebuilders in the two mounds family. Particularly the Kess Kess lack of framebuilders and reef faunal associations which instead were described from the Aferdou el Mrakib carbonate mound. Contrariwise the faunal association of the other mounds in Maider basin is absolutely confrontable with the Kess Kess fauna: abundance of auloporids corals and trilobites fragments and lack of framebuilders and buffler organisms.

The new early Givetian ivdelinid species, *Ivdelinia pulchra*, represents the youngest *Ivdelinia* species described to date. It exhibits a characteristic morphology of fold and sulcus, as well as number of ribs that enable an easy identification and, therefore, it might be a useful stratigraphic tool for the lower Givetian deposits of the Maïder Basin. *Ivdelinia pulchra* is suggested to have migrated near the Eifelian/Givetian boundary interval from today's Central Asia to Europe and North Africa. Mono specific assemblages of *Devonogypa* sp. and *Ivdelinia pulchra* are related to particular adaptation to an environment characterized by high nutrient supply, turbid water and low temperatures in a high latitude intracratonic shallow sea during the early stage of reef development.

REFERENCES

Andronov, S.M., 1961. Nekotorye predstaviteli semeistva Pentameridae iz devonskikh otlozhenii okrestnostei g. Severoural'ska. *Akademiya Nauk SSSR, Trudy Geologicheskogo Instituta 55*, 1–136. [in Russian]

Barrande, J., 1879. *Recherches paléontologiques. 5: Classe des Mollusque, Ordre de Brachiopodes. Systême silurien du centre de la Bohême 1*, 1–226.

Belka, Z. 1998. Early Devonian Kess-Kess carbonate mud mounds of the eastern Anti-Atlas (Morocco), and their relation to submarine hydrothermal venting. *Journal of Sedimentary Research 68*, 368–377.

Belka, Z., Kaufmann, B. & Bultynck, P., 1997. A conodontbased quantitative biostratigraphy for the Eifelian of the eastern Anti-Atlas, Morocco. *Geological Society of America Bulletin 109*, 643–651.

Biernat, G., 1966. Middle Devonian brachiopods of the Bodzentyn Syncline (Holy Cross Mountains, Poland). *Paleontologia Polonica 17*, 1–162.

Blodgett, R.B., Boucot, A.J., 1999. Late Early Devonian (Late Emsian) eospiriferinid brachiopods from the Shellabarger Pass, south-central Alaska, and their biostratigraphic importance; further evidence for a Siberian origin of the Farewell and allied Alaskan accreted terranes. *Senckenbergiana lethaea 79*, 209–221.

Blodgett, R.B., Rohr, D.M., Boucot, A.J., 2002. Late links among some Alaskan accreted terranes and Siberia based on megafossils. *Geological Society of America Special Paper 360*, 273–290.

Blodgett, R.B., Boucot, A.J., Rong, J.Y., 2002. Gypiduloidea, 1005–1020. *In* KAESLER, R.L. (ed.) *Treatise on Invertebrate Paleontology, Part H, Brachiopoda, revised, vol. 4.* The Geological Society of America&University of Kansas, Lawrence, Kansas.

Brice, D. 1982. Brachiopodes du Dévonien inférieur et moyen des formations de Blue Fiord et Bird Fiord des îles Arctiques Canadiennes. *Geological Survey of Canada Bulletin 326*, 1–75.

Chafetz, H.S., Buczynski, C. 1992. Bacterially induced lithification of microbial mats. *Palaios 7*, 277–293. DOI 10.2307/3514973

Dumestre, A., Illing, L.V., 1967. Middle Devonian reefs in Spanish Sahara, 333–350. *In* OSWALD, D.H. (ed.) *International Symposium on the Devonian System: Alberta Society of Petroleum Geologists 2*.

Fagerstrom, J.A., 1991. Reef-building guilds and a checklist for determining guild membership. *Coral Reefs 10*, 47–52. DOI 10.1007/BF00301908

Godefroid, J. 1972. *Pseudosieberella* (Pentameridae), noveau genre Couvinien, et genres apparentes. *Institut Royale des Sciences Naturelles de Belgique, Bulletin 48(5)*, 1–41.

Gratsianova, R.T., 1998. New species of the genus *Ivdelinia* (Brachiopoda) from the Lower Devonian of the Salair and its significance for paleobiogeography. *News of Paleontology and Stratigraphy 1 (Supplement to Russian Geology and Geophysics 39)*, 47–55. [in Russian]

Hall, J., 1867. Descriptions and figures of the fossil Brachiopoda of the Upper Helderberg, Hamilton, Portage and Chemung Groups. *Palaeontology of New York 4(1)*, 1–428.

Hollard, H., 1974. Recherches sur la stratigraphie des formations du Dévonien moyen, de l'Emsien supérieur au Frasnien, dans le Sud du Tafilalt et dans le Maïder (Anti-Atlas oriental). *Notes du Service Géologique du Maroc 264*, 7–68.

Johnson, J.G., Ludvigsen, R., 1972. *Carinagypa*, a new genus of pentameracean brachiopod from the Devonian of western North America. *Journal of Paleontology 46*, 125–129.

Jux, U., 1969. Pentameriden aus dem Bergischen Devon. *Palaeontographica A 132*, 55–93.

Kaufmann, B. 1995. Middle Devonian mud mounds of the Ma'der Basin in the eastern Anti-Atlas, Morocco, 49–57. *In* FLAJS, G., VIGENER, M., KEUPP, H., MEISCHNER, D., NEUWEILER, F., PAUL, J., REITNER, J., WARNKE, K., WELLER, H., DINGLE, P., HENSEN, C., SCHÄNFER, P., GAUTRET, P., LEINFELDER, R.R., HÜNSSNER, H. & KAUFMANN, B. *Mud Mounds: A Polygenetic Spectrum of Fine-grained Carbonate Buildups. Facies 32*.

Kaufmann, B., 1996. *Facies, stratigraphy and diagenesis of Middle Devonian reef and mud-mounds in the Maïder (eastern Anti-Atlas, Morocco)*. PhD thesis, University of Tübingen.

Kaufmann, B., 1997. Diagenesis of Middle Devonian carbonate mud buildups of the Maïder Basin (eastern Anti-Atlas). *Journal of Sedimentary Research A67*, 945–956.

Kaufmann, B., 1998a. Middle Devonian reef and mud mounds on a carbonate ramp: Maïder Basin (eastern Anti-Atlas, Morocco), 417–435. *In* WRIGHT, V.P. & BURCHETTE, T.P. (eds) *Carbonate Ramps. Geological Society of London, Special Pubblication 149*.

Kaufmann, B., 1998b. Facies, stratigraphy and diagenesis of Middle Devonian reef- and mud-mounds in the Maïder (eastern Anti-Atlas, Morocco). *Acta Geologica Polonica 48*, 43–106.

Khodalevich, A.N., 1951. Nizhnedevonskie i eifel'skie brakhiopody Sverdlovskoi oblasti. *Sverdlovskii Gornyi Institut, Trudy 18*, 1–169. [in Russian]

Khodalevich, A.N., Breivel, M.G., 1959. Nadsemeistvo Pentameracea (Superfamily Pentameracea), 14–41. *In* KHODALEVICH, A.N., BREIVEL, I.A., BREIVEL, M.G., VAGANOVA, T.I., TORBAKOVA, A.F. & YANET, F.E. (eds) *Brakhiopody i korally iz Eifelskikh boksitonosnykh otlozhenii vostochnogo sklona srednego i severnogo Urals.* Ural'skoe geologicheskoe upravlenie, Gosgeoltekhizdat, Moskva. [in Russian]

Klug, C., Schulz, H., De Baets, K., 2009. Red trilobites with green eyes from the Early Devonian of the Tafilalt (Morocco). *Acta Palaeontologica Polonica 54*, 117–123. DOI 10.4202/app.2009.0112

Li, R., Jones, B., 2002. Communities and paleoecology of Eifelian (mid-Devonian) brachiopods from the Bird Fiord Formation of Arctic Canada. *Canadian Journal of Earth Science 39*, 1485–1503. DOI 10.1139/e02-051

Malygina, A.A., Sapelnikov, V.P., 1973. Siluriskie, rannedevonskie i eifielskie Pentamerida zuzhnogo Tian'-shania. *Akademia Nauk SSSR, Uralskii Nauchnyi Tsentr, Trudy Instituta Geologii i Geokhimii 104*, 1–212. [in Russian]

Michard, A., 1976. Elements de GeÅLologie Marocaine. *Notes et Mémoires du Service Géologique du Maroc 252*, 408.

Monty, C.L.V., 1995. The rise and nature of carbonate mudmounds: an introductory actualistic approach, 11–48. *In* MONTY, C.L.V., BOSENCE, D.W.J., BRIDGES, P.H. & PRATT, B.R. (eds) *Carbonate Mud-Mounds: their origin and evolution. International Association of Sedimentologists, Special Publication 23.*

Roemer, C.F. *in* BRONN, H.G. 1850–1856. *Lethaea geognostica, oder Abbildungen und Beschreibungen für die Gebirgs-Formationen bezeichnendsten Versteinerungen*. 352 pp. E. Schweizerbart'sche Verlagshandlung und Druckerei, Stuttgart.

Sandberger, F. *in* SANDBERGER, G. & SANDBERGER, F. 1850–1856. *Die Versteinerungen des Rheinischen Schichtensystems bei Nassau.* 564 pp. Kreidel und Niedner, Wiesbaden.

Sapelnikov, V.P. 1985. *Sistema i stratigraficheskoe znachenie brakhiopod podotriada Pentamerida*. 206 pp. Nauka, Moscow. [in Russian]

Sapelnikov, V.P., Kartashova, L.E., 2003. *Ezhegodnik – 2002. Novye vidy rannedevonskikh brachiopod zeravshanskogo khrebta (Yuzhnyi Tyan'-Shan')*, 38–44. Institut geologii i geokhimii, Ural'skoe otdelenie, Rossiyskaya Akademiya Nauk, Moskva. [in Russian]

Sapelnikov, V.P., Mizens, L.I., 2005. Brachiopods from the type locality of the Pragian-Emsian boundary (Devonian). *Senckenbergiana lethaea 85*, 13–29.

Schemm-Gregory, M. 2009a. *Frequentispirifer*, a new spiriferid genus and its phylogenetic position within the Delthyridoidea (Brachiopoda, Lower Devonian). *Neues Jahrbuch für Geologie und Paläontologie, Abhandlungen 251*, 53–70. DOI 10.1127/0077-7749/2009/0251-0053

Schemm-Gregory, M. 2009b. On the genus *Quiringites* Struve, 1992 (Brachiopoda, Middle Devonian). *Bulletin of the Peabody Museum of Natural History 50*, 3–20. DOI 10.3374/014.050.0101

Schemm-Gregory, M., Jansen, U., 2008. First report of the stringocephalid genus *Paracrothyris* (Brachiopoda, Middle Devonian) from North Africa. *Bulletin of Geosciences 83*, 169–173. DOI 10.3140/bull.geosci.2008.02.169

Schuchert, C., Le Vene, C.M., 1929. Brachiopoda (Generum et Genotyporum Index et Bibliographia), 1–140. *In* POMPECKJ, J.F. (ed.) *Fossilium Catalogus I: Animalia, pars 42: Brachiopoda*. W. Junk, Berlin.

Schuchert, C., Cooper, G.A., 1931. Synopsis of the brachiopod genera of the suborders Orthoidea and Pentameroidea, with notes on the Telotremata. *American Journal of Science (series 5) 22*, 241–255.

Stampfli, G.M., Borel, G.D., 2002. A plate tectonic model for the Paleozoic and Mesozoic constrained by dynamic plate boundaries and restored synthetic oceanic isochrons. *Earth and Planetary Science Letters 196*, 17–33. DOI 10.1016/S0012-821X(01)00588-X

Tait, J.A., Bachtadse, V., Soffel, H., Franke, W., 1995. Paleozoic paleogeography of the circum Atlantic continente. Terra Nostra 8, 1-133.

Torley, K., 1934. Die Brachiopoden des oberen Massenkalkes von Bilveringen bei Iserlohn. *Abhandlungen der senckenbergischen naturforschenden Gesellschaft 43 (3)*, 67–148.

Tschernyschew, T.N., 1885. Die Fauna des unteren Devon am West-Abhange des Urals. *Trudy Geologicheskogo Komiteta 3(1)*, 1–107.

Wendt, J. 1985. Disintegration of the continental margin of northwestern Gondwana: Late Devonian of the eastern Anti-Atlas (Morocco). *Geology 13*, 815–818. DOI 10.1130/0091-7613(1985)13<815:DOTCMO>2.0.CO;2

Wendt, J. 1988. Facies pattern and paleogeography of the Middle and Late Devonian in the eastern Anti-Atlas (Morocco), 467–480. *In* MCMILLAN, N.J., EMBRY, A.F. & GLASS, D.J. (eds) *Canadian Society of Petroleum Geologists, Devonian of the World 1*.

Wendt, J., 1991. Depositional and structural evolution of the Middle and Late Devonian on the northwestern margin of the Sahara Craton (Morocco, Algeria, Libya), 2195–2210. *In*

SALEM, M.J., SBETA, A.M. & BAKBAK, M.R. (eds) *The Geology of Libya 6*. Elsevier, Amsterdam.

Wendt, J., 1993. Steep-sided carbonate mud mounds in the Middle Devonian of the eastern Anti-Atlas, Morocco. *Geological Magazine 130*, 69–83. DOI 10.1017/S0016756800023736

Wendt, J., Belka, Z., Kaufmann, B., Kostrewa, R., Hayer, J., 1997. The world's most spectacular carbonate mud mounds (Middle Devonian, Algerian Sahara). *Journal of Sedimentare Research 67*, 424–436.

Wendt, J., Belka, Z., Moussine-Pouchkine, A., 1993. New architectures of deep-water carbonate buildups: Evolution of mud mounds into mud ridges (Middle Devonian, Algerian Sahara). *Geology 21*, 723–726.

Wright, V.P. 1992. A revised classification of limestones. *Sedimentary Geology 76(3–4)*, 177–185. DOI 10.1016/0037-0738(92)90082-3

4. GEOCHEMICAL CHARACTERIZATION OF THE TAFILALT AND MAÏDER CONICAL MOUNDS (MOROCCO)

4.1. INTRODUCTION

The previous chapters reported data from the field surveys at the Hamar Laghdad Ridge, coupled with the analytical data from Seheb el Rhassel Group and Merzane Group samples (Chapter 2), and Maïder basin (Chapter 3). In this chapter the complete database obtained from a broad set of analyses carried on samples from the mounds clusters of the Hamar Laghdad ridge and the Maïder basin is reported for comparison.

From a sedimentological and genetic point of view the carbonate conical mounds of Hamar Laghdad Ridge and Maïder basin have still unclear aspects despite it seems clear the interaction between both the investigated clusters of mounds and hydrothermal fluids. Geochemistry gives powerful tools to help to elucidate the origin and the paleo-environmental fingerprints preserved within the fossiliferous limestones of these mounds. Here data coming from a broad set of analyses (XRD, XRF, SEM-EDS, EMPA and Raman microscopy) carried on 21 samples from the Hamar Laghdad Ridge and 4 samples from Maïder mounds were reported. These analyses provided new insights about geochemical composition of the limestones especially referred to the presence of secondary minerals phases deposed due to hydrothermal fluid advection. Althought the Maider mounds are younger (Middle Devonian) than the Kess Kess mounds (Early Devonian), both mound clusters developed along northern Gondwana margin in epicontinental sea, probably within analog geochemical and environmental conditions. Then a comparison between these two mound clustes would give new insights about the main subject of this thesys, the Kess Kess genesis and development.

The purpose is to complete the Kess Kess geochemical framework given in chapter 2, and compare it with several strategic samples from analogs mounds in Maïder basin.

4.2. MATERIALS AND METHODS

The studied samples were collected from the Kess Kess mounds and from several conical mounds in the Maïder Basin (Figs. 2.1 and 3.1) during two field surveys in May 2010 and February 2011. A comprehensive description of this mound, including geometry, stratigraphy and geographical position, was given in chapters 2 and 3. Table 4.1 summarizes the lithology and micro-facies of each samples analyzed and all the analyses carried on the samples. For each

samples a minimum of two thin sections (4,4x 6,9 mm surface area, 30 μm foil thickness) were prepared. A thin section of each samples was carbon/gold coated in order to be analyzed with a scanning electron microscopy and a microprobe. Au-coating was preferred for the micro-morphologies observations, and C-coating was preferred for all the sets of analyses (except for Raman microscopy: uncoated thin sections). One cm-thick polished and planar slabs were sub-sampled in order to obtain 24 mm diameter disks for high resolution scanning electron microscopy (SEM), (EDS) analyses, and Electron MicroProbe Analyses (EMPA).

The X-ray diffraction (XRD) data obtained from the powdered (bulk) samples were collected using a Philips PW 1480 X-ray diffractometer in a 2θ configuration (CuKα radiation, λ=1.54 Å). The spectra were modified and interpreted using a tool for XRD analysis in the FullProf Suite (www.ill.eu/sites/fullprof/). Major and minor element concentrations were determined by X-ray fluorescence using a PANanalytical Magix PRO X-ray Fluorescent Spectrometer on pressed pellets of bulk samples.

Scanning electron microscope (SEM) observations were conducted using a Jeol 5600 SEM (working conditions: 15 and 25 KeV accelerating voltage, 15 and 20 mm working distance) equipped with an electron back-scattering CENTAURUS system and an energy dispersive X-ray spectrometer (EDS). SEM observations were performed on etched (aqueous solutions of 1% HCl for 60 seconds), un-etched polished and freshly broken sample surfaces. The SEM and X-ray energy dispersive spectrometer (EDS) observations, which included imaging and elements analyses, were conducted on C-coated samples, using accelerating voltages between 2.5 and 20 kV. SEM observations of micro-morphologies were performed on Au-coated, etched thin sections and freshly broken samples.

EMPA analyses were carried using a Cameca SX 100 electron microprobe equipped with a SUN workstation and Peak Sight software for instrument control and data evaluation. Beam conditions were 15 kV, 6 nA, and 20 μm for energy, current, and diameter, respectively. Mg was calibrated on MgO, Al on almandine, Si on diopside, Sr on $SrSO_4$, Ca on $CaCO_3$, Ba on $BaSO_4$, Mn on rhodonite, Fe on Fe_2O_3, and Zn on ZnS. Elements were measured on their Ka lines except for Sr and Ba which were measured on La line.

In *situ*, non-destructive analyses o the different mineral were performed by using a WITec alpha300. The spectral range of the spectrometer is 100 - 4400 Δ cm^{-1}. Raman spectra were collected using a 100x Nikon objective (N.a.: 0.9) and a frequency doubled Nd: YAG (532 nm) Ar-ion 20-mW monochromatic laser source. Beam centering and Raman spectra calibration were performed daily before spectral acquisition using a Si standard (111) with a characteristic Si Raman

peak at 520.4 cm^{-1}. The optimum power for in situ analyses of different minerals was determined experimentally. Raman analyses were recorded and treated using WITecProject2.06® software, and compared with reference spectra from Mazzetti and Thistlethwaite (2002), the RRUFF Data-Base (Laetsch and Downs, 2006; White, 2009; Demoulin et al., 2010).

All these sets of analyses were performed at the SPECTRAU facilities, Faculty of Science, University of Johannesburg, during a visiting period (Nov. 2011-Feb. 2012).

SAMPLE	XRD	OXYDES CONCENTRATION (%)												
		CaO	MgO	Al_2O_3	SiO_2	Fe_2O3	Na_2O	P_2O_5	SO_3	Cl	K_2O	TiO_2	MnO	Sr	TOT
KK1	CALCITE	72,400	0,843	1,580	2,180	0,502	<<	0,059	0,055	0,030	0,000	<<	0,059	0,018	77,8
KK 2	CALCITE	70,620	0,694	1,962	2,859	0,747	0,119	0,040	0,044	<<	0,310	0,100	0,082	0,029	77,6
KK 3*	CALCITE	68,600	1,030	1,060	3,090	0,475	0,181	0,042	0,045	0,034	0,137	<<	0,117	0,065	74,8
KK 4*	CAL+QZ	72,300	0,669	0,764	1,800	0,510	<<	0,024	0,042	0,033	0,118		<<	0,055	76,3
KK 5	CAL+QZ	72,950	0,717	0,362	1,359	0,304	<<	0,050	0,041	0,037	0,068		0,057	0,023	76,0
KK 6	CALCITE	74,960	0,858	0,189	0,341	0,145	<<	0,088	0,024	0,024	0,038		0,057	0,028	76,8
KK 7	-	73,330	1,487	0,163	0,280	0,303	<<	0,060	0,073	<<	0,031		<<	0,051	75,8
KK 8	-	73,310	0,572	1,310	1,778	0,422	<<	0,020	0,089	0,022	0,247	<<	0,081	0,052	78,0
KK 9	CAL+QZ	64,760	0,458	1,823	7,574	0,831	0,041	0,032	0,072		0,282	0,126		0,013	76,0
KK 10	CALCITE	69,550	0,788	2,881	3,957	0,648	0,062	0,044	0,079		0,587	0,145	0,079	0,025	78,8
KK 11	QUARTZ	0,739	0,115	0,128	95,000	0,158		<<	0,073		0,020		0,000		96,3
KK 12	GOETHITE	0,313	0,000	0,141	1,250	85,180		0,131	0,043				0,000		87,4
KK 13	CAL+DOL+QZ	51,200	2.580	3.870	9.820	13,100		0,208	0,221	0,054	0,032	0,133	0,227	0,035	81,5
KK 14	CALCITE	66,400	1,460	2,840	3,140	6,190		0,087	0,169		0,147	0,144	0,219	0,022	80,9
KK 15	-	58,300	12,700	0,710	1,790	0,762		0,080	0,044	0,066	0,083		0,339	0,009	74,9
KK 16	CAL+DOL+QZ	56,500	8,910	1,850	6,720	0,824	<<	0,028	0,316	0,000	0,219	0,079	0,000	0,043	75,9
KK 17*	CAL+DOL	49,400	<<	1,390	1,990	5,110	<<	0,041	0,089	0,050	0,164	<<	0,355	0,016	58,6
KK 18*	CAL+HEMAT	46,900	0,908	0,642	1,520	32,000		0,340	0,125	0,027			0,130	0,025	82,6
KK 19	-	67,500	0,558	1,590	5,960	0,649		0,042	0,148	0,000	0,221	0,098	0,000	0,022	76,8
KK 20#	CAL+QZ	71,100	0,731	1,210	4,060	0,550	<<	0,052	0,071	<<	0,258	<<	0,298		78,4
KK 21#	-	75,200	0,600	0,190	0,486	0,370		0,087	0,034	0,030	0,031		0,104	0,029	77,2
KK 22#	CAL+QZ	67,900	0,770	2,790	4,400	1,230	0,048	0,071	0,066	0,000	0,455	0,132	0,082	0,023	78,0
KK 23#	CALCITE	-	-	-	-	-	-	-	-	-	-	-	-	-	-
KK 24#	-	-	-	-	-	-	-	-	-	-	-	-	-	-	-
KK 25#	CALCITE	74,500	0,531	0,515	0,718	0,306	<<	0,029	0,045	0,027	0,084		0,212	0,058	77,0

Table 4. 1. XRD and XRF analyses results from the processed samples. * Samples from Maïder mounds. # Thin sections.

4.3. RESULTS

The different lithotypes were investigated at the microscopic to sub-microscopic scale by using different analytical tools in order to obtain a comprehensive bulk and *in situ* petro-mineralogico characterization (Tab. 4.1). Thus a full set of mineralogical, chemical and geochemical characteristics were acquired for the different carbonates cement phases of the samples from the mounds o the Hamar Laghdad Ridge and Maïder basin (Figs. 4.1-4.9). Data from the analyses carried on a sample from oolitic ironstones near the Hollard Mound (Bou Tchrafine Group) was also reported.

4.3.1. XRD and XRF

4.3.1.1. Hamar Laghdad samples

The XRD analyses carried on bulk (powdered) samples outlined that the Hamar Laghdad limestones are dominated by lo-Mg carbonate. Ca-oxide content, normalized with the total amount of oxides detected with XRF analyses on bulk limestones samples, ranges between 97,4% and 62,8%. During the first set of bulk analyses several samples revealed slight contents of quartz and dolomite. Increasing the detail of field survey and analytical techniques set we detected rocks composed of pure goethite or quartz (Fig. 4.1) associated to the chimney-like structure described in figure 2.6. Within these lithologies Ca-oxide content is less than 1%.

XFR analyses confirm the XRD data showing a dominant Ca-composition with small amounts of Mg, Al and Si (Tab. 4.1). XRF analyses confirmed high abundance of Fe- and Si-minerals bearing rock and variations in dolomite content toward the top of the succession (Tab. 4.1) near the Hamar Laghdad cliff where chimney-like structures were described (**cf**. 2.4.1.2). Although the general composition of trilobites floatstone/grainstone reflects the Low-Mg carbonate composition of the whole group a significant amount of silica within the trilobites floatstone/rudstone facies (*e.g.* KK3 and KK5 in table 4.1) was detected. Within the reddish clastic facies interbedded with the upper strata of the Seheb el Rhassel Group (see paragraph 2.2.2.), XRD and XRF analyses revealed an high amount of quartz (rounded pebbles and grains, Figs. 4.3D and 4.5B) in a carbonate matrix (Tab. 4.1).

The highest concentration of Al-oxides was detected in the micrite sampled near a vein (KK14), in the reddish clastic layers (KK13) and within a sample of fossiliferous wakestone coming from a mound (KK10). High abundance of Fe-oxides coupled with high percentage of K and Al-minerals minerals were detected in the samples of oolitic ironstone collected near the Hollard Mound. In these facies where Fe is abundant the XRF analyses outlined a slight enrichment of P.

Trace elements as S, Cl, K, Ti, Mn and Sr do not show any particular trends and/or facies dependent enrichments.

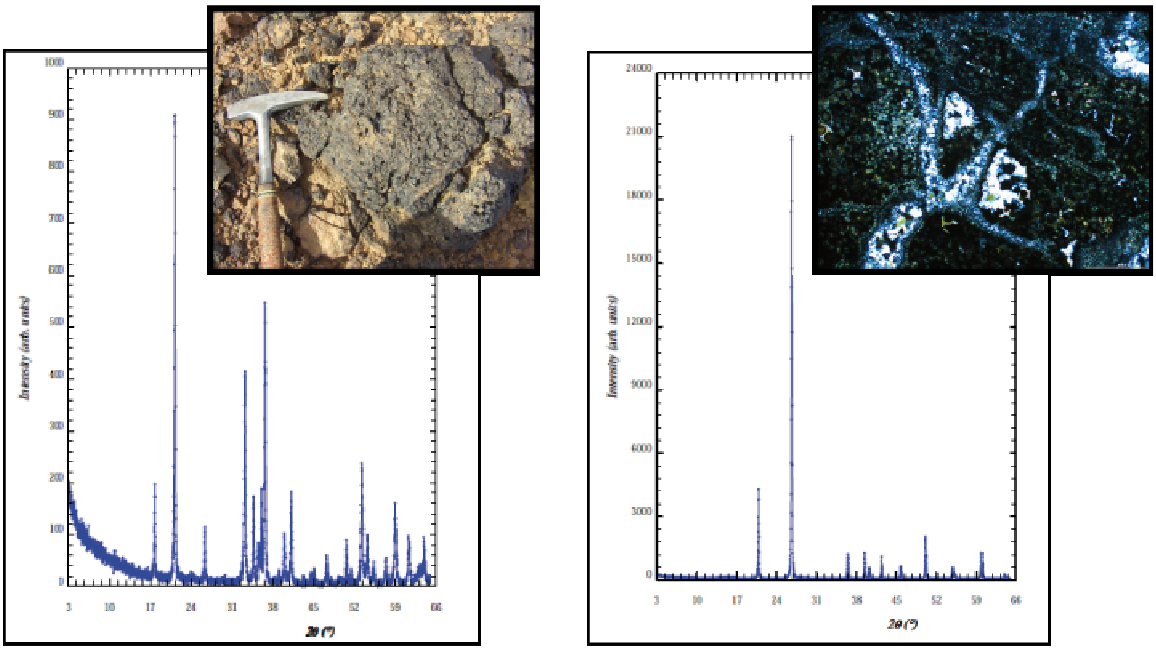

Figure 4. 1. A) XRD spectra of goethite from a chimney-like structure in the upper part of the Seheb el Rhassel Group. B) XRD spectra of quartz from the same rounded outcrop in A.

4.3.1.2. Maïder samples

The XRD analyses carried on bulk (powdered) samples showed that also the Maïder limestones are dominated by lo-Mg carbonate. Ca-oxide content, normalized to the total amount of oxides detected with XRF analyses on bulk limestones samples, ranges between 84% and 95%. Sample KK18 (Tab. 4.1) from a horizontal vein, shows lower content of Ca, near 57% and high percentage of Fe-oxides with XRD spectral fingerprint of hematite. Trilobites floatstone (KK3) analogs of the trilobites floatstone described in the Seheb el Rhassel Group was described from one of the mounds occurring in Jebel el Oftal. XRF analysis confirmed the Ca content and outlined the presence of Si mineral phases (approx. 3%) within this facies. Whereas XRF analyses carried on Maider wakestone (tentaculites) reported a bulk composition made of 95% Ca-oxides and only 5% of Si-oxides. In this sample the Si enrichment is coupled with a slight enrichmento f Al-oxides. A sample collected within a vein that cuts through the Guelb el Maharch mound (KK17; mound in fig. 3.2 B) showed a composition dominated by calcite and dolomite. XRD analyses confirmed the presence of both calcite and dolomite and XRF data reported small amount of iron (<5%), silica

(approx. 2%) and aluminium (approx. 1%). Optical analyses of this facies showed coarse grained saddle-dolomite characterized by large mm-sized crystals, curved crystals faces, crystals cleavages, undulose extinction (under crossed nicols) and ferroan composition (Fig. 4.2). Locally the saddle dolomite crystals are replaced by high-Fe calcite (Fig. 4.2).

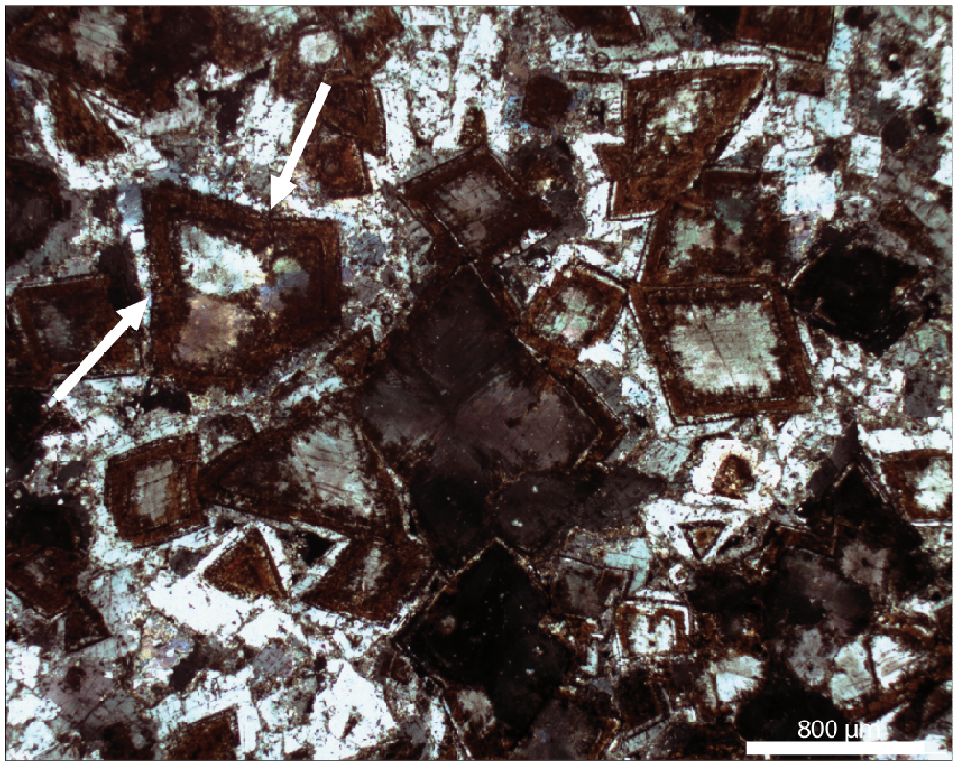

Figure 4. 2. Photomicrograph of sample KK17: euhedral mm-sized saddle-dolomite with typical undulose extinction (crossed nicols) and curved crystal faces (arrows). The crystals show red boundaries due to high iron content.

4.3.2. SEM-EDS

SEM microscopy analyses were carried on all the 25 samples both on etched thin sections and freshly broken samples. The images were coupled with EDS analyses that gave the spatial variation of elements composition in relation with different micro-morphologies.

Figures 4.3A and B show euhedral crystal of dolomite surrounded by calcite matrix from Hamar Laghdad limestones (Seheb el Rhassel Group). The dolomite crystals are zoned with sharp boundaries and partially dedolomitized core where high magnification SEM microscopy detected small framboids (average diameter 5 µm) and thin acicular iron mineral (Fig. 4.3A). EDS analyses results show an approximate Ca/Mg carbonates distribution of 1/3 and, near the euhedral dolomite crystals (Figs. 4.3A, B), show traces of Si.

From the imagines data set emerged that in the Hamar Laghdad samples meso-sparite and

micrite grains are often lined by bright materials (Figs. 4.3C - E). These bright materials stand out in the etched samples due to its higher resistance to the HCl corrosion. Investigated with EDS these lined carbonate revealed a composition made of Ca-carbonate with slight enrichment of Al and Si. In the etched samples of reddish pisolites limestone the change in composition of the cements and matrix, and the different amount of Ca-cement within the pisolite laminae were emphasized: the abundant rounded quartz clasts are condensed in lalaminae with lower relief due to a higher content of calcite that reacted with the acid (Fig. 4.3D).

Figure 4.3 E reports a microphotograph of the boundary between fibrous radiaxial calcite, with typical elongated crystals (bottom), and micrite with abundant bright material lining the crystals (top).

A sample of dark red rock from the chimney-like structure (Fig. 4.1A) was analyzed with SEM-EDS showing that the 100% of the mineral phase is made of pure euhedral goethite (KK12 in Tab. 4.1; Figs. 4.1 A, 4.3 F and 4.9). This sample of euhedral goethite is the same showed in figure 2.6B.

Several EDS analyses performed both on C-coated polished disks and thin sections, and some results from reddish infra-mound micrite (KK14) are reported in figure 4.4. The first set of spectra (Figs. 4.4C-D) is referred to a bright acicular fragment within carbonatic matrix which represents one of the few occurrences of phosphate material in the studied samples (Fig. 4.4C). The matrix is made of Ca-carbonate, with traces of Fe, Al and Si, whereas in the bottom part of the microphotograph Mn, P, and Fe are significantly enriched. Figures 4.4E and F report a portion of micrite and its EDS spectra, respectively. In this area the calcium Ca-carbonate was replaced by Si-minerals with cloudy pattern and low Al content, with XRD spectral fingerprint of quartz.

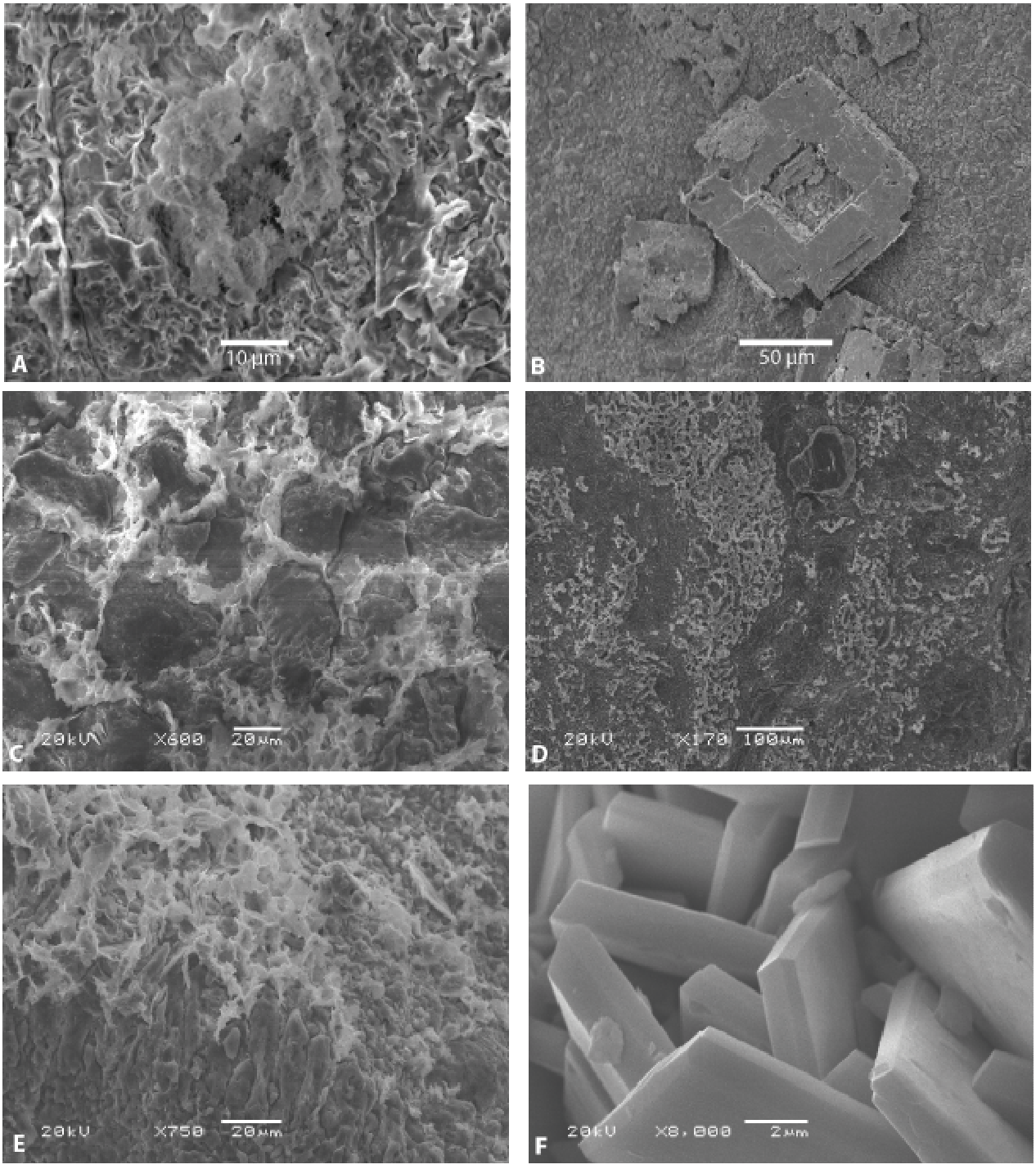

Figure 4. 3. SEI micrographs of the Hamar Laghdad samples. All the samples were etched with HCl in aqueous solution. A) KK2, Ipidiomorphic dolomite crystal with acicular framboids, in mesosparite cement. 1600x B) KK7, eudral dolomite crystal in micrite. 400x C) KK8, calcite grains lined by brighter materials. 600x D) KK9, pisolites layering with alternation of Ca content and Quatrz grain in relief. 170x E) KK10, calcite grains lined by brighter material, in the bottom of the figure elongated fibrous radiaxial calcite. 750x F) KK12, eudral goethite crystals. 8000x.

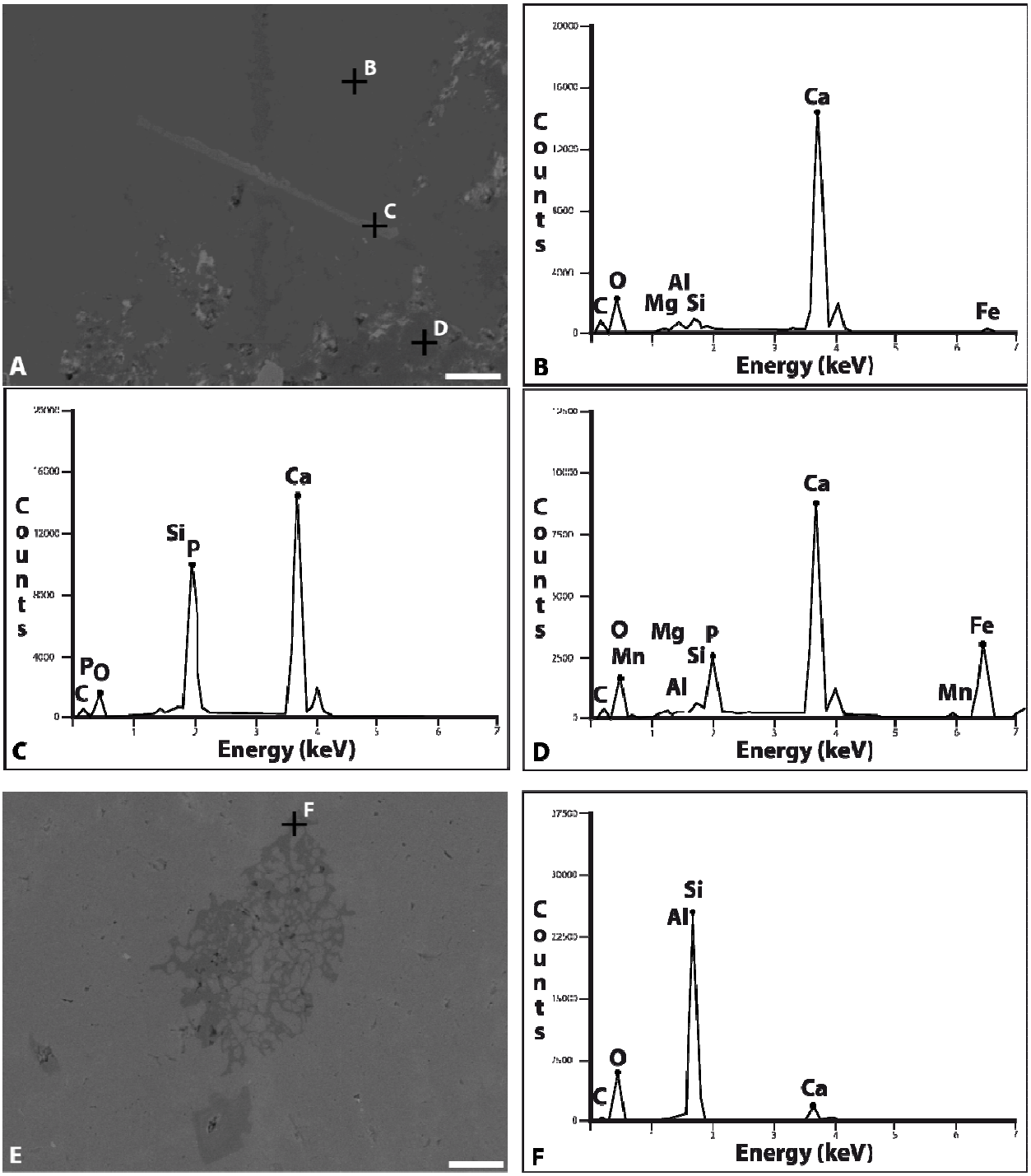

Figure 4. 4. SEM/EDS analyses of trilobites floatstone from Hamar Laghdad succession (KK14) A) BEI micrograph of an organic fragment, scale bar 20 µm. Black crosses correspond to spectra in B, C, D. B-D) EDS spectra from Ca-matrix (B), organic remain (C) and altered matrix (D). E) BEI micrograph of a cloudy inclusion in the Ca-carbonates, scale bar 50 µm. F) EDS spectra of the cloudy mineral (black cross in E) revealing prevalence of Si with low content of Ca.

4.3.3. EMPA

Some of the prominent micro-facies and micro-morphologies were analyzed via electron micro-probe spot-by-spot analysis. This procedure carried in restricted sectors allowed to produce Ca, Mg, Al, Si, Fe, Sr, Mn, Cr and Zn relatives abundances spectra from different point in the same facies. This technique due to a low detection limit allowed the study of several trace elements in the limestones.

An example of spot-by-spot analysis is in figure 4.5. The analyses carried on a trilobite shell emphasize the presence of Si along the shell where restricted sectors of micrite were replaced by high-Mg calcite, probably dolomite under XRD detection limit. BEI imagines (Fig. 4.5B) show the patchy silicification of the shell that preserved the original low-Mg calcite composition (see also 2.4.1.3 trilobites floatstone/rudstone description). Within the cloudy Si-mineral the Al is slightly present as in the rest of the investigated limestones, and Fe peaks occur in correspondence of rounded grains (Fig. 4.5A points 14, 15).

Linear analyses consist in 250-500 points of analysis along the diameter of the 24 mm disks. Despite the absence of an exact spatial collocation of the points, which are under the resolution of the imagines, the linear analyses give a continuous elements composition of the facies revealing abrupt changes of relative abundances (Fig. 4.6). The data reported in figure 4.6A evidence depletion in Ca-oxide content in correspondence of Si-oxide peaks in the trilobites floatstone (KK3) sample from the Maïder mound. Whereas in the reddish facies characterized by pisolites occurrences (Fig. 4.6B) the presence clastic Si throughout the carbonate matrix caused a chaotic spectrum reporting scattered Si peaks and Ca depletions.

Figure 4. 5. (Next page) BEI micrographs of trilobites floatstone (sample KK5) and EMPA spot-by spot analyses (numbers). A) Close-up of a trilobite shell with patchy Si-mineralization (green). B) Patchy silicified trilobites shells (red).

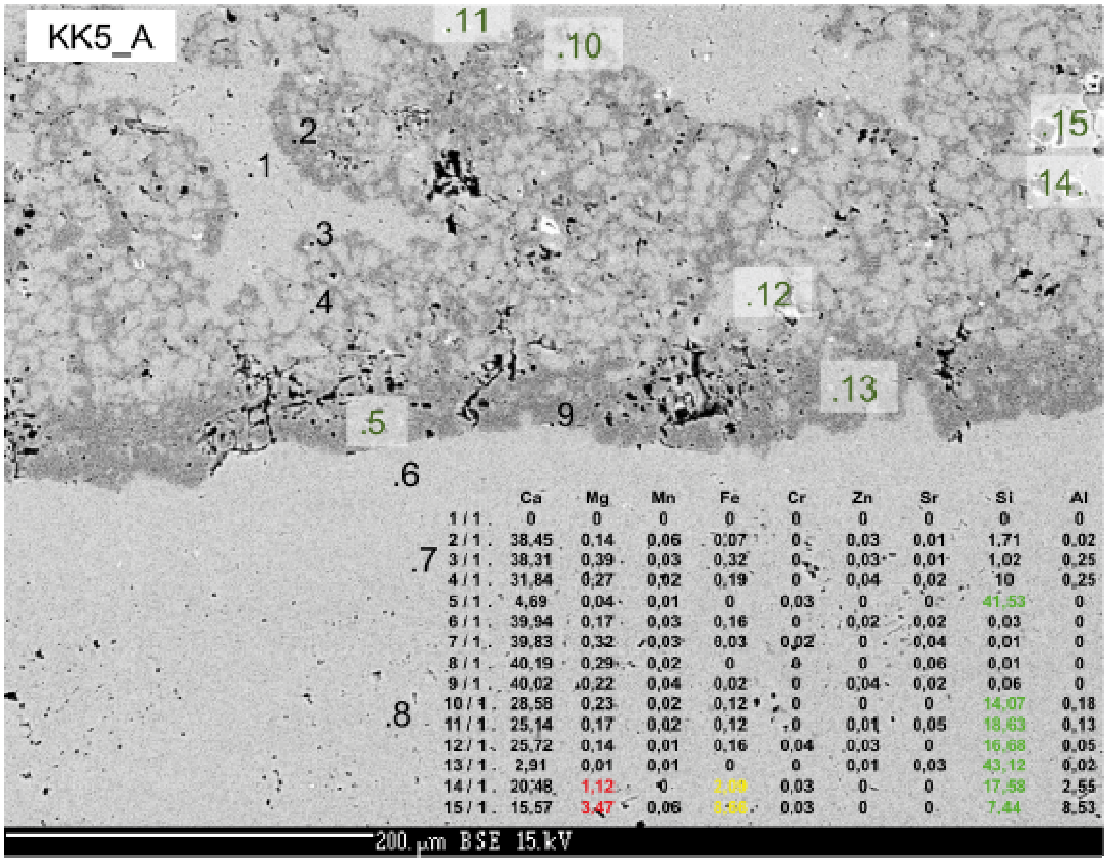

	Ca	Mg	Mn	Fe	Cr	Zn	Sr	Si	Al
1 / 1	0	0	0	0	0	0	0	0	0
2 / 1	38,45	0,14	0,06	0,07	0	0,03	0,01	1,71	0,02
3 / 1	38,31	0,39	0,03	0,32	0	0,03	0,01	1,02	0,25
4 / 1	31,84	0,27	0,02	0,19	0	0,04	0,02	10	0,25
5 / 1	4,69	0,04	0,01	0	0,03	0	0	41,53	0
6 / 1	39,94	0,17	0,03	0,16	0	0,02	0,02	0,03	0
7 / 1	39,83	0,32	0,03	0,03	0,02	0	0,04	0,01	0
8 / 1	40,19	0,29	0,02	0	0	0	0,06	0,01	0
9 / 1	40,02	0,22	0,04	0,02	0	0,04	0,02	0,06	0
10 / 1	28,58	0,23	0,02	0,12	0	0	0	14,07	0,18
11 / 1	25,14	0,17	0,02	0,12	0	0,01	0,05	18,63	0,13
12 / 1	25,72	0,14	0,01	0,16	0,04	0,03	0	16,68	0,05
13 / 1	2,91	0,01	0,01	0	0	0,01	0,03	43,12	0,02
14 / 1	20,48	1,12	0	2,09	0,03	0	0	17,58	2,55
15 / 1	15,57	3,47	0,06	1,99	0,03	0	0	7,44	8,53

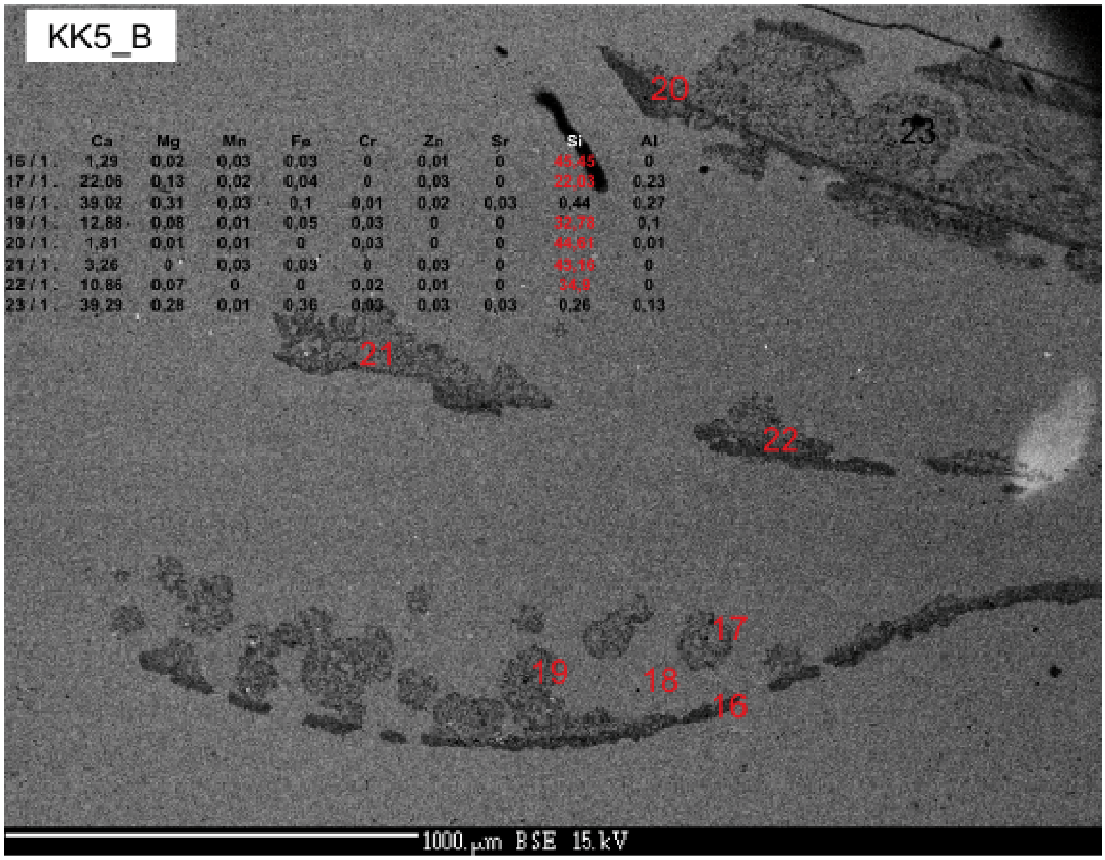

	Ca	Mg	Mn	Fe	Cr	Zn	Sr	Si	Al
16 / 1	1,29	0,02	0,03	0,03	0	0,01	0	43,45	0
17 / 1	22,06	0,13	0,02	0,04	0	0,03	0	22,03	0,23
18 / 1	39,02	0,31	0,03	0,1	0,01	0,02	0,03	0,44	0,27
19 / 1	12,88	0,08	0,01	0,05	0,03	0	0	33,78	0,1
20 / 1	1,81	0,01	0,01	0	0,03	0	0	44,81	0,01
21 / 1	3,26	0	0,03	0,09	0	0,03	0	43,16	0
22 / 1	10,86	0,07	0	0	0,02	0,01	0	34,9	0
23 / 1	39,29	0,28	0,01	0,36	0,03	0,03	0,03	0,26	0,13

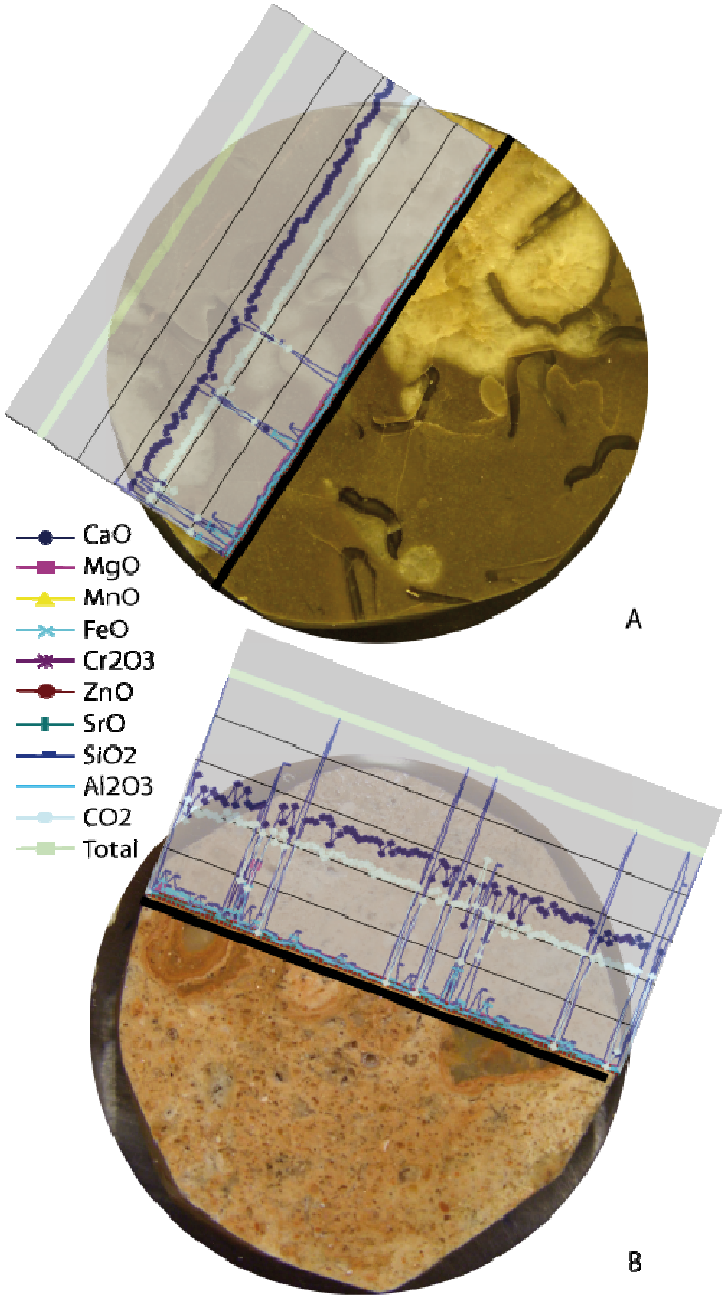

Figure 4. 6. EMPA analyses carried on 24 mm C-coated disks and plots of the oxides abundances. A) KK3, trilobites floatstone from Maïder basin mound. B) KK9, sample from the red pisolitic facies.

4.3.4. RAMAN MICROSCOPY

Representative Raman spectra of the different lithotypes from Hamar Laghdad and Maïder contain distinctive peaks 281, 711 and 1088 cm^{-1} that are characteristic of calcite (RRuff ID — R050127, 532 nm; White, 2009) (Fig. 4.7). Three of the limestones (KK5, KK6, KK7; Figs. 4.7-4.9) analyzed by Raman consist of a multiphase spectrum of calcite with disordered carbonaceous matter as indicated by the intense D1 (~1350 cm^{-1}) and G1 (~1600 cm^{-1}) Raman bands (Figs. 4.7-4.8). Raman microscopy analyses carried on 5 samples (Tab. 4.1) outlined the presence of

carbonaceous matter in the limestones and confirmed the occurrence of quartz within the trilobites floatstone (Fig. 4.7E).

The first analyzed sample is a trilobites floatstone (Fig. 4.7) showing the characteristic bimodal fabric (floatstone in the upper part and rudstone in the lower part of figure 4.7A). Raman spectra revealed that the cements contain more calcite than the micrite (Fig. 4.7B) and the first order carbonaceous matter is more abundant in the cements and around the shells (Figs. 4.7C-D and F-G). The map obtained for silica distribution does not reveal unambiguous data even if silica seems to be more abundant around the trilobites shells (Fig. 4.7E).

The scans obtained from the analysis of dark micrite collected near a vein outlined that the calcite content is greater in the cement phases respect to the micrite (Fig. 4.8A-B) whereas the first order carbonaceous matter is more abundant in the micrite (Fig. 4.8C-D). This trend is clearly represented in the close up (Fig. 4.8E-G).

Raman spectra of a dark red rock sample collected in the chimney-like structure shown in figure 4.1 A contains all the peaks (244, 300, 387, 480, 550, 680, 1000 cm^{-1}) characteristic of goethite (RRuff ID – 050142, 532 nm) (Fig. 4.9).

Figure 4. 7. (Pag. 84) Raman microscopy analysis carried on sample KK6 (trilobites floatstone). A) Polished surface and reflected light photomicrograph of the investigated surface. B) Maps of calcite distribution, C) and D) first order carbonaceous matter respectively D1 RAMAN band and G1 RAMAN band. E) Quartz distribution. All the photomicrographs have a total wide of 4 mm. F) Single Raman spectra from a shell (Calcite=green, Dolomite=blue) and G) marine cements. Calcite peak 1086 cm^{-1} ref. RRuff ID - R050127, 532 nm; Carb-D1 peak 1350 cm^{-1}; Carb-G1 peak 1600 cm^{-1}; Quartz peak 463 cm^{-1} ref. RRuff ID - R040031, 532 nm.

Figure 4. 8. (Pag. 85) Raman microscopy analysis carried on sample KK8 (dark micrite. A) Reflected light photomicrographs of the investigated surface. Inset represented in E-F. B) Map of calcite distribution, C) carbonaceous-D matter, D) carbonaceous-G matter. E) Maps of calcite, F) carbonaceous-D matter and G) carbonaceous-G matter of the inset in A. A-D scale bar 1000 µm; E-F scale bar 60 µm.

Figure 4. 9. (Pag. 86) Raman microscopy analysis carried on sample KK12 (gdark red rock from chimney-like structure). A) Reflected light photomicrographs of the investigated surface (voids filled by resin). B) Map corresponding to the 387 peak and C) corresponding to the 550 peak of goethite spectra. D) Single spectra of goethite showing the peak corresponding to goethite with the characteristic peaks (black line = sample; blue line = ruff data) and the peak corresponding to the resin. Goethite peak 387 ref. Ruff ID – R050142, 532 nm. A scale bar 80 µm; B, C scale bar 60 µm.

A
MICRITE
CEMENT
F
G
1cm
B
C
D
E
F
155
1685
G
0
3200
1088
1350
1600

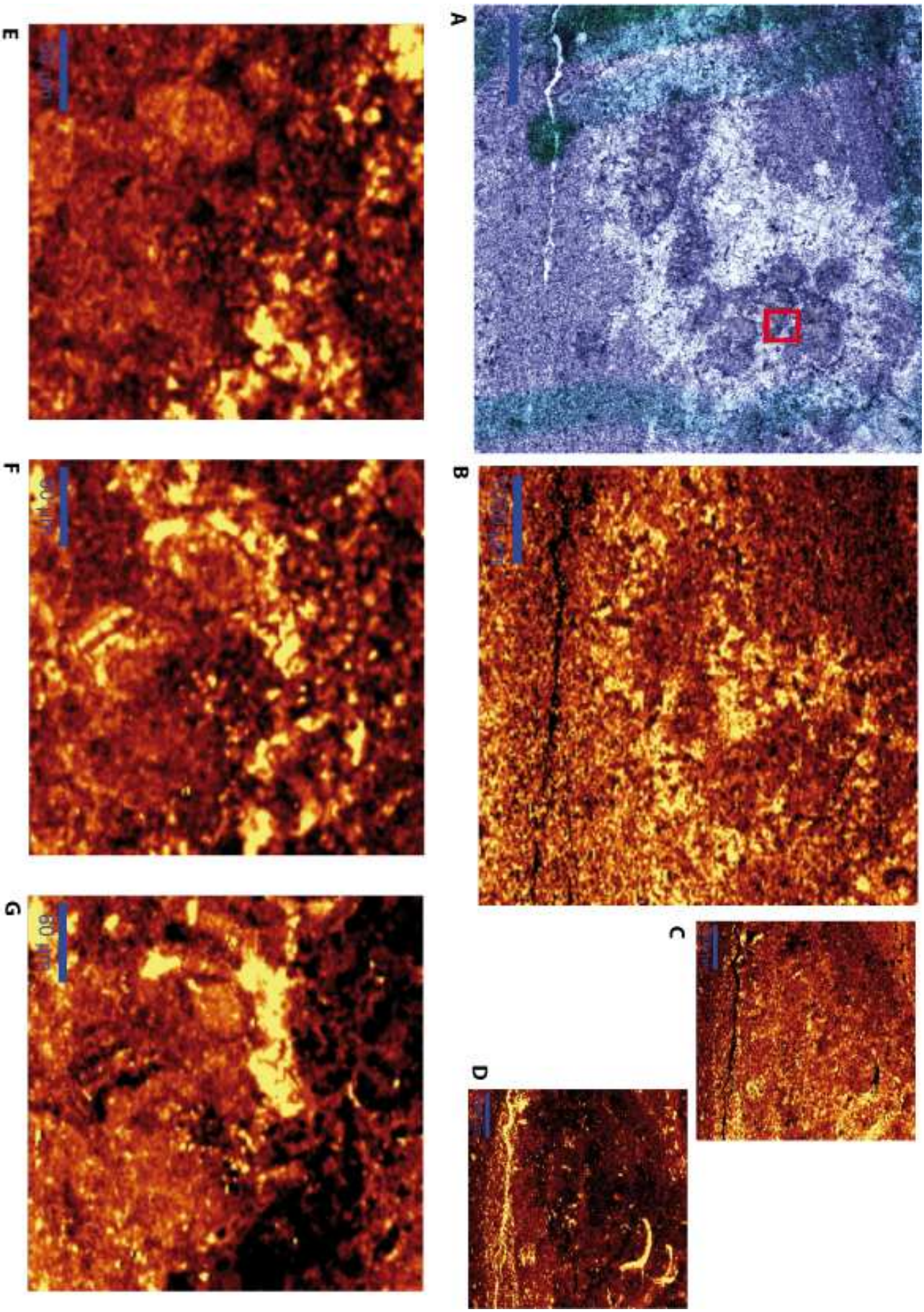
A
B
C
D
E
F
G

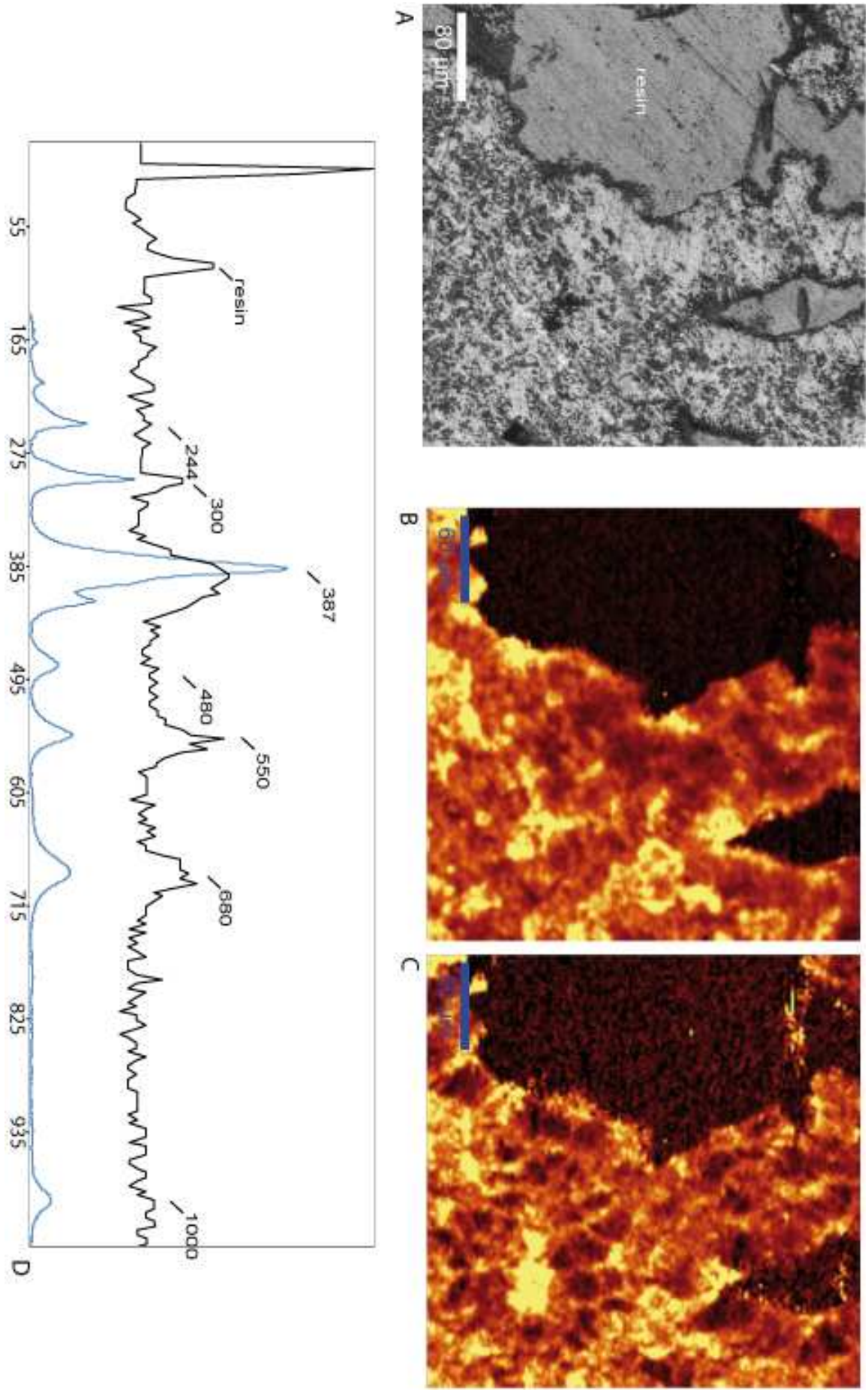
A
80 µm
resin
B
C
D
55
165
275
385
495
605
715
825
935
resin
244
300
387
480
550
680
1000

4.4. DISCUSSION

XRD data confirmed that the studied limestones are dominated by calcite with accessory minerals such as neomorphic quartz, dolomite and goethite in the Kess Kess samples and hematite, dolomite in the samples from the Maïder basin. These minerals in the two studied mounds clusters are localized in distinct facies such as chimney like structures and cavities filled by trilobites floatstone in the Hamar Laghdad and in veins cutting the mounds buildups in Maïder basin. Two samples collected in the rounded outcrops on top of Hamar Laghdad Ridge were made of 95% of quartz and 85% goethite, respectively.

XRF data endorsed the presence of these different accessory mineral phases in the considered micro-facies (Tab. 4.2). Particularly Mg is enriched in the reddish clastic facies with pisolites (Tab. 4.2). In the facies where Al is abundant it is in direct dependence with Si, on the contrary in the Si-bearing facies the two elements do not show direct dependence. These relations suggest that enrichments of Al could be due to the presence of small amounts of Al-silicates, whereas Si enrichment could be due to quartz presence. Despite the high amount of Fe-oxides in this goethite samples (KK12) from the topmost part of Hamar Laghdad ridge and in the hematite from Maïder vein (KK18), the general distribution of Fe in the studied samples do not shows a regular pattern. P is enriched where macroscopic organic remains occur, whereas other elements are in traces and do not show particular trends.

The micrite samples investigated with SEM microscopy present grains coated by bright material defined as ca-calcite from the EDS spectra but a clay origin of this lining is not excluded due to presence of Al- and Si-minerals in the EDS spectra. High-resolution imagines of euhedral dolomite crystals revealed zonation of the crystals with sharp boundaries and a dedolomitized core where dolomite were substituted by Fe-bearing calcite. Furthermore the presence of saddle-dolomite in the Maider sample (KK17) suggests high temperature of formation. Saddle-dolomite is strongly related with warm fluids circulation and more generally formed where the fluids reach higher temperatures respect to the surrounding rocks (Machel and Lonnee, 2002).

Back-scattered electrons imagines of the trilobite shells within the trilobites floatstone, in accordance with EMPA analyses, showed the patchy silicification of the low-Mg calcite shells. Silica enrichment was also detected in samples from stromatactis and vein filling, and suggests a link between the Si deposition and the fluids advection system (see chapter 2).

Raman spectra of the analyzed limestones contain the characteristic peaks of first order carbonaceous material (D1: 1350 cm^{-1}; G1: 1600 cm^{-1}). The relative intensity of the first-order D1

and G1 bands indicates that the carbonaceous matter is disordered and poorly crystalline (e.g., Marshall et al., 2010). According to the Raman maps acquired on trilobites floatstone, the carbonaceous matter are enriched in the micrite respect to the cements phase, and the contents is higher along the trilobites shells that could be explained with an original fingerprint retained from the fine grained micrite.

4.5. CONCLUSIONS

The broad set of analyses gave a complete scenario of the geochemical composition of the Kess Kess and gave new insights about the Maïder mounds geochemical composition which could be now compared.

If the 90% of the whole rocks is composed of Ca-carbonates in both localities the dolomite occur in restricted facies composed of coarse idiotopic to hypidiotopic dolomite, usually with euhedral crystals. Occurrence of saddle-dolomite in the Maïder basin limestones denotes a deposition under higher temperatures respect to the temperature registered in the Kess Kess dolomite. The high temperatures could be due to the circulation of hydrothermal fluids along the main fracture that cuts across the Guelb el Maharch mound (Fig. 3.2) where the specimen was collected

The abrupt change of the water chemo-physical conditions in restricted depositional environments is also suggested in the Kess Kess limestones by the occurrence of goethite- and quartz-bearing rocks within chimney-like structures.

Detailed analyses confirmed the presence of Si-minerals with patchy fabric in scutellid floatstone/rudstone. This localize silicification suggests the mobilization within the fluids of Si that substituted the LMC carbonate both in the Kess Kess, where this facies was firstly described, and in the Maïder mounds, where this facies is less abundant.

Although secondary mineral phases were detected in both the mound clusters in the Hamar Laghdad they are present in different facies through the Seheb el Rhassel Group whereas in the Maïder basin these secondary phases are less abundant or localized within veins that cut across the mounds.

SAMPLE	FACIES	XRD	OXYDES CONCENTRATION (%)											
			CaO	MgO	Al_2O_3	SiO_2	Fe_2O3	Na_2O	P_2O_5	SO_3	Cl	K_2O	TiO_2	MnO	Sr
KK1	Brachiopod *lumachella*	CALCITE	72,400	0,843	1,580	2,180	0,502	<<	0,059	0,055	0,030	0,000	<<	0,059	0,018
KK 2	Stromatactis	CALCITE	70,620	0,694	1,962	2,859	0,747	0,119	0,040	0,044	<<	0,310	0,100	0,082	0,029
KK 4*	Wackestones	CAL+QZ	72,300	0,669	0,764	1,800	0,510	<<	0,024	0,042	0,033	0,118		<<	0,055
KK 10		CALCITE	69,550	0,788	2,881	3,957	0,648	0,062	0,044	0,079		0,587	0,145	0,079	0,025
KK 3*		CALCITE	68,600	1,030	1,060	3,090	0,475	0,181	0,042	0,045	0,034	0,137	<<	0,117	0,065
KK 5	Trilobites floatstone	CAL+QZ	72,950	0,717	0,362	1,359	0,304	<<	0,050	0,041	0,037	0,068		0,057	0,023
KK 6		CALCITE	74,960	0,858	0,189	0,341	0,145	<<	0,088	0,024	0,024	0,038		0,057	0,028
KK 22#		CAL+QZ	67,900	0,770	2,790	4,400	1,230	0,048	0,071	0,066	0,000	0,455	0,132	0,082	0,023
KK 23#		CALCITE	-	-	-	-	-	-	-	-	-	-	-	-	-
KK 7	Layered micrite	-	73,330	1,487	0,163	0,280	0,303	<<	0,060	0,073	<<	0,031		<<	0,051
KK 14		CALCITE	66,400	1,460	2,840	3,140	6,190		0,087	0,169		0,147	0,144	0,219	0,022
KK 8		-	73,310	0,572	1,310	1,778	0,422	<<	0,020	0,089	0,022	0,247	<<	0,081	0,052
KK 9	Pisolites	CAL+QZ	64,760	0,458	1,823	7,574	0,831	0,041	0,032	0,072		0,282	0,126		0,013
KK 13		CAL+DOL+QZ	51,200	2,580	3,870	9,820	13,100		0,208	0,221	0,054	0,032	0,133	0,227	0,035
KK 11	Rounded outcrops	QUARTZ	0,739	0,115	0,128	95,000	0,158		<<	0,073		0,020		0,000	
KK 12		GOETHITE	0,313	0,000	0,141	1,250	85,180		0,131	0,043				0,000	
KK 15	Clastic	-	58,300	12,700	0,710	1,790	0,762		0,080	0,044	0,066	0,083		0,339	0,009
KK 16		CAL+DOL+QZ	56,500	8,910	1,850	6,720	0,824	<<	0,028	0,316	0,000	0,219	0,079	0,000	0,043
KK 19		-	67,500	0,558	1,590	5,960	0,649		0,042	0,148	0,000	0,221	0,098	0,000	0,022
KK 18*	Vein filling	CAL+HEMAT	46,900	0,908	0,642	1,520	32,000		0,340	0,125	0,027			0,130	0,025
KK 20#		CAL+QZ	71,100	0,731	1,210	4,060	0,550	<<	0,052	0,071	<<	0,258	<<	0,298	
KK 21#		-	75,200	0,600	0,190	0,486	0,370		0,087	0,034	0,030	0,031		0,104	0,029
KK 25#		CALCITE	74,500	0,531	0,515	0,718	0,306	<<	0,029	0,045	0,027	0,084		0,212	0,058

Table 4.2. Results of the XRD and XRF analyses grouped for lithofacies. T* Samples from Maïder mounds. # Thin sections.

REFERENCES

Demoulin, A., Trigance, C., Neff, D., Foy, E., Dillmann, P., L'Hostis, V., 2010. The evolution of the corrosion of iron in hydraulic binders analysed from 46-and 260-year-old buildings. Corrosion Science 52, 3168–3179.

Laetsch, T.A., Downs, R.T., 2006. Software for identification and refinement of cell parameters from powder diffraction data of minerals using the RRUFF Project and American Mineralogist Crystal Structure Databases. Program and Abstracts of the 19th General Meeting of the International Mineralogical Association in Kobe, Japan, pp. P08–25. http://rruff.info/.

Machel, H.G., Lonnee, J., 2002. Hydrothermal dolomite: a product of poor definition and imagination. Sedimentary Geology 152, 163-171.

Marshall, C.P., Edwards, H.G.M., Jehlicka, J., 2010. Understanding the application of Raman spectroscopy to the detection of traces of life. Astrobiology 10, 229–243.

Mazzetti, L., Thistlethwaite, P.J., 2002. Raman spectra and thermal transformations of ferrihydrite and schwertmannite. Journal of Raman Specroscopy 33, 104–111.

White, S.N., 2009. Laser Raman spectroscopy as a technique for identification of seafloor hydrothermal and cold seep minerals. Chemical Geology 259, 240–252.

5. SEDIMENTARY PROCESSES AND FLUIDS EXPULSION IN CROMMELIN CRATER AREA (ARABIA TERRA, MARS)*

5.1. INTRODUCTION

Roughly at the Noachian-Hesperian transition (3.7–3 Ga; Hartmann and Neukum, 2001), the Martian climate began to shift toward more arid conditions. This climate transition was characterized by gradual change of geologic processes as slowing and then cessation of water activity. The spectral analyses evidenced that during this transition the mineral formation switched from phyllosilicate- to sulfate evaporite-dominated (Bibring et al., 2006). This climate change probably resulted in the Martian equatorial regions in a transition from erosion to deposition of evaporites and playa deposits (e.g. Michalski et al., 2013). This scenario, active during the climatic transition at the Noachian–Hesperian boundary, was described in Meridiani Planum (Arvidson et al., 2006; Andrew-Hanna et al., 2007; 2010; Zabrusky et al., 2012). Lobate and crudely layered sediments from Meridiani Planum and Arabia Terra were interpreted as playa deposits triggered by a regional long-wavelength groundwater upwelling driven by region topography (Andrew-Hanna et al., 2007; 2010; Zabrusky et al., 2012; Michalski et al., 2013).

Outside of Meridiani Planum region, outcrops of layered sediments are observed throughout much of the Arabia Terra region (Malin and Edgett, 2000; Edgett, 2005; this study). These layered deposits, formerly named ELDs (Malin and Edgett, 2000), are exhumed throughout the whole Arabia Terra region exposed surface, particularly in the Crommelin and Firsoff craters area. Within the ELDs distinctive morphologies such as mounds, furrows and concentric concave strata were described.

Recently proposed hydrological models predict a fluctuating water table, producing sub-planar deposit with consistent dip directions toward the North, both within Meridiani Planum and throughout Arabia Terra regions(Andrews-Hanna et al., 2010). Thus fluids upwelling along the direction of the regional flow from the southern highlands toward the northern lowland, should have reached the surface in the main depression such as the craters throughout Arabia Terra and Meridiani. Where this flow possibly reached the surface might have given rise to peculiar morphologies such as lobate flows (Michalski et al., 2013), layered deposits (Andrew-Hanna et al.,

* This chapter consists of a paper in preparation by Fulvio Franchi, Angelo Pio Rossi, Monica Pondrelli: “Importance of fluid expulsion processes in the geological evolution of Mars: an example from Crommelin Crater”.

2007; 2010; Zabrusky et al., 2012; this study), mound and knobs (Michalski et al., 2013; Pondrelli et al., 2011). Mounds and spring mounds on Mars have been described in different setting such as Elysium Planitia (Greeley and Fagents, 2001; Lanagan et al., 2001), Acidalia Planitia (Crumpler, 2003a; 2003b; Farrand et al., 2005; Keszthelyi et al. 2010; Komatsu et al., 2011; Oehler and Allen, 2010; 2012; Skinner and Mazzini, 2009), Isidis Planitia (Keszthelyi et al. 2010; Skinner and Mazzini, 2009), Utopia Planitia (Burr et al., 2009; Clarke et al., 2007; Komatsu et al., 2011; de Pablo and Komatsu, 2007; Skinner and Tanaka, 2007; Skinner and Mazzini, 2009), Candor Chasma (Chan et al., 2010), Valles Marineris (Rossi et al., 2007; 2008a) and Arabia Terra (Pondrelli et al., 2011; Rossi et al. 2008a). These morphologies are settled within meter-scale layered formations interpreted as water induced sedimentary rocks (Malin and Edgett, 2000; Edgett and Malin, 2002; Edgett, 2005) probably affected by climate-controlled periodicity (Andrew-Hanna et al. 2010; Lewis et al., 2008), and are of primary relevance in astrobiology (Walter and Des Marais, 1993).

In this work we describe and reconstruct the stratigraphic framework of the Crommelin area detailing the occurrence of ELDs within the Crommelin, Firsoff craters and smaller crater several kilometers south from Firsoff, here (hereafter referred to as Southern crater) (Fig. 5.1). Therefore, after the evaluation of the original crater geometries and crater filling sediment packages, HiRISE-based DEM of mounds and furrows were generated. These tridimensional imagines/reconstruction allow to infer morphological and geometrical relation between ELDs, mounds and furrows. The obtained dataset allowed to compare Crommelin ELDs and related morphologies with the geological record of Meridiani Planum for which a strong relation with fluids upwelling was proposed (Andrew-Hanna et al. 2010; Michalski et al., 2013). The groundwater upwelling could have triggered biological activity (Michalski et al., 2013) potentially preserved in the water related morphologies such as the mounds and furrows in Crommelin region.

The aim of this paper is to describe the ELDs geological setting in the Crommelin crater region, which includes even Firsoff crater and a smaller crater southwest from Firsoff, and to point out their relation with ground water flow. Furthermore we will discuss about the mound and other morphologies development within the ELDs focusing on their astrobiological significance in relation with Mars and terrestrial analogs.

5.2. DATA AND METHODS

Combinations of several different data sets were utilized for characterizing strata setting and morphologies of the studied area (Fig. 5.1A). The NASA Context Camera (CTX, Malin et al., 2007) images form the framework for targeted high-resolution HiRISE (High Resolution Imaging Science

Experiment on Mars Reconnaissance Orbiter, McEwen et al., 2007). Low to mid-resolution topographic data and DEM reconstruction, are based on Mars Orbiter Laser Altimeter (MOLA) and High Resolution Stereo Camera (HRSC) data sets. High resolution HiRISE DEMs (~30 cm/pixel) have been generated from PSP_003432_1850 and ESP_020679_1820 (e.g. Moratto et al., 2010). These digital elevation models provided the base for 3D processing of the HiRISE images of interesting morphologies that permitted to discern and describe individual landforms. The landforms described are represented in the HiRISE images: PSP_003432_1850, PSP_002021_1850, ESP_020679_1820, ESP_020534_1825, ESP_016766_1810. These data sets were integrated and mapping carried out using Geographic Information Systems (GIS) tools: ESRI (ArcGis) and QGis (www.qgis.org).

Mapping of the geological unit is derived from those proposed by Scott and Tanaka (1986) and Pondrelli et al. (2011). The morpho-stratigraphic units were mapped with respect to abrupt changes of color, albedo and surface morphology (Fig. 5.1B). The geometries of the original crater dimensions and the estimation of the craters filling sediments package were performed using the equations given by Garvin et al. (1999, 2000, 2002, 2003). Using the high-resolution stereo-derived topography and imagery, orthogonal projections of the mounds in Firsoff were generated.

5.3. GEOLOGICAL SETTING

The Crommelin and Firsoff impact craters are located in the equatorial southern lowlands of Arabia Terra respectively centered at 4,9° N – 10,5° E and 2,6° N – 9,2° E (Fig. 5.1A). The Southern crater is centered at 1° N – 9° E. Figure 1B shows the large-scale geological setting of the study area.

The stratigraphic succession studied in the Crommelin area begins with the Plateau Sequence (Noachian in age) that is represented in this region by the Cratered Unit (and Subcratered Unit). The Cratered Unit is the most extensive unit of the western equatorial region (Tanaka, 1986) and was interpreted by as a mixture of lava flows, pyroclastic deposits and impact breccias (Scott and Tanaka, 1986). These deposits are non-conformably overlapped by the ELDs (e.g. Hynek et al., 2002; Malin and Edgett, 2000; Pondrelli et al., 2011). Despite thickest exposed succession of ELDs occurs inside Crommelin and Firsoff craters, layered deposits are present even outside the craters at least in part as aeolian transported debris, especially in the southern region (Fig. 5.1B) where they cover extensively a flat topography (Pondrelli et al., 2011). Mounds and other structures suggestive of spring activity are exclusively within the ELDs and are a common features in the southeastern region of the Firsoff crater, where we observe the higher density of mound buildups, and in the

crater below Firsoff (Fig. 5.1B). Inside to the three craters considered here the ELDs onlap the crater rims (Fig. 5.1C) whereas outside the craters the ELDs are buried by the Hummocky Material (Pondrelli et al., 2011). The Hummocky Material unit is made of dark-toned rocks of probable volcanic origin, and unconformably overlies the succession. Despite crater counts dataset is dated (Scott and Tanaka, 1986) there are stratigraphic evidences that during the Late Noachian many areas were largely draped by a thin mantle of reworked (aeolian and volcanic) sediments (Scott and Tanaka, 1986). In the southern and western sector of Arabia Terra, the Hesperian flood basalts belonging to the Ridge Plain Material Unit (Scott and Tanaka, 1986), buried the Noachian units.

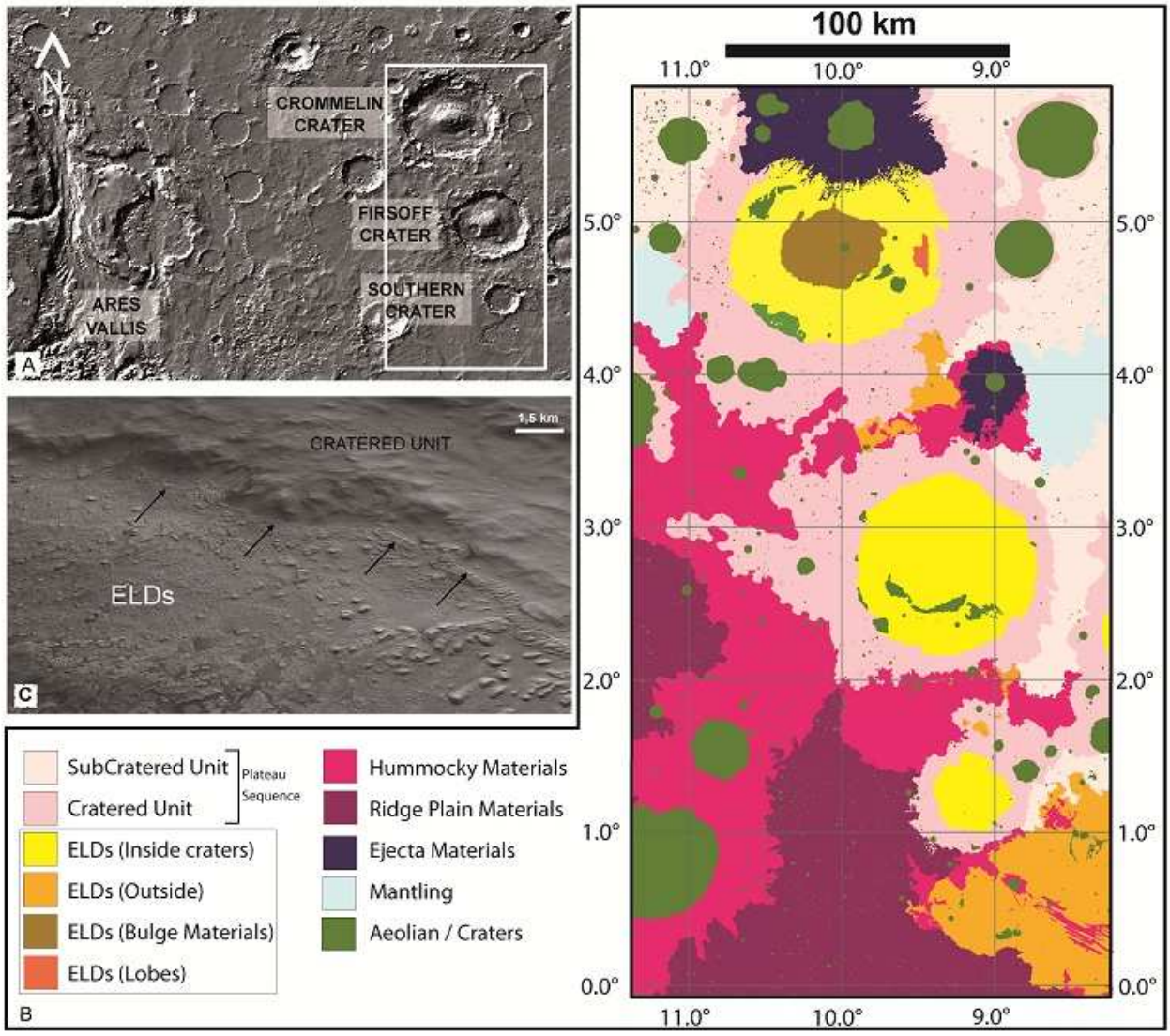

Figure 5. 1. A) Location map of the study area (MOLA MEGDR-based shaded relief). Boxed area is detailed in B. B) Schematic geological map of the Southern Arabia Terra region on Mars (with box in A). Stratigraphic units defined after Scott and Tanaka (1986) and Pondrelli et al. (2011). C) ELDs strata onlapping the Crommelin crater rim sediments (arrows) in its northern sector.

Within this stratigraphic framework the ELDs lower boundary is represented by the

Noachian Plateau Sequence (Cratered unit) whereas the flood basalts (Ridge Plain Materials) represent the upper constrain for the ELDs, which span from the upper Noachian to the lower Hesperian (Scott and Tanaka, 1986). In this time span Mars was characterized by abundant water related features like valley networks (Fasset and Head, 2008), relict lakes and channels within which has been suggested the presence of water-related carbonates associated with phyllosilicate-bearing rocks (Ehlmann et al., 2008; 2010).

The ELDs unit is a succession of meters-thick strata that covers almost the whole inner part of the studied craters, and a large area southeast from Firsoff Crater (Fig. 5.1B). The ELDs pinch out against the internal walls of the crater onlapping the crater rims (Fig. 5.1C) and the central bulge sediments (Fig. 5.2). ELDs elsewhere have been described as Etched terrain (ET) unit characterized by high thermal inertia and warm nighttime temperature in THEMIS thermal infrared images (Hynek, 2004). Particularly in the Crommelin area the ELDs present a peculiar scalloped pattern (Fig. 5.3A) dotted by mounds (Fig. 5.3B) and concave concentric troughs (hereafter referred to as ridge-and-troughs).

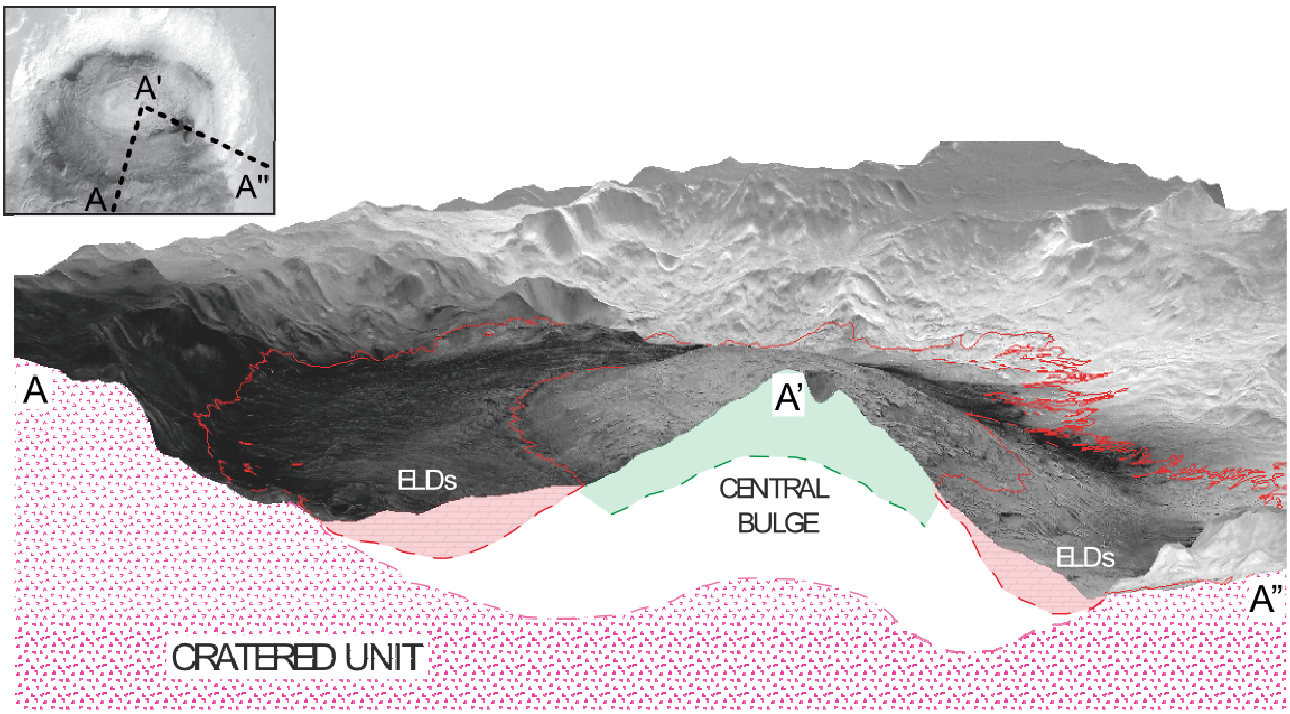

Figure 5. 2. Interpretative block diagram sketching the geometrical and stratigraphical relations within the Crommelin crater. The inset shows the indicative direction of the geological profile. The ELDs (red pattern) and Cratered Unit (pink pattern) contact (red lines). The ELDs are clearly in onlap with the underlying Cratered Unit. The ELDs strata corresponding to central bulge unit are in green.

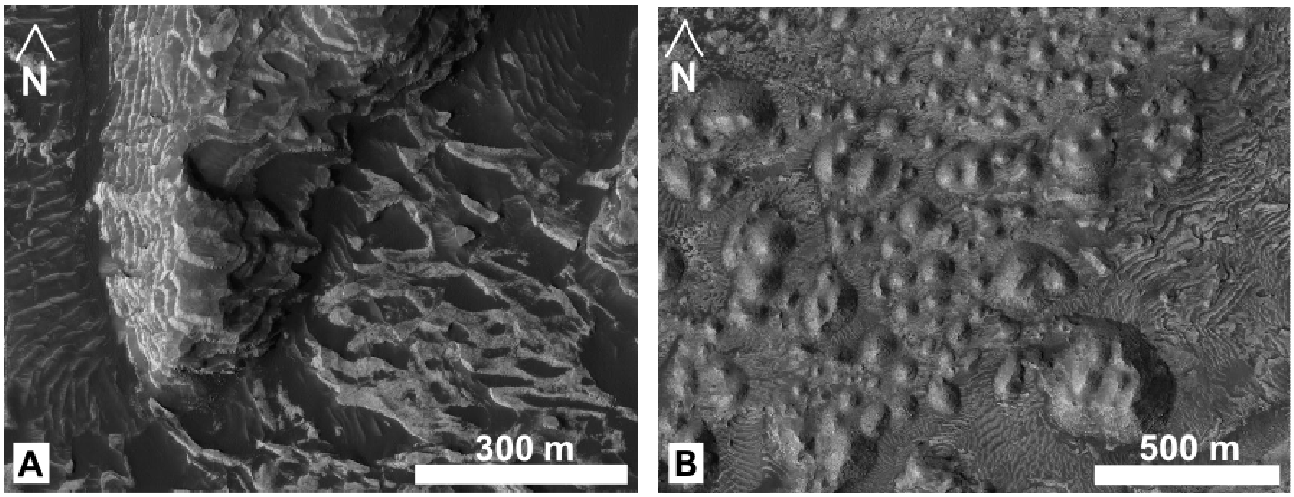

Figure 5. 3. A) High sinuous ELDs strata (*etched terrains,* REF) observed in the southwestern sector of the Firsoff crater (HiRISE ESP_020534_1825). B) The mounds field in the southeastern sector of the Firsoff crater. (HiRISE ESP_020679_1820).

5.4. RESULTS

5.4.1. ELDs filling geometries

The morphometric equations used in this work were defined by Garvin et al. (1999, 200, 2002, 2003) on the basis of MOLA topographic profiles and a suite of more than 20 geometric properties of fresh impact craters. By comparing these properties, several equations were generated that relate geometric properties with the crater diameter, and give the original geometry of the impact craters. These original geometry compared with the extant topography allow to inferred the total supposed thickness of the sediments package within craters and, eventually, the unconformity within the stratigraphic succession.

The expected dimensions of Crommelin and Firsoff craters sediment packages were calculated starting from measurements on the MOLA data set (Tables 5.1 and 5.2). The sediment package is irregularly distributed inside the craters showing a maximum thickness southward where landforms and morphologies (furrows, ridge-and-trough s and mounds) are pervasive, and a minimum northward where landforms and morphologies are dispersed (Fig. 5.2A).

According to definitions of crater basins given by Garvin et al. (2003), Crommelin and Firsoff craters are “peak-ring” whereas Southern crater is a *complex crater.*

PARAMETER	EQUATION
Depth	$0,36\ D^{0,49}$
Rim height	$0,02\ D^{0,84}$
Central bulge height	$0,04\ D^{0,51}$
Central bulge diameter	$0,25D^{1,05}$

Table 5. 1. Morphometric equations from Garvin et al. (2003).

CROMMELIN CRATER		
PARAMETER	**CALCULATED**	**MEASURED**
Diameter	-	110
Depth	3,6	1,5 - 2
Rim height	1	0,6
Central bulge/peak height	0,4	1,8
Central bulge diameter	34,8	40-70
FIRSOFF CRATER		
PARAMETER	**CALCULATED**	**MEASURED**
Diameter	-	90
Depth	3,3	1,5
Rim height	0,9	0,3
Central bulge height	0,4	1,2
Central bulge diameter	16,9	40

Table 5. 2. Calculated and measured geometric parameters of the Crommelin and Firsoff craters. All the values are in kilometers.

5.4.1.1. Crommelin crater

Crommelin crater is ca. 110 Km in diameter with an exposed (measured from crater floor to crater rim) depth of about 1,7 km (Fig. 5.4A). The original crater depth was estimated as 3,6 km, and the thickness of the total package of its filling sediments as between 1,7 and 1,2 km (Fig. 5.4A). Crommelin central bulge is elongated in the East-West direction, resulting in an elliptical shape with the major axis 70 km long and the minor axis 40 km long. The morphometric equation gave a central bulge diameter of 34,8 km and 0,4 km height, less than ¼ of the central bulge height measured from the MOLA data set (1,8 km, Fig. 5.4A). Based on the morphometric equations, the expected height of the crater rims (1 km) is slightly greater than the measured one (0,6 km, Fig. 5.4A). The average level of the sediments outside the crater was assumed as reference height for morphometric calculations (Fig. 5.4A, horizontal dotted line). The schematic N-S section of the Crommelin crater (Fig. 5.4A) shows that the package of sediments is thicker in the southern sector of the crater. Assuming a package of the filling sediments settled on top of a flat crater's floor, the difference in thickness between North and South is of ca. 500 meters.

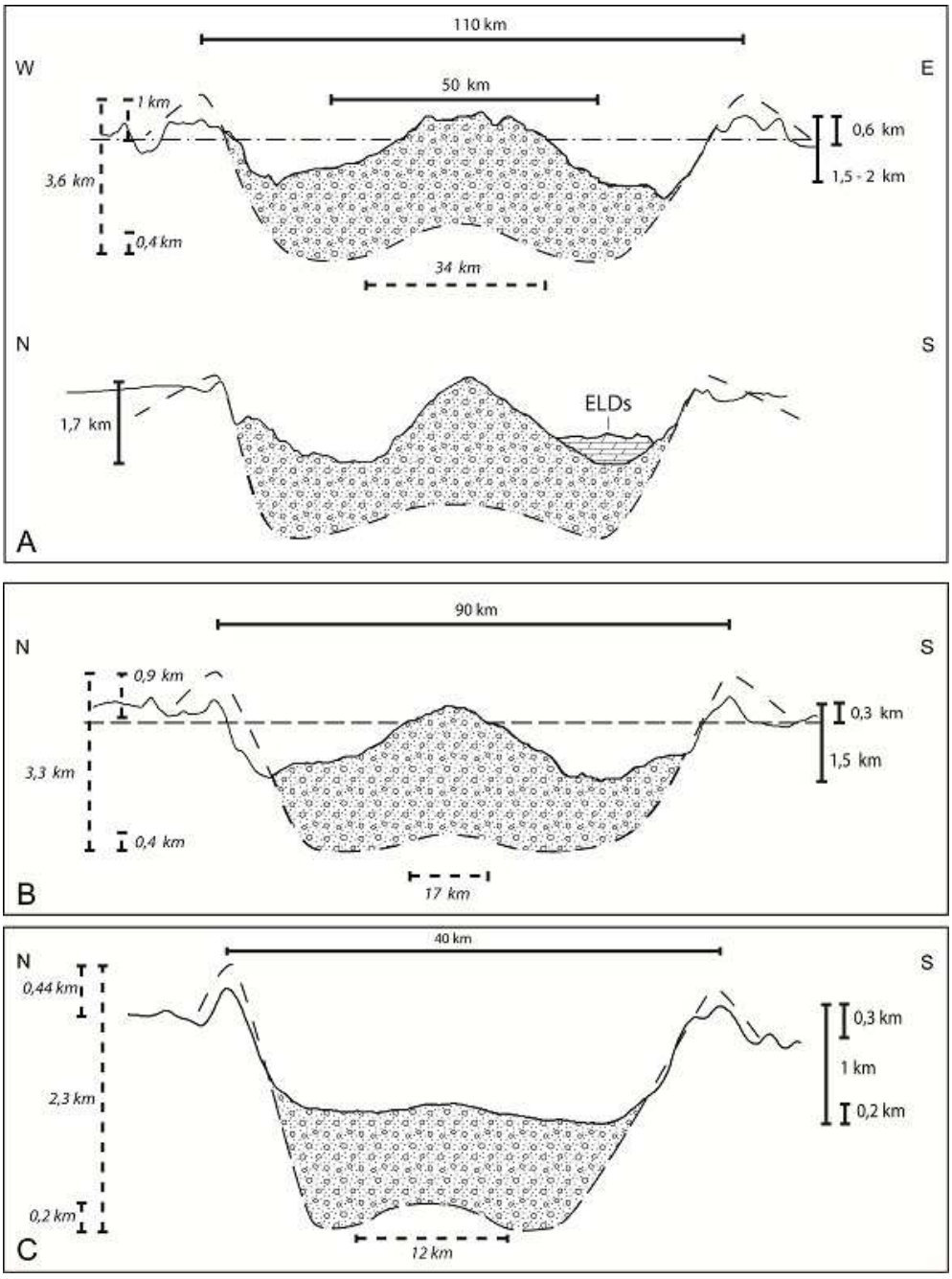

Figure 5. 4. Geometries of the craters and sediment packages. Black lines and related values are relative to the crater profile inferred by MOLA data. The broken lines and realted values correspond to the crater profile estimated with the Garvin et al. (2003) equation. Horizontal dashed lines are the datum used for the reconstruction. Areas with filled pattern correspond to the inferred thickness of sediment package. A) Crommelin crater : schematic North-South and West-East sections. Calculated parameters: 3,6 km deep; 1 km rim height; 34 km central bulge diameter; 0,4 km central bulge height. The area with filled pattern in the N-S section corresponds to the exceeding thickness of the sediments package in the south. B) Firsoff crater: Schematic section North-South section. Calculated parameters: deep = 3,3 km; rim height = 0,9 km; central bulge diameter = 17 km; central bulge height = 0,4 km. The dashed line is the datum used for the reconstruction. C) Schematic section of the Southern crater. Parameters calculated from the equations: deep = 2,3 km; rim height = 0,44 km; central bulge diameter = 12 km; central bulge height = 0,2 km.

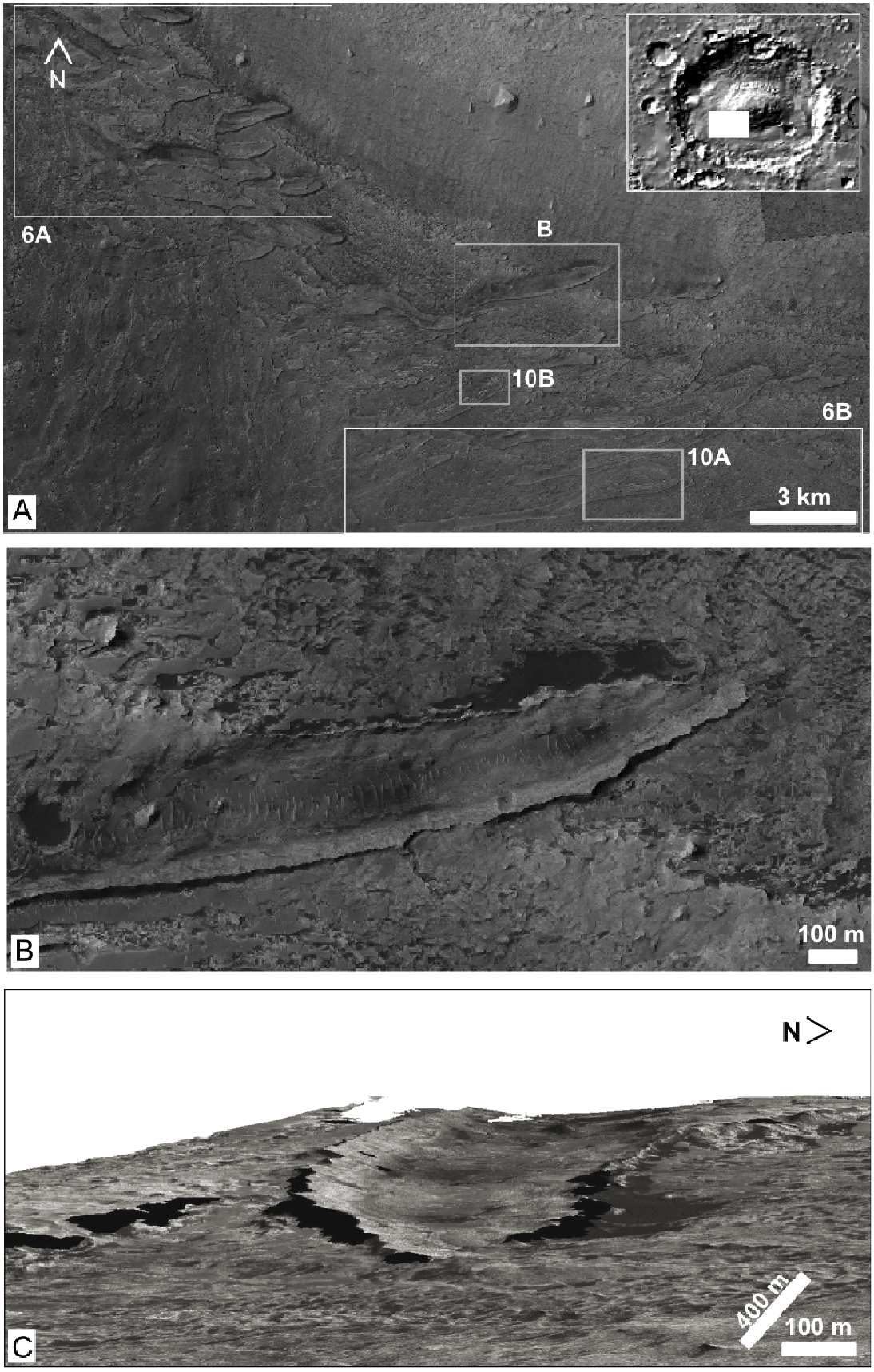

Figure 5. 5. A) Southwester sector of the Crommelin crater with the furrows along the edge of the central bulge. (CTX B11_013875_1833). The boxed areas are showed in figures 5B, 6A-B and 10A-B. B) East-West oriented furrow (HiRISE PSP_002021_1850). C) 3D view of a furrow (HiRISE PSP_002021_1850).

5.4.1.2. Firsoff Crater

Firsoff crater is ca. 90 Km in diameter with an exposed depth of about 1,5 km measured from crater floor to crater rim (Fig. 5.4B). The estimated original crater depth was as 3,3 km, and the thickness of the total package of sediments within crater was ca. 1,2 km (Fig. 5.4B). The morphometric equations gave a central bulge height of 0,4 km whereas the measured central bulge height is of 1,2 km. The Firsoff bulge has a rounded shape with a measured diameter of ca. 40 km whereas the expected diameter is 16,9 km. The expected height of the craters rims (0,9 km) is 0,6 km higher than the measured rim height (Fig. 5.4B). For these computations we also assumed as reference the mean height of the sediments outside the crater, as with Crommelin.

5.4.1.3. Southern Crater

The Southern crater, ca. 30 km south from Firsoff crater, has a diameter of ca. 40 km and is filled by highly convoluted ELDs (Fig. 4C). The shape of this crater is substantially different from Crommelin and Firsoff craters. The central bulge is only few kilometers wide and few tens of meters high. The morphometric equations gave for this crater a central bulge diameter of 12 km and a calculated height of 0,2 km. The rims height is of about 0,3 km only few tens of meter lower than the measured one (0,4 km, Fig. 4C). This crater show a wide mound cluster covering the whole The southeastern sector where the mounds are aligned along rectilinear kilometric fractures.

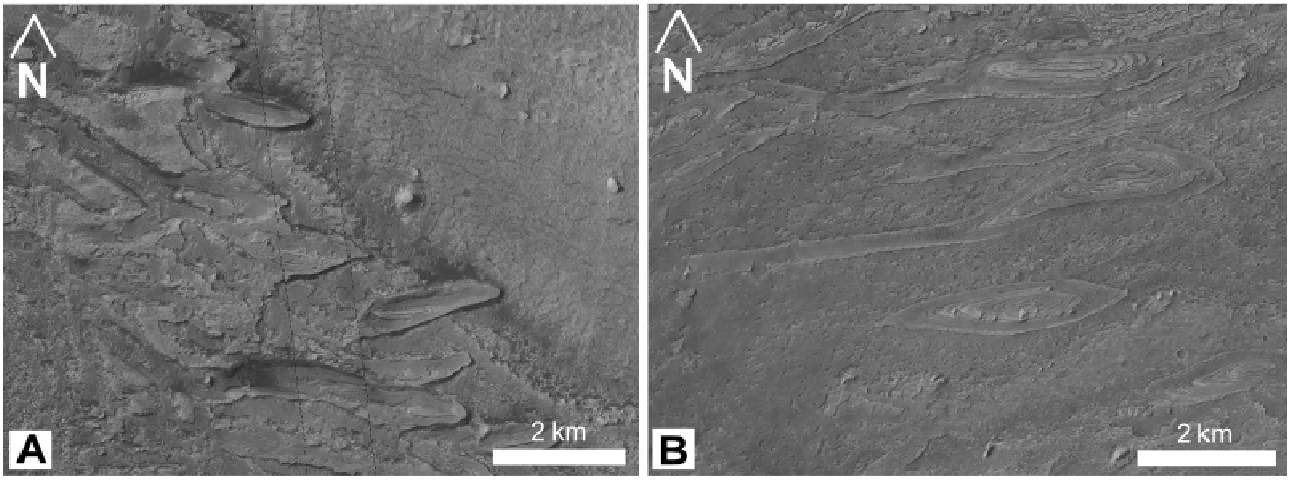

Figure 5. 6. Southern sector of the Crommelin crater (white box in 6A). A) Northernmost East-West oriented channels with sharp inward-dipping edges and high relief. B) Southernmost WSW-ENE oriented channels showing more elongated concentric strata with lower relief.

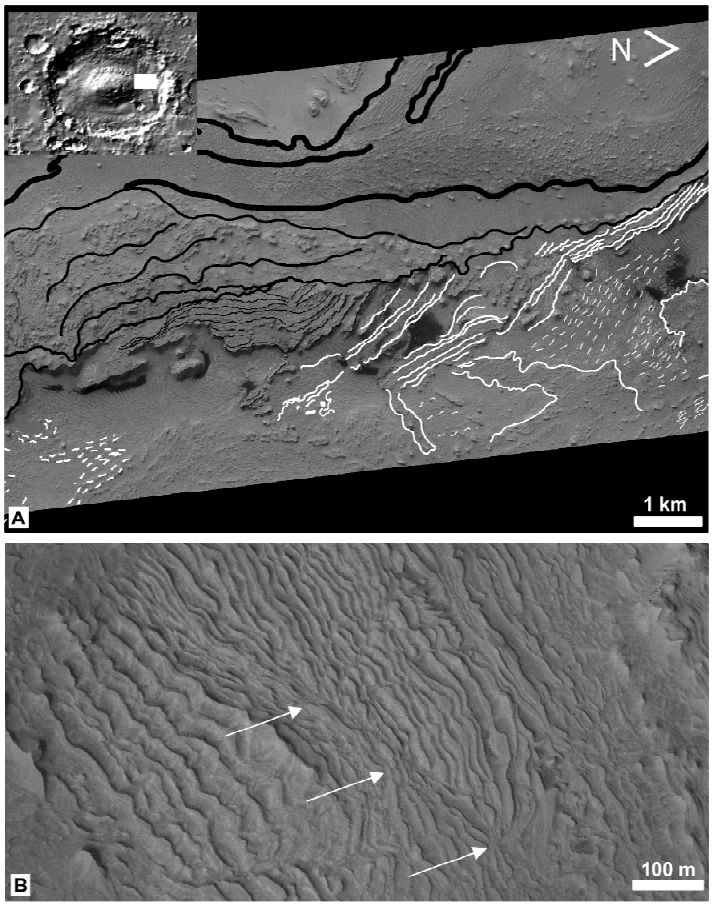

Figure 5. 7. A) ELDs in the north sector of the Crommelin crater (HiRISE PSP_003432_1850) corresponding to the white boxed area of the inset. Overlapped lobes of crudely stratified ELDs: strata boundaries are underlined with different line patterns corresponding to different lobes. B) Detail of the contact between two lobate strata (white arrows).

5.4.2. ELDs morphologies

5.4.2.1. Furrows and ridge-and-troughs

In the southern sector of the Crommelin crater the scalloped ELDs strata are cutted by characteristic furrows several kilometers long and few hundred meters large (Figs. 5.5-5.6). In the northern sector furrows are not observed and the ELDs strata show an irregular stratification organized in few tens kilometers wide overlapped lobes (Fig. 5.7A) divided by unconformities (Fig. 5.7B). On top of the lobate ELDs many small (ca. 10 meters) remnants and mounds are exhumed. The lobate ELDs are widespread in the Northeastern sector of Crommelin crater (Fig. 5.1B), exactly at the opposite side of the furrows that are more abundant in the Southwester sector. The lobes have

a slightly curved front and an inclination around 5° which is the steeper slope of the Crommelin crater sediments package (Fig. 5.8A and Fig. 5.9, WE profile).

The geometry and spatial relation of the Crommelin furrows are summarized in figures 5.5 and 5.6. The furrows branch out from the base of the crater central bulge and their elongation trend is about 35-45 degrees respect to the E-W direction (Figs. 5.5 and 5.8). Figure 5.8A reports the average slopes of the whole Crommelin crater showing higher inclination in the northern side of the central bulge (where the lobes were described). Particular relevance for further discussion about the furrows is the slope of the central bulge in the sector where the furrows are more abundant (southwestern sector). As shown in figures 5.8B and C the furrows (white lines) do not follow the main slope of the bulge. The furrows developed only in the region with lower inclination, ca. 2°-3° (Fig. 5.9), that coincides with the thicker package of ELDs (Fig. 5.4A). There are no evidences of strata truncations along the furrows, which seem to be developed along a single stratum. The furrows appear substantially smooth with polygonal texture, covered by unconsolidated aeolian sediments (dark dunes, Fig. 5.5B). The raised edges of those furrows are few tens of meters high (Fig. 5.5C) and do not show substantial difference of albedo with the furrows bed and ELDs. In the northern part of the southwestern sector the furrows have high relief and they do not exceed 2 km in length (Figs. 5.6A). Further south the furrows display a lower relief and are more elongated in WSW-ENE direction (Figs. 5.6B). These furrows terminate in elongated structures with concentric stratification (hereafter named “ridge-and-troughs”) (Figs. 5.6B) typically not wider than 1 km. These ridge-and-troughs have lower relief respect to the furrows. The ridge-and-troughs strata are partially covered by recent dust and dunes made of dark-toned material, whereas the strata edges appear light toned, sharp and inward-dipping (Fig. 5.10). The ridge-and-through structures developed where the topography is flat.

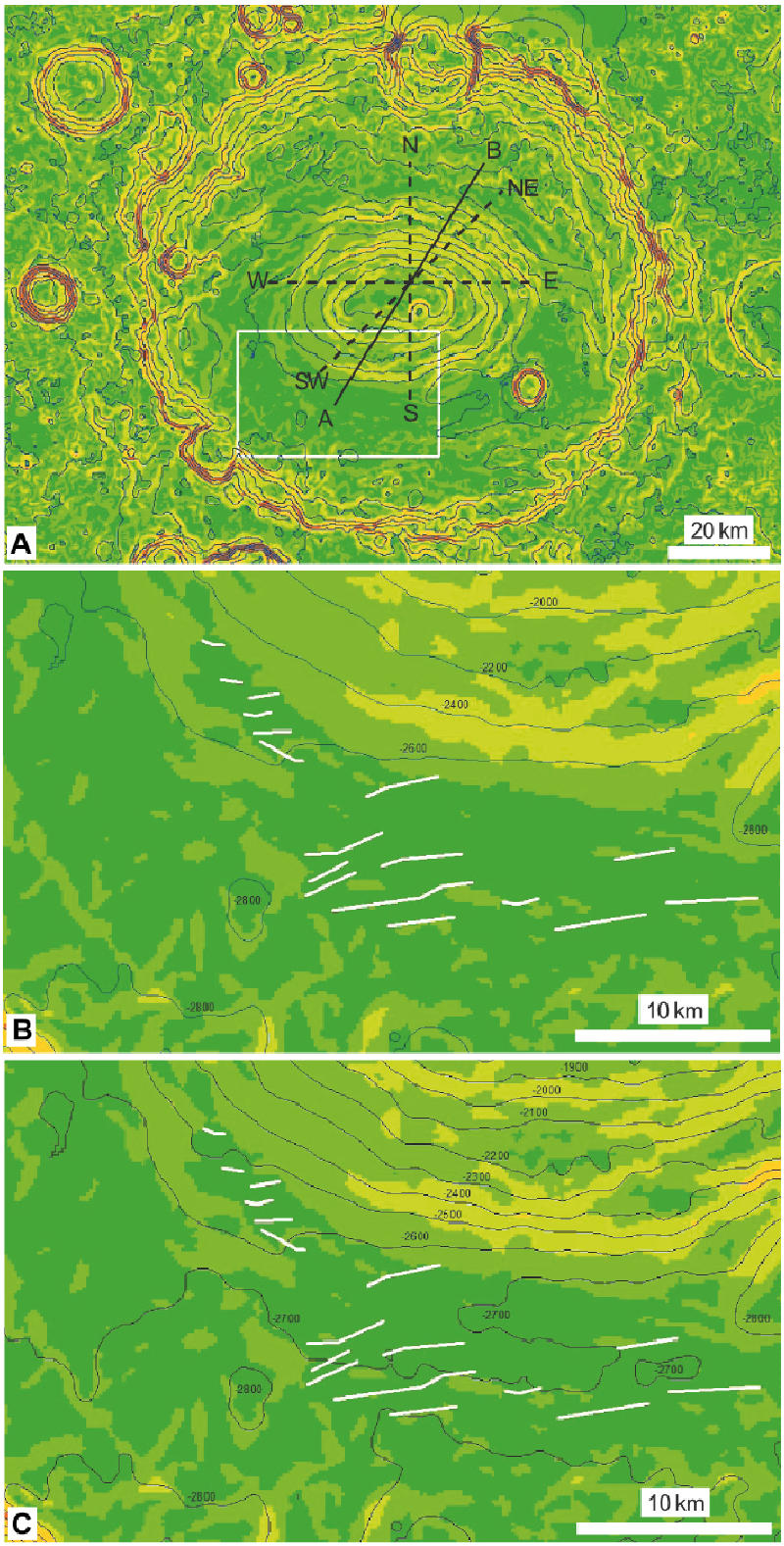

Figure 5. 8. DEM-derived slopes-map of Crommelin crater. A) Crommelin crater slopes from 0° (dark green) to almost vertical walls (red). Dotted grey lines represent sections of the central bulge for which slope was calculate. Topographic contours (200 m spacing) based on HRSC DEM. B) Southwestern sector of Crommelin crater (white box A) showing the direction of the major furrows (white lines). Topographic contours with 200 m spacing and 100 m spacing (C) based on HRSC DEM.

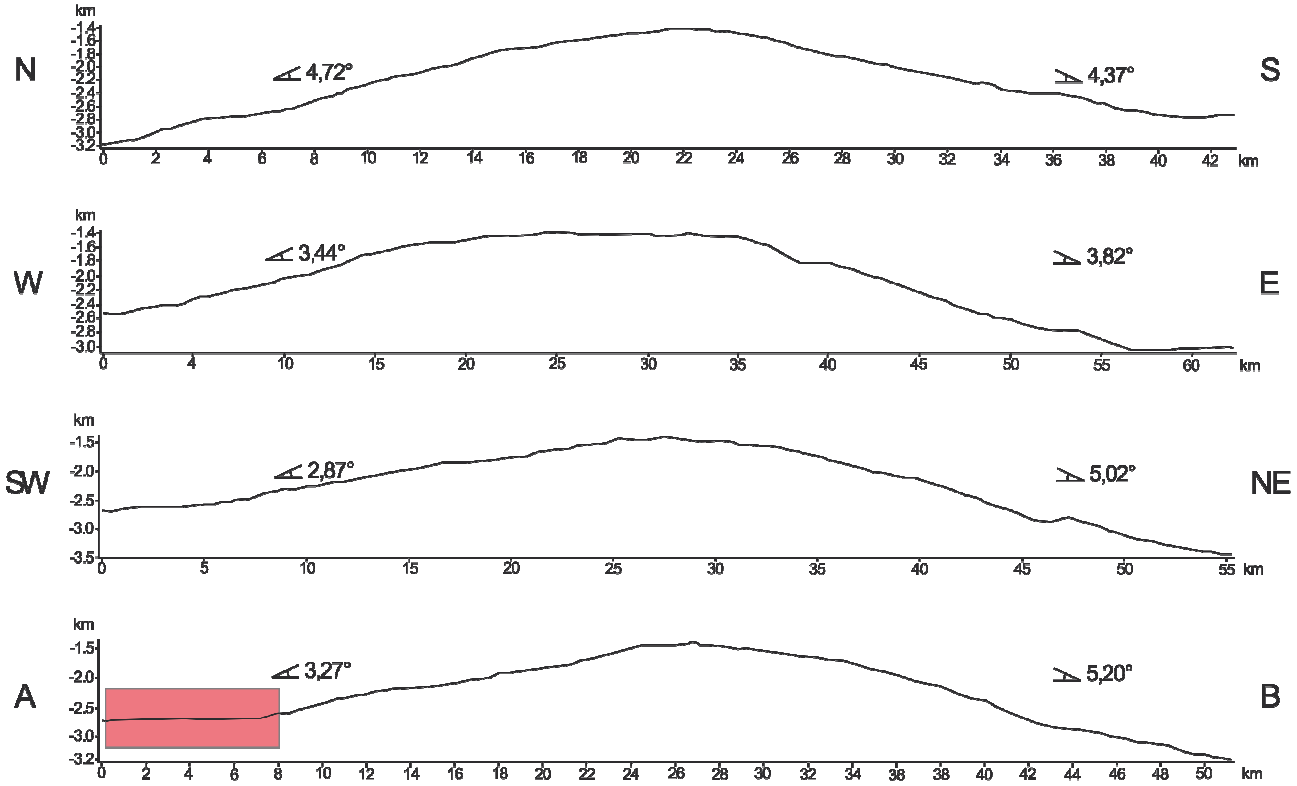

Figure 5. 9. North-South, West-Est and Southwest-Northeast profiles of the Crommelin crater central bulge (dotted line in 8A), and A-B section passing through the sector with major amount of furrows. Slope toward: N = 4,72° - 8,2%; S = 4,37° - 7,6%; SW = 2,87° - 5%; NE = 5,02° - 8,75%; W = 3,44° - 6%; E = 3,82° - 6,7%; A = 3,27° - 5,7%; B = 5,20° - 9%.

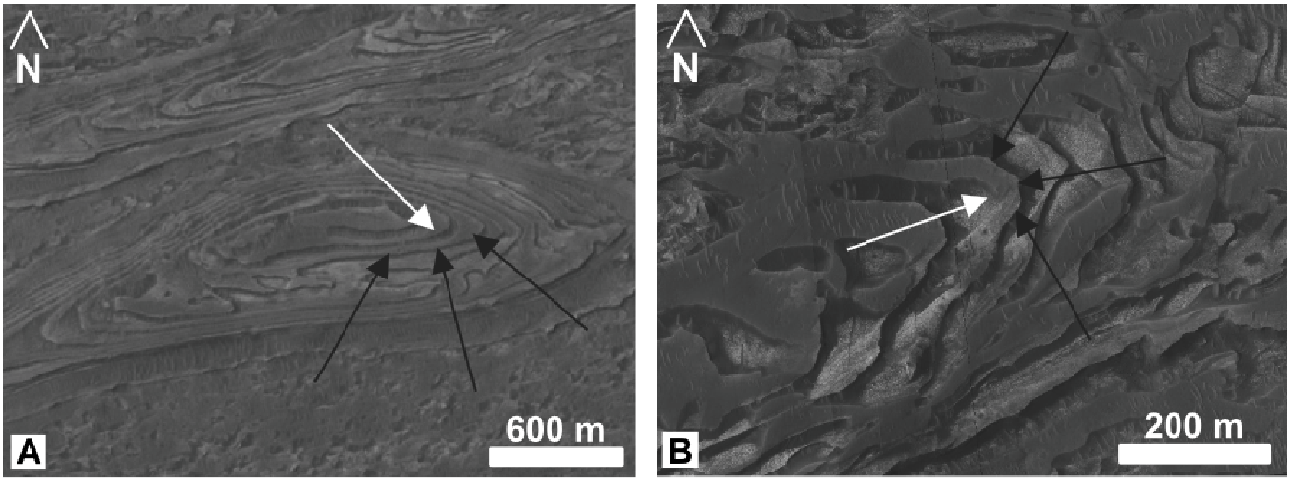

Figure 5. 10. Ridge-and-Through structures in the Southwestern sector of the Crommelin crater (white boxes in figure 4A). A) Elongated ridge-and-trough structure: the white arrow points to the inner part of the ridge-and-trough and the black arrows to the inward-dipping edges (CTX B11_013875_1833). B) Detail of a ridge-and-trough structure, the white arrow points to the ridge-and-trough and the black arrows to the inward-dipping edges. In C and D the dip direction coincides with the north-south direction of the figure. (HiRISE PSP_002021_1850).

5.4.2.2. Conical mounds

Conical mound clusters occur in southern Arabia Terra, centered in the southern sector of Firsoff crater, inside the Southern crater and in the Crommelin northern sector (Figs. 5.1B). The mound occurrences throughout the studied area are exclusive of the ELDs inside the craters. All the conical mounds are ca. 50 to 100 meters high and few hundred meters wide. Where exposed the inner part of the mounds shows clear stratification with strata draping the morphology. However, several smaller mounds (ca. 50 meters high) in the North of Crommelin crater show distinct planar bedding. Common features of these conical mounds are the asymmetry of their flank and the presence of apical hole (Fig. 10). Distribution of the mounds and ellipticity of the mounds base increase toward the South.

The conical mounds at the Crommelin crater (Fig. 5.11A) occur within the lobate ELDs (Fig. 5.6). Collapsed conical structures with a 50 - 30 meters wide diameter, were also described aligned along straight km-long faults in the northern sector of the Crommelin crater (Fig. 5.11B).

The highest density of mound buildups is observed in the southeastern sector of the Firsoff crater (Fig. 5.3B) where the ELDs strata are less scalloped and show thinner stratification respect to the southwestern sector characterized by highly sinuous pattern (Fig. 5.3A) and absence of mounds. The density of the mounds (ranging between 500 and 200 meters in width) in Firsoff crater reaches the value of 20 mounds for km2 (Fig. 5.12). Many of these mounds are characterized by a well-rounded apical hole, local fractures and dikes that branch out from the buildups (Figs. 5.11C and E). A HiRISE based 3D reconstruction (resolution of 1 m/pixel) of the mounds field in figure 5.11 allowed the investigation of the framework of each single mound and related structures (Fig. 5.12). The well-exposed mounds show internal stratification and strong flank asymmetry, with the northward flank steeper than the southward (against the rim) (Figs. 5.12B-E).Using the high-resolution stereo-derived topography and imagery, an orthogonal projections of the ELDs setting was built, from which resulted the strata are significantly folded under the buildups (Fig. 5.11D). The Firsoff crater mounds do not show horizontal stratification and their morphology appear to be inconsistent with remnants generated by wind erosion.

The mounds of the Southern crater have the same morphological characteristics of all the Firsoff mounds except for a major axial elongation (2:1) resulting in an elliptical shape (Fig. 5.13). The density of the mounds in this crater is less than in Firsoff and many solitary mounds are settled on top of the ELDs edges or show a direct mutual connection with the inward-dipping edges of the ridge-and-trough via elongated structures (Fig. 5.13C). As well as the furrows these elongated structures do not follow the maximum dip direction and do not show relation with gravitational events. The mounds, which are normally scattered within the ELDs, in the Southern crater are

aligned along kilometer-long straight faults and anticline. Figure 5.13 shows a group of buildups developed along straight kilometric fractures and/or on top of syncline structures (Fig. 5.13B).

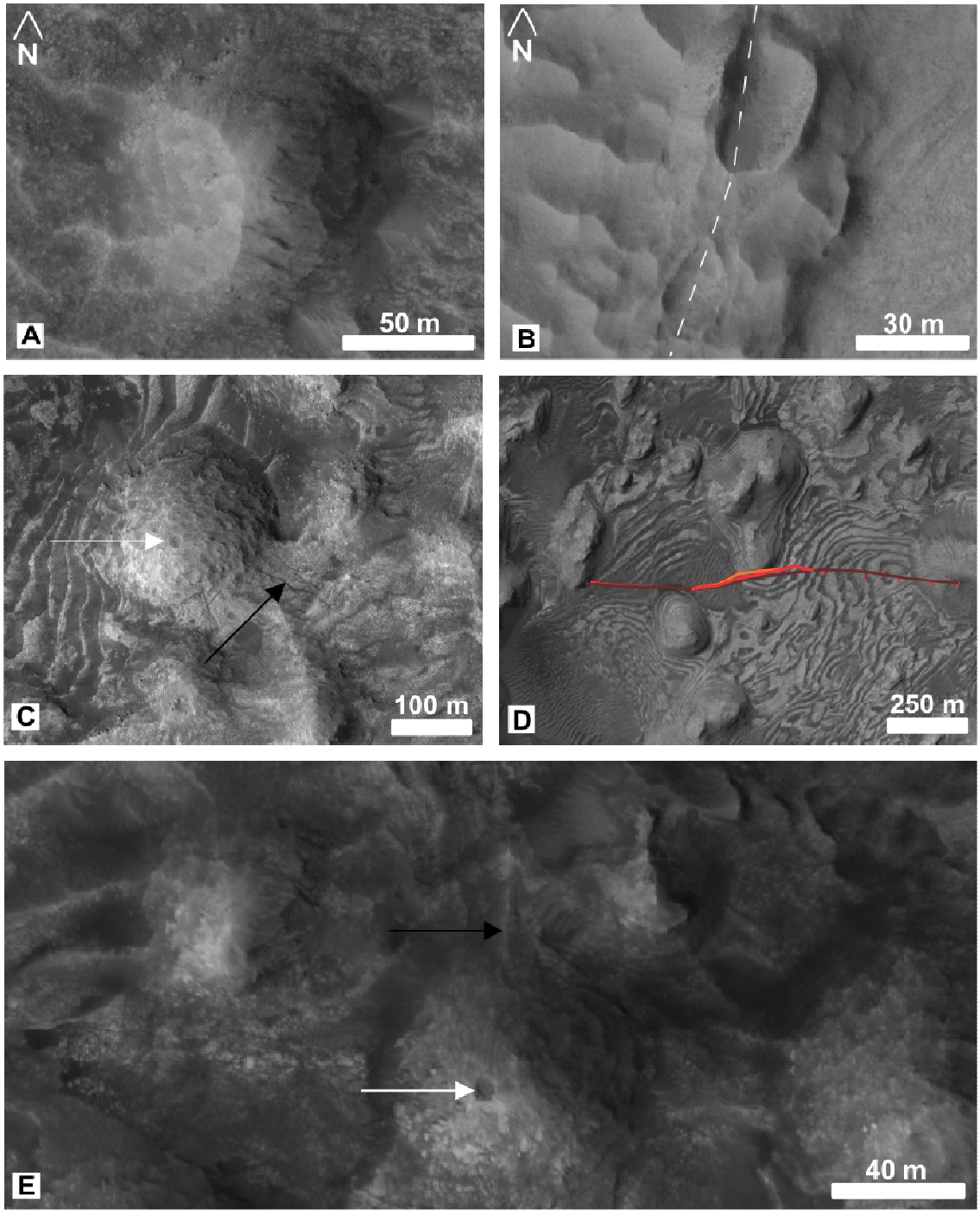

Figure 5. 11. A) Conical mound in the northern sector of Crommelin crater. B) Collapsed conical structure in the northern sector of Crommelin crater. These structures are aligned along straight kilometer-long faults (dotted line). A and B from HiRISE PSP_003432_1850. C) Mound buildups within the ELDs settled on top of a fracture or vein (black arrow) showing a well-rounded apical hole (white arrows) (HiRISE ESP_020679_1820). D) View of the ELDs in the southern sector of the Firsoff crater (8 km southwest to area in A), the colored lines represent the folded strata (anticline structure) under the mound; vertical exaggeration 2:1 (CTX B18_016776_1818). E) Conical mound with an apical hole (white arrow) and dike or vein branching out from the mound base (HiRISE ESP_020679_1820).

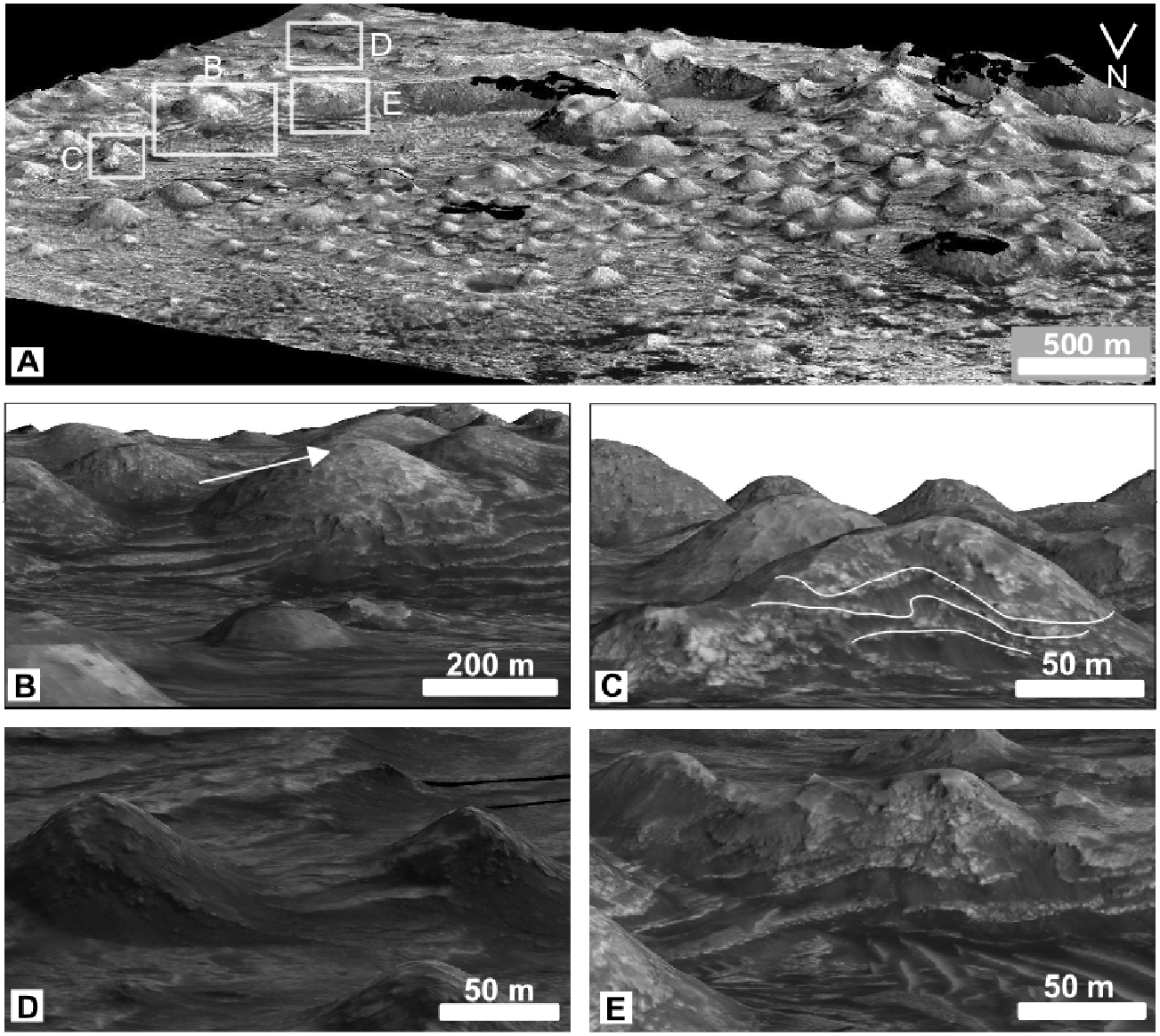

Figure 5. 12. A) Tridimensional reconstruction of the mounds field (same as figure 10A) in the southeastern sector of the Firsoff crater. White boxes outline the areas showed in B, C, D and E. Rim of the crater is on the upper part of the picture. B) Tridimensional view of the mound showed in figure 10B characterized by an apical hole (arrow) settled on top of folded strata. C) Tridimensional view of a mound with exposed internal stratification (white lines). D) Tridimensional view of two mounds where the folded strata drape the mound morphologies. E) Layered strata below a conical mound. (HiRISE ESP_020679_1820)

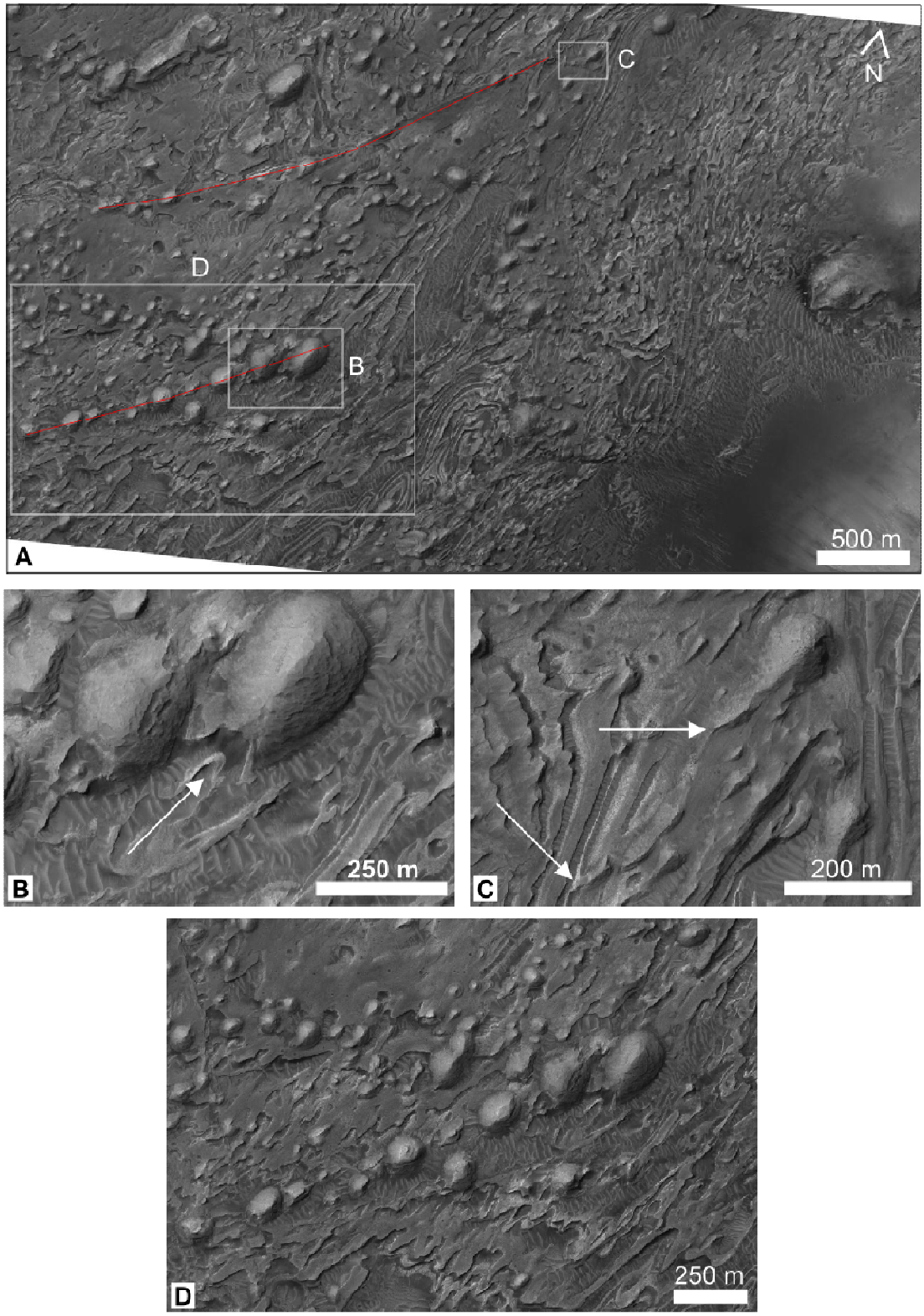

Figure 5. 13. Cluster of conical mounds with circular to elliptical base, Southern crater. A) Mound clusters aligned along kilometric faults (red lines) in the southeastern sector of the crater. Crater rim is on the right of the picture. Details are illustrated in B-D (boxed areas). B) Elliptical mound settled on top of an anticline structure. The white arrow points to the axe of the anticline. C) Elongated structure (arrows) branching out from a isolated mound. D) Mound cluster aligned along a straight fault (ESP_016776_1810).

5.5. DISCUSSION

The detailed geological and morphological study of the Crommelin area ELDs reported a clear distribution of several meso-scale morphologies in the crater lowlands, particularly in the southern sectors of each crater covered by thick package of ELDs.

ELDs are widespread in the whole study area covering almost the 25% of the exposed surface (Fig. 5.1B). From the morphometric equations (Garvin et al., 2003) resulted an enormous amount of sediments within the three craters. Firsoff and Southern craters present an isopachous sediments package whereas Crommelin in the southern sector presents a thicker (500 m) sediments package than the northern sector (Fig. 5.4A, N-S section). This sector of the Crommelin crater is crossed by kilometer-long furrows branching out from the lower part of the crater central bulge. The crater profiles inferred from the morphometric equations indicate that the furrows developed in the sectors with lower inclination (Fig. 5.9) and their direction of elongation do not coincide with the slope dip direction. Hence gravity driven processes can reasonably be excluded as genetic processes for furrows and the related ridge-and-troughs within the ELDs. The more so because the crater central bulge is avoid of gullies and aprons that could be generated by drebris flows and other gravitative events (e.g. Levy et al., 2010).

The ELDs, in the study area, are characterized by presence of diffused conical mounds with asymmetric shape and steep flanks (Figs. 5.11-5.13) some of those have an apical hole. Several mounds in Arabia Terra are seemingly settled on top of tectonic structures (Figs. 5.11B, D and 5.13) and the ELDs folding could have generated fractures along the crest of the anticline where subsequently the mound buildups developed (Fig. 5.13B). These fractures, probably linked with a deep fracture system generated in the impact, could have acted as preferential ways for fluids upwelling (Pondrelli et al., 2011).

The ELDs genetic process are still under debate, anyway some of the depositional processes invoked to explain their origin include sub-glacial volcanism (Chapman and Tanaka, 2001; Komatsu et al., 2004), aeolian/airfall (Malin and Edgett, 2000; Edgett and Malin, 2002), lacustrine deposition (Newsom et al., 2003), lacustrine/volcanic (Ori and Baliva, 1999), spring deposition (Rossi et al., 2008a; 2008b) and mud volcanism (Pondrelli et al., 2011; Oeheler and Allen, 2012).

ELDs were described even in the Vernal crater within a 30 km wide outcrop of high thermal inertia sediments organized in meters thick strata gently dipping to the North (Allen and Oehler, 2008). Two elliptical structures with characteristic high albedo and concentric halos interpreted as spring-related morphologies (Allen and Oeheler, 2008) were exhumed on top of these layered

deposits. The proposed model for development of the Vernal crater mounds involves the groundwater upwelling along the structural and sedimentary preferential ways pumped by the regional hydraulic head (Okubo and McEwen, 2007). ELDs-like strata are also present in the Candor Chasma (Chan et al., 2010; Okubo and McEwen, 2007; Ormö et al., 2004) characterized by the presence of mound (knobs) organized along faults or scattered, and ridge-and-troughs strata pattern (*sensu* Okubo and McEwen, 2007) analogues of the ridge-and-troughs described in this work with inward-dipping edges ascribed to fluid-driven recrystallization. The knobs described by Chan et al. (2010) resemble remnants with some original planar stratification rather than mounds formed by syndepositional fluid migration or escape events. The Candor Chasma mounds have the same size (types 1-2-3) and setting (type 1 knobs aligned along faults) of the ELDs mound buildups and their abrupt shape should involve early lithification (Chan et al., 2010). Anyway the Firsoff mounds do not show remnant features like the “type 1 knobs”. Even if erosional processes are more consistent for most of these knobs, several of them display evidence of fluid movements and injections, such as indurated layers, apical hole, and hydrated sulfates. Mound apical holes have been interpreted as evidence for spring origin (Allen and Oehler, 2008; Clarke et al. 2007; Farrand et al., 2005), fluid seepage (Chan et al., 2010) and/or mud volcanism (Komatsu et al. 2011; Farrand et al., 2005; Oehler and Allen, 2010; Skinner and Mazzini, 2009). Chan et al. (2010) reported the presence of apical hole in the 10% of the “type 2 knobs” (potentially fluid-related buildups), which are the most similar to the ELDs mounds in Arabia Terra, and are characterized by fluid-driven recrystallization and reworking.

The thick package of sedimentary deposits (ELDs) detected across the lowlands of Arabia Terra region, showing morphological similarities with the Meridiani deposits, are the exhumed part of the deposits that once covered a vast area of the martian surface (Zabrusky et al., 2012). These sedimentary deposits, that are both morphologically similar to and in close proximity to the Meridiani deposits, might have formed under Meridiani-like conditions. Thus, this may implies that the hydrological processes responsible for forming the Meridiani deposits (Andrews-Hanna et al., 2007, 2010) were active even in Arabia Terra. Depressions such as Crommelin and Firsoff craters would have filled with Meridiani-type layered sediments due to the migration of the groundwater flow from the highlands (South) to the lowlands (North) (Andrews-Hanna et al., 2010). Due to the regional northward monocline slope in Arabia Terra, the likely rising point of the flow should have been in the southern sector of each crater.

Previous theories refer to local occurrences of layered deposits whereas the regional groundwater upwelling theory explains the occurrence of ELDs throughout the Meridiani Planum and Arabia Terra (Allen and Oheler, 2008; Andrews-Hanna et al., 2007, 2010; Michalski et al., 2013; Zabrusky et al., 2012). Cyclic fluids upwelling were supposed to generate evaporites and/or layered deposits (e.g. playa deposits) and thus triggered the early lithification of lose sediments (Andrews-Hanna et al., 2007, 2010; Grotzinger et al., 2005: Murchie et al., 2009) preserving mounds and other morphologies that otherwise would have been consumed by eolian erosion over geological timescales.

Layering of sediments could be generally due to periodical fluctuation of the groundwater flow similar to the one described by Lewis et al. (2008) and Zabrusky et al. (2012) in the Becquerel Crater (Arabia Terra) and it could be strongly suggestive of climatic control, and be consistent with a climatic modulation of the precipitation and evaporation flux able to drive variations in the groundwater upwelling and evaporation rates (Andrews-Hanna et al., 2010). The periodical rise of the water table should have triggered the early lithification of the loose sediments and deposed thick package of hydrate rocks. Analogue process was invoked by Zabrusky et al. (2012) to describe the genesis of peculiar knobs occurring within the layered deposits in Meridiani Planum.

5.6. TERRESTRIAL ANALOGUES

In the last years hydrothermal activity and fluids seepage were identified as the most attractive features on Mars for the astrobiologists due to their intrinsic relation with fluid and supposed high preservation potential of life signatures. Hydrothermal vents and related buildups on Earth represent the perfect laboratory for studying past and present microbial life (Campbell, 2006) because many of the most primitive organisms are supposed to be hyperthermophiles, which implies that the arise of early life on Earth could have started in hydrothermal environments (Allen and Oehler, 2008 and citations therein). Hydrothermal activity has many implications: from a general point of view the fluids-sediment interaction influences the biological activity, increases the potential of preservation of biological signatures and forms peculiar morphologies such as mounds, knobs, evaporitic sediments, etc. The mud mounds are well-documented microbial-related morphologies and could be influenced by hydrothermal activity on Earth and are important analogues for astrobiological study, the more so because of the discovery of mounds clusters on Mars.

Terrestrial mounds may have different origins spanning from mud volcanism to microbial activity (Riding, 2002) and all of them are characterized by strong potential of preservation and

abundant biological activity (Campbell, 2006). The Kess Kess mounds, broadly described in chapter 2, represent suitable morphological analogues of the mounds described in the Crommelin region and a powerful tool for astrobiological research. The stabilization of the steep flanks of these mounds should have involved early lithification of the sediments induced by fluid circulation (see chapter 2) and probably triggered by microbial activity (Chafetz and Buczynski, 1992). Some of the morphological features in common between the Kess Kess and the Martian buildups are shown in figure 5.14 (see also fig. 5.12 for a comparison): conical shape, asymmetry (steeper flak down-slope) and internal layering. Veins and fractures (see figure 2.5, pag 18), are widespread structures both in the Kess Kess and Arabia Terra mounds, and probably they were the likely way for fluid seepage (Okubo and McEwen, 2007).

A regional groundwater upwelling scenario, analogs of the one described in Arabia Terra, was described in the Dalhouise region (central Australia). In the Dalhouise region where the groundwater flux, driven by topography, reaches the surface, deposition of evaporitic deposits occurs, and the deposition is coupled with positive morphologies like conical mounds and spring mounds. Furthermore in the Dalhouise elongated and narrow channels branch out of the spring mound buildups suggesting a water circulation analogues of the one described in Crommelin crater with “flow-channels” and pools. Due to the authigenic carbonates strong potential of preservation the Dalhouise mounds abound of microbial signatures and micro-morphologies (Clarke et al., 2007, 2009). This region, in which water circulation, formation of authigenic minerals and Mars analog morphologies co-exist, was already proposed by Mann et al. (2004) as a potential terrestrial analogues for astrobiological purposes.

5.7. CONCLUSIONS

Arabia Terra and Meridiani Planum are two of the few zones interested by deposition of layered deposits and not buried by younger geological units, such as flood basalts (Fig. 5.1). Therefore the ELDs in Crommelin area represent clear examples of how the geological processes, at the Noachian-Hesperian transition, shift and gave rise to mass deposition of sedimentary rocks accompanied by peculiar morphologies. Several studies proposed these particular geomorphological setting as generated by a long wave-length groundwater upwelling. Where the groundwater reached the surface the sediments package is thicker (Fig. 5.2) and the ELDs are characterized by abundant prominent morphologies such as furrows and mounds.

The ELDs coupled with furrows, ridge-and-trough and mounds are present merely inside the craters. In all the crater studied mound clusters were described aligned along the crater rims or along straight faults. Thus their origin could have been triggered by the deep fractures system originated during the impact. If mounds could be evidence of deep water upwelling, furrows and ridge-and-troughs structures could be likely evidences of surface processes, probably due to the water stagnation in the lower and flat topography. Hence, the groundwater flowing through the fractures induced by the impact reached the surface and gave rise to the mound clusters, then the water filled the flat bottom of the crater and generated furrows and ridge-and-trough structures during the water table standstill. As a result of the arid climate assumed in the models, groundwater reaching the surface, in the crater lowland, will evaporate and leave behind evaporitic deposits and cemented the loose sediments that were infiltrated by the rising groundwater table and indurated into an erosion resistant deposit. This upwelling/evaporation system was triggered by a regional long-wavelength groundwater flow, with upwelling centered in the topographic depressions.

Despite the estimated high sedimentation rate the discharge was maintained even when the depressions have been filled with sediment, because the hydraulic head was maintained. If upwelling-evaporation system was maintained the discharge migrated toward the lowlands with consequent migration of the depocenter from Meridiani to Crommelin. As a matter of facts the study area is topographically below Meridiani Planum and the assumed static water table model implies a migration of the groundwater upwelling seepage southeastward to the highlands after the lowlands filling.

Despite on Mars detailed mineralogical and petrographic analyses are lacking from the images database emerged clear morphological analogies between the Crommelin mounds and terrestrial conical mounds. Thus improvement of knowledge about the terrestrial mounds may give new insights about the geochemical processes that gave rise to analogues morphologies on Mars. Further analyses on the Dalhouise mounds, for example, could clarify how the groundwater upwelling influence the activity of microbial communities and how the biological signatures are preserved within carbonate conical mounds.

The data discussed in chapter 2 and 4 for the Kess Kess prove that the particular environmental condition that sustained the development of Kess Kess mounds were preserved in the rocks record as geochemical signatures and could be studied with proper analytical tools. Therefore terrestrial conical mounds are suitable geological and geochemical laboratories for the study of the sediment-water-life interaction as it is on Earth and may be on Mars.

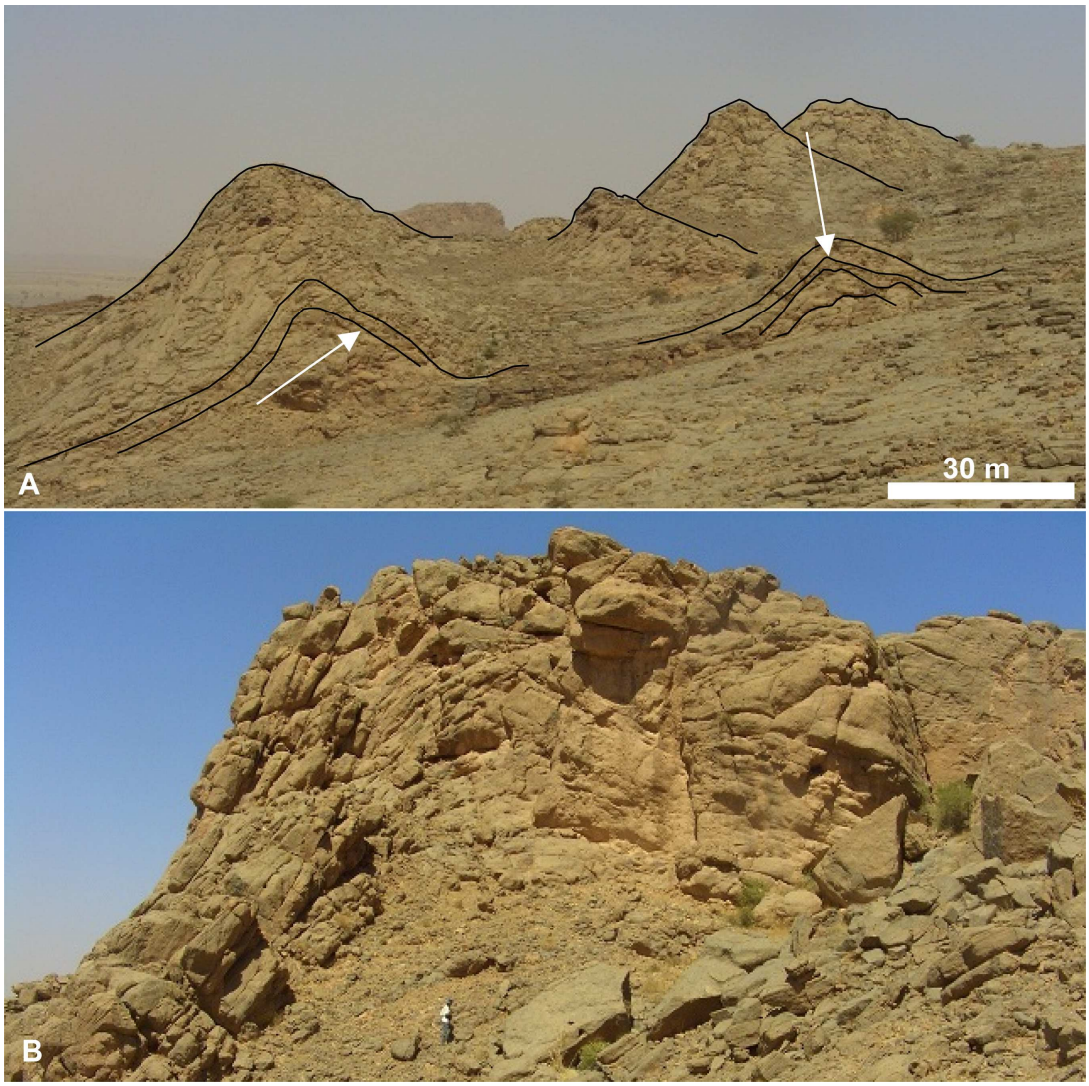

Figure 5. 14. Panoramic view of the Hamar Laghdad ridge with some well exposed conical mound. A) Example of several mounds dissected bya fault showing the internal stratification (black lines) draping the mound buildup (arrows) B) One of the rare Kess Kess cutted in a half showing the core facies, the inner stratification draping the morphology, the conical shape and the strong asymmetry with the steeper down-slope flank (man for scale) (N31° 22' 37.3'' W4° 02' 35.9'').

REFERENCES

Aitken, S.A., Collom, C.J., Henderson, C.M., Johnston, P.A., 2002. Stratigraphy, paleoecology, and origin of Lower Devonian (Emsian) carbonate mud buildups, Hamar Laghdad, eastern Anti-Atlas, Morocco, Africa. Bulletin of Canadian Petroleum Geology 50, 217-243.

Andrews-Hanna, J., Phillips, R., Zuber, M., 2007. Meridiani Planum and the global hydrology of Mars. Nature 446, 163-166.

Andrews-Hanna, J.C., Zuber, M.T., Arvidson, R.E., Wiseman, S.M., 2010. Early Mars hydrology: Meridiani playa deposits and the sedimentary record of Arabia Terra. Journal of Geophysical Research 115, E06002.

Allen, C.C., Oehler, D.Z., 2008. A case for ancient springs in Arabia Terra, Mars. Astrobiology 8 (6), 1093–1112.

Arvidson, R.E., Poulet, F., Morris, R. V., Bibring, J.-P., Bell III, J. F., Squyres, S. W., Christensen, P.R., Bellucci, G., Gondet, B., Ehlmann, B.L., Farrand, W.H., Fergason, R.L., Golombek, M., Griffes, J.L., Grotzinger, J., Guinness, E.A., Herkenhoff, K.E., Johnson, J.R., Klingelhöfer, G., Langevin, Y., Ming, D., Seelos, K., Sullivan, R.J., Ward, J. G., Wiseman, S.M., Wolff, M., 2006. Nature and origin of the hematite-bearing plains of TerraMeridiani based on analyses of orbital and Mars Exploration rover data sets. J. Geophys. Res. 111. http://dx.doi.org/10.1029/2006JE002728.

Burr, D.M., Tanaka, K.L., Yoshikawa, K., 2009. Pingos on Earth and Mars. Planetary and Space Science 57, 541-555.

Burt, D.M., Knauth, L.P., 2003. Electrically conducting, Ca-rich brines, rather than water, expected in the Martian subsurface. J. Geophys. Res. 108, 8026.

Campbell, K.A., 2006. Hydrocarbon seep and hydrothermal vent palaeoenvironments and paleontology: past developments and future research directions. Palaeogeogr. Palaeoclimatol. Palaeoecol. 232, 362-407.

Chafetz, H.S., Buczynski, C. 1992. Bacterially induced lithification of microbial mats. *Palaios 7*, 277–293. DOI 10.2307/3514973

Chan, M.A., Ormö, J., Murchie, S., Okubo, C.H., Komatsu, G., Wray, J.J., McGuire, P., McGovern, J.A., 2010. Geomorphic knobs of Candor Chasma, Mars: New Mars Reconnaissance Orbiter data and comparisons to terrestrial analogs. Icarus 205, 138-153.

Chapman, M.G., Tanaka, K.L., 2001. Interior trough deposits on Mars: subice volcanoes? Journal of Geophysical Research: Planets 106, 10087-10100.

Clarke, J.D.A., Bourke, M., Nelson, P., Manga, M., Fonseca, J., 2007. The Dalhousie Mound Spring Complex as a guide to Martian Landforms, Processes, and Exploration. Proceedings 7th Australian Mars Exploration Conference, Perth, Western Australia.

Clarke, J.D.A., Bourke, M.C., 2009. Recognition criteria of spring deposits on Mars at all scales: evidente fromthe Dalhouise Springs analog (Australia). 40th Lunar Planetary Science Conference, Houston, Texas, [1102].

Crumpler, L.S., 2003a. Physical characteristics, geologic setting, and possible formation processes of spring deposits on Mars based on terrestrial analogs. 6th International Conference on Mars, Lunar and Planetary Institute, Houston, Texas [3228].

Crumpler, L.S., 2003b. Spring deposits on Mars: physical processes from terrestrial analogs. 6th International Conference on Mars, Lunar and Planetary Institute, Houston, Texas [2002].

de Pablo, M.A., Komatsu, G., 2007. Pingo fields in the Utopia Basin, Mars: geological and climatic implications. 38th Lunar Planetary Science Conference, Houston, Texas [1278].

Dohm, J.M., Tanaka, K.L., Hare, T. M., 2001. Paleotectonic Map of the Thaumasia Region, Mars. USGS, Geologic Investigation Series I–2650, Atlas of Mars: Thaumasia Region, Sheet 2 of 3.

Edgett, K. S. and M. Malin, 2002. Martian sedimentary rock stratigraphy: Outcrops and interbedded craters of northwest Sinus Merdiani and southwest Arabia Terra. Geophysical Research Letters 29 (24), 2179, doi:10.1029/2002GL016515.

Edgett, K. S. 2005. The sedimentary rocks of Sinus Meridiani: Five key observations from data acquired by the Mars Global Surveyor and Mars Odyssey orbiters. Mars 1, 5-58, 2005. doi:10.1555/mars.2005.0002

Ehlmann, B. L., Mustard, J.F., Murchie, S.L., Poulet, F., Bishop, J.L., Brown, A.J., Calvin, W.M., Clark, R.N., Des Marais, D.J., Milliken, R.E., Roach, L.H., Roush, T.L., Swayze, G.A., Wray, J.J., 2008. Orbital identification of carbonate-bearing rocks on Mars. Science 322, 1828-1832, doi:10.1126/science.1164759.

Ehlmann, B. L., Mustard, J.F., Murchie, S.L., 2010. Geologic setting of serpentine deposits on Mars. Geophysical research letters 37, L06201, doi:10.1029/2010GL042596.

Ehlmann, B.L., Mustard, J.F., Murchie, S.L., Bibring, J.-P., Meunier, A., Fraeman, A.A. Langevin, Y., 2011. Subsurface water and clay mineral formation during the early history of Mars. Nature 479, 53-60, doi: 10.1038/nature10582.

Farrand, W.H., Gaddis, L.R., Keszthlyi, L., 2005. Pitted cones and domes on Mars: Observations in Acidalia Planitia and Cydonia Mensae using MOC, THEMIS, and TES data. Journal of Geophysical Research 110 E05005. doi:10.1029/2004JE002297.

Fassett, C.I., Head, J.W., 2008. The timing of martian valley network activity: Constraints from buffered crater counting. Icarus 195, 61-89.

Garvin, J. B., S. E. H. Sakimoto, Schnetzler, C., Frawl, J.J., 1999. Global geometric properties of martian impact craters: A preliminary assessment using Mars Orbiter Laser Altimeter (MOLA) topography. 5th International Conference on Mars, Pasadena, California. [6163]

Garvin, J.B, Frawley, J.J., Sakimoto, S.E.H., Schnetzler, C., 2000. Global geometric properties of Martian impact craters: an Assessment from Mars Orbiter Laser Aaltimeter (MOLA) Digital Elevation Models. 31st Lunar and Planetary Science Conference, Houston, Texas. [1619]

Garvin, J. B., Sakimoto, S. E. H., Frawley, J.J., Schnetzler, C., 2002. Global Geometric Properties of Martian Impact Craters. 33rd unar and Planetary Science Conference, Houston, Texas. [1255]

Garvin, J.B., Sakimoto, S.E.H., Frawley, J.J., 2003. Craters on Mars: global geometric properties from gridded MOLA topography. 6th International Conference on Mars, Pasadena, California. [3277]

Glotch, T. D., Christensen, P. R., 2005. Geologic and mineralogic mapping of Aram Chaos: Evidence for a water-rich history. Journal of Geophysical Research 110, E09006, doi:10.1029/2004JE002389.

Glotch, T. D., Rogers, A. D., 2007. Evidence for aqueous deposition of hematite□ and sufate□rich light□toned layered deposits in Aureum and Iani chaos, Mars. Journal of Geophysical Research 112, E06001, doi:10.1029/ 2006JE002863.

Greeley, R., Fagents, S. A., 2001. Icelandic pseudocraters as analogs to some volcanic cones on Mars. Journal of Geophysical Research 106 (20), 527-546.

Griffes, J. L., Arvidson, R. E., Poulet, F., Gendrin, A., 2007. Geologic and spectral mapping of etched terrain deposits in northern Meridiani Planum. Journal of Geophysical Research 112, E08S09, doi:10.1029/2006JE002811.

Grotzinger, J., Arvidson, R., Bell III, J., Calvin, W., Clark, B., Fike, D., Golombek, M., Greeley, R., Haldemann, A., Herkenhoff, K., 2005. Stratigraphy and sedimentology of a dry to wet eolian depositional system, Burns formation, Meridiani Planum, Mars. Earth Planetary Science Letters 240, 11-72.

Hartmann, W.K., Neukum, G., 2001. Cratering chronology and the evolution of Mars. Space Science Review 96, 165-194.

Hynek, B.M., Arvidson, R.E., Phillips, R.J., 2002. Geologic setting and origin of Terra Meridiani hematite deposit on Mars. Journal of Geophysical Research 107, 11-18.

Keszthelyi, L.P., Jaeger, W.L., Dundas, C.M., Martínez-Alonso, S., McEwen, A.S., Milazzo, M.P.,

2010. Hydrovolcanic features on Mars: Preliminary observations from the first Mars year of HiRISE imaging. Icarus 205, 211-229.

Komatsu, G., Ori, G.G., Ciarcelluti, P., Litasov, Y.D., 2004. Interior layered deposits of Valles Marineris, Mars: analogous subice volcanism related to Baikal Rifting, Southern Siberia. Planetary and Space Science 52 (1–3), 167-187. 10.1016/j.pss.2003.08.003.

Komatsu, G., Ori, G.G., Cardinale, M., Dohm, J.M., Baker, V.R., Vaz, D.A., Ishimaru, R., Namiki, N., Matsui, T., 2011. Roles of methane and carbon dioxide in geological processes on Mars. Planetary and Space Science 59, 169-181.

Lanagan, P. D., McEwen, A. S., Keszthelyi, L. P., Thordarson, T., 2001. Rootless cones on Mars indicating the presence of shallow equatorial ground ice in recent times, Geophysical Research Letters 28, 2365-2367.

Levy, J., Head, J., Marchant , D., 2009. Thermal contraction crack polygons on Mars: Classification, distribution, and climate implications from HiRISE observations. Journal of Geophysical Research 114, E01007.

Levy, J.S., Marchant, D.R., and Head, J.W., 2010, Thermal contraction crack polygons on Mars: A synthesis from HiRISE, Phoenix, and terrestrial analog studies: Icarus 206, 229-252.

Lewis, K.W., Aharonson, O. Grotzinger, J.P., Kirk, R. L., McEwen, A.S., Suer, T.A., 2008. Quasi-periodic bedding in the sedimentary rock record of Mars. Science 322, 1532-1535. doi:10.1126/science.1161870.

Malin, M., Edgett, K., 2000. Sedimentary rocks of early Mars. Science 290, 1927.

Malin, M.C., Bell III, J.F., Cantor, B.A., Caplinger, M.A., Calvin, W.M., Clancy, R.T., Edgett, K.S., Edwards, L., Haberle, R.M., James, P.B., Lee, S.W., Ravine, M.A., Thomas, P.C., Wolff, M.J., 2007. Context Camera Investigation on board the Mars Reconnaissance Orbiter. J. Geophys. Res. 112, E05S04. doi:10.1029/2006JE002808.

Mann, G.A., Clarke, J.D.A., Gostin, V.A., 2004. Surveying for Mars Analogue Research Sites in the Central Australian Deserts. Australian Geographical Studies 42 (1), 116–124.

Mounji, D., Bourque, P.A., Savard, M.M., 1998. Hydrothermal origin of Devonian conical mounds (kess-kess) of Hamar Lakhdad Ridge, Anti- Atlas, Morocco. Geology 26, 1123-1126.

McEwen, A.S., Eliason, E.M., Bergstrom, J.W., Bridges, N.T., Hansen, C.J., Delamere, W.A., Grant, J.A., Gulick, V.C., Herkenhoff, K.E., Keszthelyi, L., Kirk, R.L., Mellon, M.T., Squyres, S.W., Thomas, N., Weitz, C.M., 2007. Mars Reconnaissance Orbiter's High Resolution Imaging Science Experiment (HiRISE). J. Geophys. Res. 112, E05S02. doi:10.1029/2005JE002605.

McLennan, S. M., Bell III, J.F., Calvin, W.M., Christensen, P.R., Clark, B.C., de Souza, P.A.,

Farmer, J., Farrand, W.H., Fike, D.A., Gellert, R., Ghosh, A., Glotch, T.D., Grotzinger, J.P., Hahn, B., Herkenhoff, K.E., Hurowitz, J.A., Johnson, J.R., Johnson, S.S., Jolliff, B., Klingelhöfer, G., Knoll, A.H., Learner, Z., Malin, M.C., McSween Jr., H.Y., Pocock, J., Ruff, S.W., Soderblom, L.A., Squyres, S.W., Tosca, N.J., Watters, W.A., Wyatt, M.B., Yen, A., 2005. Provenance and diagenesis of the evaporite-bearing Burns formation, Meridiani Planum, Mars. Earth Planetary Science Letters 240, 95-121, doi:10.1016/j.epsl.2005.09.041.

McLennan, S.M., Sephton, M.A., Allen, C., Allwood, A.C., Barbieri, R., Beaty, D.W., Boston., P., Carr, .M, Grady, M., Grant, J., Heber. V.S., Herd, C.D.K., Hofmann, B., King, P., Mangold, N., Ori., G.G., Rosii, A.P., Raulin, F., Ruff, S.W., Sherwood Lollar, B., Symes, S., Wilson, M.G., 2011. Planning fo Mars returned sample science: final report of the MSR End-to-End International Science Analysis Group (E2E-Isag). Astrobiology 12, 175-300.

Mellon, M.T., 1997. Small-scale polygonal features on Mars: Seasonal thermal contraction cracks in permafrost: Journal of Geophysical Research– Planets 102, 25,617–25,628.

Michalski, J.R., Cuadros, J., Niles, P.B., Parnell, J. Rogers, A.D., Wright, S.P., 2013. Groundwater activity on Mars and implications for a deep biosphere. Nature Geoscience 6, 133-138. doi:10.1038/ngeo1706

Moratto, Z.M., Broxton, M.J., Beyer, R.A., Lundy, M., Husmann, K., 2010. Ames Stereo Pipeline, NASA's Open Source Automated Stereogrammetry Software. 41st Lunar and Planetary Institute Science Conference, Houston, Texas [2364].

Murchie, S. L., Roach, L., Seelos, F., Milliken, R., Mustard, J., Arvidson, R., Wiseman, S., Lichtenberg, K., Andrews-Hanna, J., Bishop, J., Bibring, J., Parente, M., Morris, R., 2009. Evidence for the origin of layered deposits in Candor Chasma, Mars, from mineral composition and hydrologic modeling. Journal of Geophysical Research 114, E00D05. doi:10.1029/2009JE003343.

Newsom, H.E., Barber, C.A., Hare, T.M., Schelble, R.T., Sutherland, V.A., Feldman, W.C., 2003. Paleolakes and impact basins in southern Arabia Terra, including Meridiani Planum: implications for the formation of hematite deposits on Mars. Journal of Geophysical Research 108, 8075.

Noe Dobrea, E. Z., Poulet, F., Malin, M. C., 2008. Correlations between hematite and sulfates in the chaotic terrain east of Valles Marineris. Icarus 193, 516-534, doi:10.1016/j.icarus.2007.06.029.

Oehler, D.Z., Allen, C.C., 2010. Evidence for pervasive mud volcanism in Acidalia Planitia, Mars. Icarus 208, 636-657.

Oehler, D. Z., and Allen, C. C., 2012, Giant Polygons and Mounds in the Lowlands of Mars: Signatures of an Ancient Ocean? Astrobiology 12 (6), 1-15. doi:10.1089/ast.2011.0803

Okubo, C.H., McEwen, A.S., 2007. Fracture-Controlled Paleo-Fluid Flow in Candor Chasma, Mars. Science 315, 983-985. doi: 10.1126/science.1136855

Okubo, C.H., Lewis, K.L., McEwen, A.S., Kirk, R.L., 2008. Relative age of interior layered deposits in southwest Candor Chasma based on high-resolution structural mapping. J. Geophys. Res. 113, E12002. doi:10.1029/2008JE003181.

Ori, G.G., Baliva, A., 1999. Large bulges at the center of impact craters on Mars. 30th Lunar and Planetary Science Conference, Huston, Texas [1758].

Ormö, J., Komatsu, G., Chan, M.A., Beitler, B., Parry, W.T., 2004. Geological features indicative of processes related to the hematite formation in Meridiani Planum and Aram Chaos, Mars: A comparison with diagenetic hematite deposits in southern Utah, USA. Icarus 171, 295-316. doi:10.1016/j.icarus.2004.06.001.

Pondrelli, M., Rossi, A.P., Ori, G.G., van Gasselt, S., Praeg, D., Ceramicola, S., 2011. Mud volcanoes in the geologic record of Mars: The case of Firsoff crater. Earth and Planetary Science Letters 304 (3-4), 511-519.

Riding, R., 2002. Structure and composition of organic reefs and carbonate mud mounds; concepts and categories. Earth-Sciences Reviews 58, 163–231.

Rossi, A.P., Neukum, G., Pondrelli, M., Zegers, T., Mason, P., Ori, G.G., Fueten, F.,Oosthoek, J., Chicarro, A., Foing, B., 2007a. The case for a large-scale spring deposits on Mars: light-toned sediments in crater bulges, Valles Marineris and chaos. 38th Lunar and Planetary Science Conference, Houston, Texas, [1549].

Rossi, A.P., Neukum, G., Pondrelli, M., Van Gasselt, S., Zegers, T., Hauber, E., Chicarro, A., Foing, B., 2008a. Large-scale spring deposits on Mars? Journal of Geophysical Research 113, E08016.

Rossi, A.P., Pondrelli, M., Van Gasselt, S., Zegers, T., Hauber, E., Neukum, G., 2008b. Gale crater bulge: a candidate multi-stage large spring mound. 39th Lunar and Planetary Science Conference, Houston, Texas [1611].

Scott, D., Tanaka, K., 1986. Geologic map of the western equatorial region of Mars. US Geol. Surv. Misc. Invest. Ser., Map I-1802-A.

Skinner Jr., J., Tanaka, K.L., 2007. Evidence for and implications of sedimentary diapirism and mud volcanism in the southern Utopia highland-lowland boundary plain, Mars. Icarus 186, 41-59.

Skinner Jr., J., Mazzini, A., 2009. Martian mud volcanism: terrestrial analogs and implications for formational scenarios. Marine Petroleum Geology 26, 1866-1878.

Tanaka, K.L., 1986. The stratigraphy of Mars, in Lunar and Planetary Science Conference, 17th, Houston, Texas. Proceedings, pt. 1: Journal of Geophysical Research 91 (B13), E139–E158.

Walter, M.R. and Des Marais, D.J., 1993. Preservation of Biological Information in the Thermal Spring Deposits: Developing a Strategy for Search of Fossil Life on Mars. Icarus 101, 129-143.

Zabrusky, K., Andrews-Hanna, J.C., Wiseman, S.M., 2012. Reconstructing the distribution and depositional history of the sedimentary deposits of Arabia Terra, Mars. Icarus 220 311-330.

6. GENERAL CONCLUSIONS

Since the Devonian Kess Kess mounds were first described in the Hamar Laghdad Ridge (Anti-Atlas, Morocco), a lively debate has surrounded the hypothesis about their origin. Although after the discovery of the first chemosynthetic communities a hydrothermal origin for these mounds was proposed, currently they are still considered controversial vent deposits. This study combines an updated research review with detailed field investigations and new analytical results aimed at defining a more complete scenario about the origin of the Kess Kess mounds. It also includes an updated discussion on the effects of hydrothermal fluids circulation through sediments, as well as a discussion on their astrobiological potential. Because of their well-documented morphologies and their relationship with the hydrothermal activity, the Kess Kess mounds could represent reliable analogues useful for astrobiological studies, the more so because many mound clusters were discovered on the Martian surface.

In the first part of this thesis the Kess Kess conical mounds were described and a detailed genetic model intended to provide answers to still open questions, such as the nature of their interaction with hydrothermal fluids. This goal was achieved with the combination of field survey in the Hamar Laghdad Ridge and laboratory analyses carried on samples from the Merzane volcanic breccia and from the Seheb el Rhassel Group which also includes the Kess Kess buildups (chapter 2). Overall, a full set of petrographic, mineralogical, chemical, geochemical, and paleobiological features from the different carbonate type of the mounds and infra-mounds deposits, and for the volcanic breccia were discussed to strengthen the Kess Kess genetic framework. The new data allowed a distinction between the effect of hydrothermal advection that influenced the stable isotopes composition and the mineralogical composition of the limestone.

1- The distribution of the temperature values extrapolated from the isotopic compositions of the Seheb el Rhassel Group attests that during the deposition of the primary micrite the water temperature was approx. 40-45°C. The $\delta^{18}O$ values of micrite sampled from the Kess Kess mounds were more depleted than those measured in the underlying strata. This probably depends on a direct precipitation of the micrite from heated fluids that reached the surface during the mounds development. At the stratigraphic level of the mounds, however, there is a pronounced excursion to less negative $\delta^{18}O$ values moving from the mounds to the infra-mound areas that localized the fluid advection in the mounds occurrence. The isotopic data set allowed to infer that $\delta^{13}C$ values in the Kess Kess mounds appear not sufficiently depleted to be directly attributable to methane derived CO_2; alternatively, the $\delta^{13}C$ values could be related to the contribution of hydrothermal crustal CO_2 ($\delta^{13}C \sim -7‰$).

2- The consistence of this low-temperature hydrothermalism cyclically activated during the Devonian in the Tafilalt Platform was tracked by the occurrence in different stratigraphic levels of secondary potentially hydrothermal minerals and structures, such as: 1) low-Si olivine-rich basaltic breccia cemented by quartz, clinochlore and anatase (Merzane Group); 2) two levels of silicized trilobite skeletal remains in the Seheb el Rhassel Group (Emsian) and in the overlying Bou Tchrafine Group (Eifelian); 3) several generations of mounds in the Emsian (the Kess Kess) and Eifelian (Hollard Mound) up to the Frasnian (minor vents) with faunal associations adapted to particular environmental conditions (scutellid trilobites, vents ostracods and thermophilic corals) 4) chimney-like structures with goethite, quartz and euhedral dolomite.

In the second part of the thesis we described a Middle Devonian mounds cluster exhumed in the Maïder Basin (chapter 3) and then compared these mounds with the Kess Kess. Although both these mound clusters developed within an intracratonic basin along the African northern margin during Devonian, their geological setting and mineralogical compositions are different. Our results suggest that the Kess Kess were strongly influenced by the volcanic breccia underlying the Seheb el Rhassel Group, whereas in the Maïder Basin a volcanic-derived heating flux was lacking and minero-petrographic evidences of fluids circulation and mineral alteration are less abundant. In addition, reef builders macroinvertebrate guilds were founded in the Maïder Basin mounds and, therefore, biological activity appears to be a main cause for the mounds development.

The third part of this thesis (chapter 5) was aimed to improve the understanding of how certain conical mounds developed on Mars and what these mounds could potentially tell us on early Mars. To achieve this goal we have used terrestrial hydrothermalism as an analog for the formation of conical mounds and furrows described in the Crommelin and Firsoff craters (Arabia Terra, Mars). This area is covered by Equatorial Layered Deposits (ELDs) described in literature as potential fluids related sediments bounded by volcanic rocks. The ELDs were deposited in a regional long wavelength groundwater upwelling system. The groundwater migrating through Mars equatorial lowlands reached the surface in the depressions, such as Crommelin and Firsoff craters, and deposited a considerable amount of sediments and catalyzed the early lithification of the conical mounds. Within the ELDs we described peculiar landforms such as pools, furrows and mounds, that because of their shape and geometry we interpreted as morphologies potentially related.to fluid escapes. The conical mounds in Arabia Terra were studied with particular emphasis and thanks to a detailed imagines database we outlined common features between these Martian mounds and the terrestrial carbonate mounds such as the internal bedding, the asymmetric shape, the size fo the buildups, the links with veins and dikes and the steep flanks.

The multidisciplinary approach to the study of different mounds clusters on Earth and the further comparison with Mars mounds provided additional value to the study of ancient terrestrial extreme environments. The new data acquired on the the Kess Kess revealed that the limestones preserved evidences of hydrothermal activity and the comparison of these mounds with the Martian mounds suggested that the physical components that contribute to the growth of hydrothermal mounds on Earth are consistent with Arabi Terra geological setting. This study warrants further consideration of hydrothermalism as a extensive geologic process on Mars suggesting that conical mounds on Mars are suitable sites for astrobiological study.

AKNOWLEDGEMENTS

I would like to thank my supervisor that introduced me to the Red Planet, and Barbara Cavalazzi for her help during the submission of the paper on the Kess Kess genesis, I have learned a lot! I also thank Mena Shemm-Gregory (University of Coimbra) for her foundamental contribution during the preparation of the paper on “my brachiopod”. Then, I would like to thank Luca Martire (University of Torino) for his valuable advices, Daniela Fontana (University of Modena and Reggio Emilia), Giorgio Gasparotto (Univeristy of Bologna), Catherine Pierre and Giovanni Aloisi (University Pierre at Marie Curie), Christian Reinke and Eve Fisher (University of Johannesburg) for their valuable scientific support and technical assistance. And finally I would thank my colleagues that shared with me these three years.

Then I would like to thanks my parents for their support during all these years. And last but not the least, I would like to thank Vera... and myself.

LIST OF PUBBLICATIONS

Journal paper

Franchi, F., Cavalazzi, B., Pierre, C., Barbieri, R., 2012. Influence of hydrothermal processes in the genesis and development of the Devonian Kess Kess mounds (Anti-Atlas, Morocco). Sedimentary Geology, SUBMITTED.

Fanti, F., Contessi, M., **Franchi, F.**, 2012. The "Continental Intercalaire" of southern Tunisia: stratigraphy, paleontology, and paleoecology. Journal of African Earth Sciences, 73-74C, pp. 1-23.

Franchi, F., Schemm-Gregory, M. and Klug, C., 2011. A new species of *Ivdelinia* Andronov, 1961 from the Moroccan Givetian and its palaeoecological and palaeobiogeographical implications**.** Bullettin of Geosciences, vol. 87 (1), pp. 1–11.

Refereed Conference proceedings

Oral communications

Sgavetti, M., Tampella, G., Serventi, G., **Franchi,. F.**, and Baioni, D. Spectral characteristics of the Hamar Laghdad area: an analogue for identification of Mars methanogenic features. 3rd Conference on Terrestrial Mars Analogues, 25-27 October 2012, Marrakech, Morocco.

Pondrelli, M., Rossi, A.P., van Gasselt, S., Le Deit, L., Glamoclija, M., Cavalazzi, B., Fueten, F., **Franchi, F.**, Haubert, E. and Zegers, T. Equatorial Layered Deposits in the Firsoff crater: geological characterization and possible Earth analogues. 3rd Conference on Terrestrial Mars Analogues, 25-27 October 2012, Marrakech, Morocco.

Franchi, F., Rossi, A.P., Pondrelli, M., Cavalazzi, B., Barbieri, R. Ancient fluid escape and related features in the equatorial Arabia Terra (Mars). 12th European Workshop on Astrobiology (EANA), 15-17 October 2012, Stockholm, Sweden. [02.4]

Franchi, F., Rossi, A.P., Pondrelli, M., Cavalazzi, B., Barbieri, R. Ancient fluid escape and related features in the equatorial Arabia Terra (Mars). European Planetary Science Congress, 23-28 September 2012, Madrid, Spain. [EPSC2012-132]

Franchi, F., Cavalazzi, B., Barbieri, R., Ori, G. G. Overview of the geology of the

Devonian Kess-Kess mounds of the Anti-Atlas, Morocco. COCARDE meeting, October 2011, Rabat, Morocco.

Franchi, F., Pierre, C., Schemm-Gregory, M., Cavalazzi, B. and Barbieri, R. Methane-related Ca-carbonates and other evidences of seepage in the Kess Kess conical mounds (Eastern Anti-Atlas, Morocco). 28th IAS meeting, July 2011, Zaragoza, Spain.

Poster communications

Franchi, F., Cavalazzi, B., Rossi, A. P., Pondrelli, M., Barbieri, R. Kess Kess Hydrothermal Mounds in Morocco: A Unique Analog for Exploring Possible Fossil or Extant Life on Mars. 43rd Lunar and Planetary Science Conferente, March 2012, The Woodlands, Texas. [2245].

Franchi, F., Cavalazzi, B., Rossi, A. P., Pondrelli, M., Barbieri, R. Ancient Fluid Escape and Conical Mound Fields in Firsoff Crater, Arabia Terra (Mars). 43rd Lunar and Planetary Science Conferente, March 2012, The Woodlands, Texas. [1062]

Franchi, F., 2011. Diagenesis of the Devonian conical mounds of the eastern Anti-Atlas (Morocco). 28th IAS meeting, July 2011, Zaragoza, Spain.

Franchi, F., Barbieri, R., Cavalazzi, B. Evidences of hydrothermal activity in the Kess Kess carbonate mounds, Morocco. 23rd CAG meeting 2011, Johannesburg.

Franchi, F. (Ed. Fanti, F., Spalletta, C.) Stratigraphic revision of the Cretaceous 'Continental Intercalaire', Tataouine region, Southern Tunisia: palaeogeographic implications. International Conference on Vertebrate Paleobiogeography 2009, Bologna.

Giglio, F., Romano, S., Ravaioli, M., **Franchi, F.** Heavy metals distribution in the Adriatic sea sector influenced by sediment input from Neretva River. Geoitalia 2007, Rimini.